INFLUENCE OF MICROSTRUCTURE OF BI-LAYERED POLYMERIC ANTIMICROBIAL SCAFFOLDS IN VASCULAR TISSUE ENGINEERING

A THESIS PRESENTED BY

SOUMYA COLUMBUS K C

TO

SREE CHITRA TIRUNAL INSTITUTE FOR MEDICAL
SCIENCES AND TECHNOLOGY
THIRUVANANTHAPURAM
INDIA

IN PARTIAL FULFILMENT OF THE REQUIREMENTS
FOR THE AWARD OF
DOCTOR OF PHILOSOPHY

2015

DECLARATION

I, **Soumya Columbus K C**, hereby certify that I had personally carried out the work depicted in the thesis entitled, ***"Influence of microstructure of bi-layered polymeric antimicrobial scaffolds in vascular tissue engineering",*** except where due acknowledgment has been made in the text. No part of the thesis has been submitted for the award of any other degree or diploma prior to this date.

Thiruvananthapuram
06-05-2015

Soumya Columbus K C
Reg.No: 2010/PhD/20

SREE CHITRA TIRUNAL INSTITUTE FOR MEDICAL SCIENCES & TECHNOLOGY
BIOMEDICAL TECHNOLOGY WING, POOJAPPURA
THIRUVANANTHAPURAM – 695011, INDIA
(An Institute of National Importance under Govt. of India)
Phone-(91)0471-2520221 Fax-(91)0471-2341814 www.sctimst.ac.in

Dr. V. Kalliyana Krishnan
Scientist G (Senior Grade)
Dental Products Laboratory
BMT Wing, SCTIMST
email: kalyankv@sctimst.ac.in

This is to certify that **Ms. Soumya Columbus K C**, in the Dental Products Laboratory of this Institute has fulfilled the requirements prescribed for the Ph. D. degree of the Sree Chitra Tirunal Institute for Medical Sciences and Technology, Thiruvananthapuram. The thesis entitled, ***"Influence of microstructure of bi-layered polymeric antimicrobial scaffolds in vascular tissue engineering"*** was carried out under my direct supervision. No part of the thesis was submitted for the award of any degree or diploma prior to this date.

* Clearance was obtained from the Institutional Ethics Committee/ Institutional Animal Ethics Committee for carrying out the study.

Thiruvananthapuram
06-05-2015

Dr. V. Kalliyana Krishnan
(Research Supervisor)

The thesis entitled

"INFLUENCE OF MICROSTRUCTURE OF BI-LAYERED POLYMERIC ANTIMICROBIAL SCAFFOLDS IN VASCULAR TISSUE ENGINEERING"

Submitted by

SOUMYA COLUMBUS K C

for the degree of

Doctor of Philosophy

of

SREE CHITRA TIRUNAL INSTITUTE
FOR
MEDICAL SCIENCES AND TECHNOLOGY, TRIVANDRUM

Is evaluated and approved by

…….	……..
Dr. V. Kalliyana Krishnan	Examiner
(Research Supervisor)	

Dedicated to

GOD ALMIGHTY & MY FAMILY

ACKNOWLEDGEMENTS

It is with a deep sense of gratitude, satisfaction and with the divine blessings of God almighty that I submit this dissertation. I take this opportunity with much pleasure to thank all those who have contributed in many ways for the success of this study.

I have no words to express my deepest sense of gratitude and respect to my Guide Dr. V Kalliyana Krishnan, Scientist G (Senior Grade), DPL, SCTIMST who offered continuous advice and encouragement throughout the course of my study. He introduced me into the scientific world with systematic guidance and support which motivated me always for achieving the targets of the study. He was always accessible and took significant effort for the successful completion of this endeavour.

I thank members of Doctoral Advisory Committee, Dr. Lissy K Krishnan, Scientist G, TRU, Dr. P P Lizymol, Scientist D, DPL and Dr. G.S.Bhuvaneshwar, former Head, BMT Wing, SCTIMST for their timely suggestions, ideas and comments which helped in the improvement of the quality of this work. I extend my special gratitude to Dr. Lissy K Krishnan who provided constant encouragement and support throughout the study. She gave me complete freedom in Thrombosis Research Unit to carry out the biological aspects of the study which enabled me to work efficiently in an interdisciplinary area like tissue engineering.

I am grateful to the Director of SCTIMST and the Head, BMT Wing for all support provided during the course of my work. I thank Department of Biotechnology, Government of India and Kerala State Council for Science Technology and Environment, Kerala, India for providing project funding which includes my fellowship during the study.

I am thankful to the Dean Prof. Suresh Nair, Associate Dean Dr. Prabha D. Nair for their support during the course. I am also acknowledging Dr. Jaysingh, the Deputy Registrar and all members of academic division for their assistance.

I thank Dr. H K Varma, Dr. Suresh Babu, Mr Vijayan, Mr. Nishad and all members of BCL who helped in ICP, XRD and SEM analysis. I would like to acknowledge Dr. K Sreenivasan, Dr. C Radhakumary and Mr P R Hari, LPA for DSC and GPC analysis; Dr. Prabha D Nair, Ms. Geetha and staff, DTERT for contact angle measurements; Dr Annie John, Ms. Susan Mani of Transmission electron microscope lab for TEM analysis. I also acknowledge Er.V Ramesh Babu and Staff of Precision fabrication facility for fabricating molds for different experiments.

I am extending sincere thanks to Dr. T V Kumary, Dr. P R Anil Kumar, Ms. Usha Vasudev and staff of Tissue Culture Lab for cyto-compatibility evaluation of scaffolds; I am grateful to Dr. P R Umasankar, Dr. Sachin Shenoy and all staff, DIMT & Dr. Harikrishnan V.S and staff, DLAS for helping in experiments with sheep and rabbit. I thank Department of Physics, CUSAT and Department of Chemical Sciences, MG University for helping in the AFM and SEM analysis.

I am acknowledging all TRU members especially to Ms. Renu Ramesh who trained me in the cell isolation and culture experiments. I am thankful to Ms. Priyanka Manoj and Mr. Anil Kumar for the help with hemolysis evaluation. I extend my thanks to all other members Dr. Anugya Bhatt, Ms. Mary Vasantha, Mr. Renjith S, Ms. Tara S, Ms. Subha S and Ms. Indu for their timely help and friendship. I am grateful to Dr. Asha S Mathews who was with me during the initial stages of study and also to Dr. Ragaseema V M, Dr. Unnikrishnan S for their help.

I am extremely thankful to my labmates for their help during the study. I thank Mr. Renjith P Nair for the help in fibrin coating of scaffolds and analysis of cell seeded scaffolds; Mr. R Satheesh and Mr. Arun Torris for training the Micro-CT operation; Ms. Ariya Saraswathy and Mr. P R Rejin for providing training of UTM testing. Dr. Diksha Painuly gave me valuable advice which helped me during paper communication and thesis writing. I also thank Ms. Rethikala P K, Ms. Vibha C, Mr. Shameem Mohammed, Ms. Jasmin Joseph, Ms. Sreelekshmi, Ms. Priya for their friendship which relieved my stresses and made my days memorable.

I am extremely grateful to all my teachers within the campus who were involved in my PhD course work. Cooperation from staff of various administrative departments and library of the Institute is fondly remembered. Cordial attitude and support from my fellow students from other departments of our campus is acknowledged especially Ms. Remya, Ms. Mayuri, Ms. Sudhin Thampi, Mr. Arjun Namboothiri and Dr. Priya of POP, Ms. Sunitha of TEM and Ms. Rakhi of DTERT.

I have no words to express gratitude to my family members who provided the most precious support. I am indebted to my parents and my sister for their endless support, encouragement, love and prayers. I am gratified to my mother-in-law and father-in-law for their support for overcoming difficult times. My Husband Nithin has been the pillar of my strength and supported me wholeheartedly whenever it was most required.

God almighty I kneel down before you for giving me strength, courage and for providing good health for completing this work.

TABLE OF CONTENTS

LIST OF FIGURE

LIST OF TABLES

ABBREVIATIONS

AGF	: Angiogenic Growth Factor
ASTM	*:* American Society for Testing and Materials
bMSCs	: Bone Marrow Stromal Cells
BS	: Bi-layered
BVTE	: Blood Vessel Tissue Engineering
CAD	: Computer Aided Designing
CAM	: Computer Aided Modelling
CVD	: Cardio Vascular Diseases
DAPI	: 4',6-Diamidino-2-Phenylindole
DSC	: Differential Scanning Calorimetry
EC	: Endothelial Cell
ECM	: Extra Cellular Matrix
EDS	: Electron Dispersive Spectroscopy
EDTA	: Ethylene diamine tetra acetic acid
ES	: Electro Spun
ESEM	: Environmental Scanning Electron Microscopy
EPC	: Endothelial Progenitor Cell
E	: Elongation
ePTFE	: expanded poly tetrafluoroethylene
ETO	: Ethylene Oxide
FBS	: Fetal Bovine Serum
FDA	: Food and Drug Administration
GAG	: Glycosaminoglycan
GPC	: Gel Permeation Chromatography
Hb	: Haemoglobin
HBSS	: Hank's Balanced Salt Solution
HDPE	: High Density Polyethylene
HPLC	: High Performance Liquid Chromatography
HUVEC	: Human Umbilical Vein Endothelial Cell
IAEC	: Institutional Animal Ethics Committee
ICP/OES	: Inductively Plasma Optical Emission Spectroscopy
ISO	: International Organization for Standardization
IU	: International Unit
M	: Modulus

Micro-CT	: Micro-Computed Tomography
MGG	: May-Grunwald-Giemsa
Mn	: Number average molecular weight
MSC	: Mesenchymal Stem Cells
MW	: Molecular Weight
PBMNC	: Peripheral Blood Mono Nuclear Cell
PBS	: Phosphate Buffered Saline
PCL	: Poly(ε-caprolactone)
PDLLA	: Poly(DL-lactic acid)
PEG	: Poly(ethylene glycol)
PET	: Polyethyelene terephthalate
PGA	: Poly(glycolic acid)
PGF	: Platelet derived Growth Factor
PGS	: Poly(glycerol sebacate)
PLA	: Poly(lactic acid)
PLCL	: Poly(lactide-co-caprolactone)
PLGA	: Poly(lactic-co-glycolic acid)
P(LLA-CL)	: Poly(L-lactide-co-caprolactone)
PU	: Polyurethane
RBC	: Red Blood Cell
SC	: Solvent Cast
SCPL	: Solvent Casting and Particulate Leaching
SD	: Standard Deviation
SEM	: Scanning Electron Microscopy
SIS	: Small Intestinal Submucosa
SMC	: Smooth Muscle Cell
SMPC	: Smooth Muscle Progenitor Cell
SNP	: Silver Nanoparticles
TE	: Tissue Engineering
TIPS	: Thermal Induced Phase Separation
TS	: Tensile Strength
UTM	: Universal Testing Machine
VEGF	: Vascular Endothelial Growth Factor
XRD	: X-ray diffraction
ZIA	: Zone of Inhibition

SYNOPSIS

Pathological conditions such as atherosclerosis and thrombosis that affect small diameter blood vessels adversely are major causes of mortality and morbidity globally. Autologous grafts such as sephenous vein and internal mammary artery are considered to be the gold standards for replacing the diseased blood vessels. Lack of availability of these grafts has led to the development of synthetic grafts mainly using polyethylene terephthalate (Dacron) and poly(tetrafluroethylene) (PTFE). Unlike in case of large and medium diameter applications, synthetic small diameter grafts (<5 mm diameter) are found to be highly prone to thrombosis and associated with high failure rates. In this scenario, tissue engineering (TE) is evolving as a promising strategy, whose purpose is to create vascular tissue in the laboratory with the aid of a biodegradable scaffold on which cells may be grown. Design strategies of the scaffold mimicking the natural blood vessel structure are expected to provide better cell attachment and multilayered organization of vascular cells. Moreover, the regulation of micro-architectural parameters such as pore size and porosity at the individual layers of scaffold may provide suitable homing sites for specific cell type, similar to native extra-cellular matrix. Some TE approaches emphasized on multilayered scaffolds, but the gradient porosity characteristics at the scaffold strut has not been addressed so far. The mechanical properties and degradation characteristics of scaffold also need to be optimized in terms of microstructure present within it. Further the incorporation of a suitable agent during scaffold fabrication can impart antimicrobial activity to the scaffold, which may be effective to prevent contamination during *in vitro* culture.

In this background, the main goal of the study was to evaluate an antimicrobial bi-layered scaffold design strategy for small diameter blood vessel applications. The study is presented in six chapters. The background and introduction to the work are presented in Chapter 1. It explains in detail the anatomy of blood vessel, pathology affecting blood vessel, treatment modalities, vascular grafting and classifications. It also briefly introduces TE strategies and various aspects of scaffolds for blood vessel construction. Major challenges in scaffold design for blood vessel such as relevance of multilayered scaffold design, need for gradient pore size within the scaffold strut for facilitating the growth of vascular cells and mechanical integrity of scaffolds while undergoing degradation have also been briefed. Properties of biodegradable polymers employed in TE and suitable agents for imparting antimicrobial activity have also been described.

Hypotheses put forward on the basis of current knowledge are: *(1) Optimization of morphology of PCL based scaffolds can be done by suitable selection of fabrication parameters during solvent casting and electrospinning (2) Antimicrobial property may be induced by incorporating appropriate agent during scaffold fabrication process (3) Multilayered scaffold with a pore size gradient across the layers may be fabricated for TE of small diameter blood vessels while satisfying the mechanical and degradation characteristics (4) Microstructure of scaffolds may be a determining factor in deciding the final performance of vascular grafts.* In order to prove the hypotheses, a 5-pronged approach was employed such as (i) the optimization of properties of scaffolds fabricated by solvent casting and particulate leaching (SCPL) method, (ii) evaluation of solvent cast scaffolds after silver nanoparticle (SNP) incorporation, (iii) optimization of

electrospun scaffold properties by varying fabrication parameters, (iv) evaluation of electrospun scaffold properties after SNP incorporation and (v) design strategy for constructing a tissue engineered antimicrobial bi-layered scaffold (BS) and its evaluation. Major objectives of the current study are identified as follows.

- To standardize the fabrication parameters to obtain appropriate scaffold microstructure and optimum properties using SCPL and electrospinning
- To investigate the effect of SNP incorporation on properties of selected solvent cast and electrospun scaffolds
- To evaluate the potential of the scaffold systems to support the growth of primary endothelial cells
- To design a antimicrobial bi-layered scaffolds with pore size gradient across the scaffold strut
- To evaluate the physico-mechanical properties of BS scaffold and compare with native blood vessel
- To investigate the potential of bi-layered scaffolds for supporting the growth of endothelial cells (ECs) and smooth muscle cells (SMCs) in a bioreactor system.

In Chapter 2, literature is reviewed to understand the current status of vascular TE. The topics reviewed include history of vascular grafts, various strategies adopted for development of small diameter vascular grafts including various TE approaches. It also reviews multilayered scaffold design strategies in vascular TE, importance of scaffold porosity characteristics in TE: influence on cellular growth and proliferation, mechanical properties and degradation

characteristics of scaffolds. Review also summarises the incorporation strategies of antimicrobial agents into polymer systems for various biomedical applications.

In Chapter 3, experimental design in order to achieve the objectives of the proposed study is elaborated. It includes detailed description of materials employed, experimental protocols and instruments employed for the present study. Fabrication of tubular scaffolds using SCPL is described in Section 1. Electrospinning strategies are provided in Section 3 and bi-layered scaffold construction by combining the two methodologies is detailed in Section 5. Synthesis protocols of poly(ethylene glycol) [PEG] protected SNP is described in Section 2 and incorporation methods of SNPs into the scaffolds is also provided in Section 2 and Section 4. Porosity analysis methods such as SEM, micro-CT and gravimetric analysis are described. Description of mechanical testing of scaffolds such as tensile testing, burst strength and suture retention strength evaluation using UTM is given. Protocol of *in vitro* degradation study of scaffolds up to one year is provided which has been monitored and analyzed by GPC and gravimetric methods. Measurements and analysis of surface wettability using goniometer, surface roughness using AFM, scaffold crystallinity using DSC and XRD are also detailed. Descriptions are also given for silver nanoparticle distribution analysis (TEM and EDS), SNP release profile (ICP/OES) and antimicrobial activity demonstration (Zone of Inhibition Assay). Cyto-compatibility estimation of SNP incorporated scaffolds using direct contact and MTT assay, hemo-compatibility evaluation of scaffolds using hemolysis assay as per ISO 10993-part4 are provided. Procedures of EC and SMC culture from rabbit blood are described. Experimental design of co-culture system of EC and SMC on the bi-layered scaffold in two channel bioreactor system is also provided. Examination details of cell seeded

scaffolds have been carried out using fluorescence microscopy after staining with Texas red conjugated Phalloidin for actin filaments and DAPI for cell nuclei.

Chapter 4 includes results presented in the form of figures, tables and graphs. Properties of solvent cast (SC) poly(ε-caprolactone) (PCL) scaffold were optimized by varying molecular weight of PEG and its concentration. Tubular scaffolds having 4mm inner diameter were fabricated by SC and particulate leaching (PL) method using PEG as porogen. Scaffolds with 4:4 PCL-PEG ratio were found to possess better tubular consistency, wall thickness, porosity with required tensile strength for blood vessel tissue engineering (BVTE). Further these selected scaffolds were screened after subjecting to degradation 6 months and found that scaffolds containing lower molecular weight PEG possess better retention of properties after degradation. Growth potential of the scaffolds was evaluated using EC. Further SNP solution was synthesized and characterized using TEM, XRD and UV-VIS spectroscopy. It was found that SNP incorporation did not result in significant alteration in morphological and mechanical properties of SC scaffolds. Cytotoxicity results showed that SNP incorporated scaffolds (SC-SNP) were cyto and hemo compatible. Uniform coverage of EC was observed after 3 days static culture. Further flow rate was varied and electrospinning parameters were optimized to generate electrospun mats. Depending upon porosity characteristics and mechanical properties appropriate electrospun scaffold (ES) was selected. These scaffolds maintained structural integrity even after one year degradation. After SNP incorporation, fiber diameter and pore size of ES-SNP scaffolds were found to shift towards lower values. Mechanical properties, Crystalline properties, surface wettability and surface roughness of the ES-SNP scaffolds also showed variation compared to bare scaffolds. ES-SNP scaffolds were

found to be cyto and hemo-compatible. ES-SNP scaffolds showed more uniform EC growth compared to bare scaffolds after 5 days of static culture. Further design strategy has been projected to construct an antimicrobial bi-layered scaffold (BS) by combining SCPL and electrospinning technologies where SC-SNP serves as luminal layer which can provide smooth, antimicrobial and hemocompatible layer and ES as abluminal layer which can provide mechanical integrity to the graft. Physico-chemical evaluation showed that BS scaffold possess adequate mechanical integrity for BVTE. EC and SMC were isolated from rabbit blood and seeded into BS scaffold. After 3 days of culture, EC were found to align along the direction of flow and SMC were found to grow on abluminal fibrous layer.

In Chapter 5 results are discussed and analyzed with the aid of current literature. It is shown that multilayered scaffold design with optimized microstructure, mechanical properties and degradation characteristics will be important criteria to achieve successful small diameter vascular construct. The importance of present study has also been highlighted.

Chapter 6 summarises the results and conclusions drawn from the present study. The antimicrobial bi-layered scaffold could provide mechanical properties and degradation characteristics for BVTE. It can also serve as a suitable matrix for vascular tissue generation by providing suitable homing sites for EC and SMC. The work establishes the importance of microstructure on bi-layered polymeric antimicrobial scaffolds in blood vessel construction. The limitations of the current study have been identified and future areas of research to produce a suitable implantable blood vessel have been projected. Citations are listed in the bibliographic section.

CHAPTER 1

INTRODUCTION

Vascular network in the human body consists of conduits carrying blood and together with the heart constitutes the circulatory system. Atherosclerosis is a major condition that can drastically deteriorate the normal functioning of small diameter blood vessels. This often leads to coronary heart diseases, which is a major cause of mortality and morbidity (Ross *et al*., 1993). Cardiovascular disease (CVD) is estimated to cause about 17.3 million deaths globally and 1.7 to 2 million deaths in the Indian population annually (Go *et al*., 2013, Gupta *et al*., 2011). In cardiac and peripheral surgical procedures, the diseased vessels are most often replaced by patient's own healthy vessel. It is reported that ~1.4 million surgical procedures are annually performed in the United States alone (Langer *et al*., 1993). However 30-40% patients suffer from lack of suitable grafts for revascularization due to prevalence of vascular diseases, trauma and previous surgery (Faries *et al*., 2000). In addition, surgical harvesting of autologous graft is associated with unavoidable donor site morbidity and additional surgical costs (Swenne *et al*., 2006). To circumvent this problem, synthetic prosthetic grafts have been employed successfully in large diameter vessel replacements. However, these grafts are highly prone to thrombosis and associated with high failure rates when employed as small diameter grafts (< 5mm). Despite more than 50 years of research, development of a small diameter graft with a patency rate equivalent to that of native tissue remains a big challenge which has been hailed as `Holy Grail' of vascular surgery (L' Heureux *et al*,. 2007).

In this context, tissue engineering is emerging as a promising approach in vascular research towards the development of functional small-diameter vascular grafts (SDVG). The strategy adopted earlier has been to combine biodegradable scaffolds with biological components such as cells, extracelluar matrix and growth factors (Campbell & Campbell, 2007). Design approaches of the scaffold which mimic the natural blood vessel structure is expected to provide better opportunities to regenerate the multilayered organization of vascular tissue. Several attempts which emphasized on multilayered scaffold fabrication have been reported earlier (Han *et al*., 2013, Zhang *et al*., 2008, Williamson *et al*., 2006). However, most of studies fail to highlight the need to address the micro-structural characteristics at the individual layers of scaffolds to facilitate the growth of different vascular cells (Zhang *et al*., 2008). Other important parameters such as mechanical properties and degradation profile of scaffold can also influence the fate of the construct after implantation. Lack of careful consideration of these factors may affect the performance of the graft leading to aneurysm formation, rupture etc (Pavcnik *et al*., 2009). The present study details the fabrication of a bi-layered scaffold with a pore size gradient across the scaffold wall to favour optimum tissue generation while maintaining appropriate mechanical properties and degradation characteristics suitable for small diameter blood vessel tissue engineering.

The construction of a tissue-engineered vascular graft requires seeding vascular cells onto the scaffolds and maturation *in vitro* which poses a threat of microbial contamination. In order to address this, a suitable antimicrobial agent has been identified and incorporated during scaffold fabrication and evaluated for small

diameter blood vessel applications. The proper understanding of the anatomy and physiology of blood vessel, pathology affecting blood vessels, current treatment modalities, various aspects of vascular grafting, basic concepts of tissue engineering, need for a scaffold, biodegradable polymers employed in scaffold fabrication and strategies for imparting antimicrobial activity to the tissue engineering scaffolds which are helpful for the present study are outlined below.

1.1. Anatomy and physiology of blood vessels

Blood vessels carry blood from the heart and are distributed throughout the body. They form a branched system of arteries and veins that vary in size, mechanical properties and structural organization depending on their location and specific function (Ratcliffe, 2000). The large and medium sized arteries are characterized by a distinct tri-lamellar structure consisting of inner *intima*, middle *media* layer and outer *adventitia*, though these are less obvious in the smaller arterioles and do not exist in the capillaries.

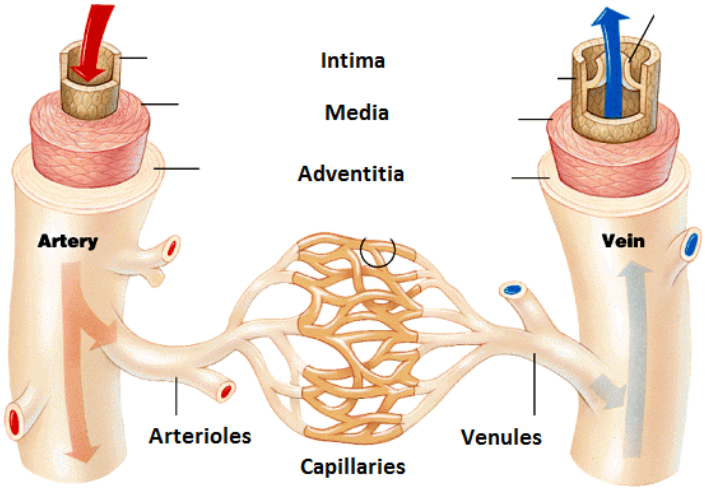

Figure 1: Schematic image representing the structure of blood vessels

(Reference: http://science.kennesaw.edu)

The aorta is the largest artery which carries blood from the heart and delivers blood to smaller arteries and then to smaller arterioles. Arterioles are further divided to form capillaries, which distribute blood to the nearby tissues as shown in Figure 1. Capillaries then form venules and once again join into the larger veins through which impure blood returns to the heart.

1.1.1. Tunica Intima

The intima consists of a lining of endothelial cells (ECs) attached to the basement membrane and forms the luminal layer closest to the blood flow. Endothelium is a dynamic cell layer which plays a critical role in regulating vascular homeostasis (Vanhoutte, 1989 and Rubanyi, 1993). By secreting specific molecules like nitric oxide, endothelial cells inhibit platelet activation and prevent thrombus formation. Endothelial injury or dysfunction may lead to the activation of its pro-thrombotic properties and result in vascular diseases such as atherosclerosis, re-stenosis, and altered immune response (Sumpio *et al.*, 2002). It is thus important to reproduce the functional integrity of the endothelium in tissue-engineered vascular graft (TEVG) for long-term vessel patency. Moreover, a confluent and quiescent EC monolayer is likely to inhibit smooth muscle cell (SMC) proliferation by favouring a contractile SMC phenotype which is needed for long-term inhibition of myoinitimal hyperplasia.

1.1.2. Tunica Media

The media consists of smooth muscle cells (SMCs) embedded in an extracellular matrix (ECM), which is composed of mainly collagen, elastin and proteoglycans

(Patel *et al*., 2006). The media in arterioles and arteries have multiple layers of SMCs, oriented in the circumferential direction of the vessel wall. Media confers mechanical strength to the vessel and controls vessel calibre by contracting and relaxing. The mechanical properties of the vessel are enhanced substantially by ECM that interpenetrates into the SMC layers. While collagen provides the tensile strength for resisting against rupture, elastin dictates elasticity properties and proteoglycans contribute to the compressibility of blood vessel (Ratcliffe, 2000). Lack of elastin and collagen deposition, misalignment of SMCs in the longitudinal rather than circumferential direction and low densities of SMCs are the major pitfalls leading to the limited performance of many tissue-engineered grafts (Chan-Park *et al*., 2009).

1.1.3. Tunica Adventitia

The outer adventitial layer comprises collagenous ECM within which fibroblasts are embedded. It also contains the *vasovasorum* and nerves. The function of adventitial layer is to add rigidity to the blood vessel and fix the vessel to the adjacent tissues.

1.2. Pathology affecting blood vessels and treatment modalities

Atherosclerosis has a key role in the drastic deterioration of functioning of the blood vessels (Benditt & Schwartz, 1988). It involves deposition of fatty plague in the arterial wall, followed by calcification of the plaque resulting in progressive narrowing and hardening of blood vessel. The occlusion of vascular conduit may also be caused by the formation of blood clot or thrombus. Vascular disability at different locations such as heart, brain and legs may lead to heart attack, stroke and peripheral vascular diseases respectively. Depending upon the severity, therapeutic

methodologies such as angioplasty, stenting or bypass surgery can be adopted to correct the diseased blood vessel. While minor narrowing of the blood vessel can be treated with angioplasty and stenting, vessels occluded to a considerable extent may be replaced by healthy grafts in a bypass procedure. Reports suggested that 10 % of patients with coronary artery diseases undergo bypass surgery (Michaels & Chatterjee, 2002).

1.3. Vascular grafting

Conduits used to replace the diseased or blocked blood vessels are called vascular grafts. Primarily an ideal vascular graft should have adequate mechanical strength and matching compliance to withstand long term hemodynamic blood pressures experienced by the native artery. The graft should also have thrombus resistant lumen which is critical in deciding the graft patency. While biocompatibility and non-immunogenicity of the graft is crucial, low susceptibility towards infection is also favoured. Handling characteristics, suturability, off-the-shelf availability and reasonable manufacturing costs are also factors considered to achieve an ideal vascular graft (Yow *et al*., 2006).

1.3.1. Classification of vascular graft based on size

Depending upon size, grafts can be classified as large caliber, medium caliber and small caliber grafts (Chlupac *et al*., 2009).

***1.3.1.1. Large calibre vascular grafts*:** Grafts with diameter greater than 8 mm are considered as large diameter. Due to large vessel radius, the resistance to blood flow

is low in large diameter grafts. Hence the occurrence of thrombosis is less and these are associated with high patency rates.

1.3.1.2. Medium calibre vascular grafts: Grafts with diameter ranging 6-8 mm but greater than 5 mm are regarded as medium diameter grafts. These grafts have shown comparably high patency rates similar to those of large diameter ones.

***1.3.1.3. Small calibre vascular grafts*:** Grafts whose diameters are lower than 5 mm are considered as small diameter grafts. In these grafts, lower vessel radius results in high resistance to blood flow. Hence these grafts are highly prone to thrombosis.

1.3.2. Classification of vascular graft

Based on origin, grafts can be classified as *natural* and *synthetic*.

***1.3.2.1. Natural Grafts*:** Usually autologous grafts such as sephenous vein from the leg, internal mammary artery and radial artery from arm are most preferable options during vascular surgery (Hoenig *et al*., 2005). These grafts possess physiological properties akin to the native vessel and are considered as gold standard. The lack of availability of these grafts due to various factors such as prevalence of other vascular diseases and need for multiple grafts are major concerns in vascular surgery.

***1.3.2.2. Synthetic grafts*:** Synthetic prosthetic grafts are being employed as grafts during vascular surgery. Polymers such as expanded polytetrafluoroethylene (Teflon) (ePTFE), polyethylene terephthalate (Dacron) (PET) and polyurethane (PU) are employed for vascular graft applications (Chlupac *et al*., 2009). Acute thrombogenicity, compliance mismatches and high susceptibility to infection increase the failure rates of small diameter prosthetic grafts (L' Heureux *et al*., 2007).

There is tremendous demand currently for developing a functional small-diameter graft for use in the clinical scenario.

1.4. Tissue engineering approaches

Tissue engineering (TE) is an interdisciplinary field that applies the principle of engineering and life sciences towards the development of functional substitutes for replacing diseased or damaged tissues or organ (Langer & Vacanti, 1993). It is emerging as a potential solution to solve the issues related with conventional therapeutic approaches including organ transplantation and replacement with artificial implants.

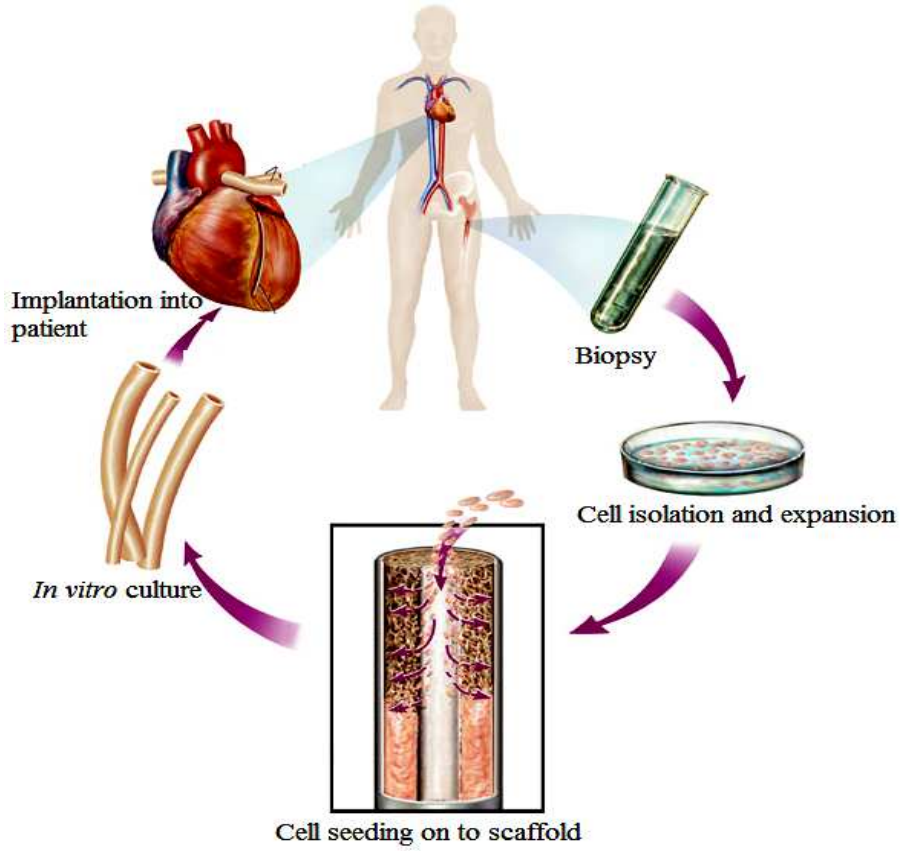

Figure 2: Representative figure conveying the concept of vascular tissue engineering

(Reference: www.yalescientific.org)

The construction of a tissue-engineered vascular graft requires the assembly of three major components such as scaffold, vascular cells and bioactive agents or growth factors. In principle, autologous cells can be isolated from appropriate sources and can be expanded *in vitro* to get the adequate number of cells. These cells can be accommodated into three dimensional temporary entities called scaffolds. *In vitro* conditioning of the cell seeded construct with the aid of a bioreactor can mimic the native tissue environment which could further facilitate structural organization of vascular tissue within the construct. After optimizing *in vitro* pre-conditioning, the new blood vessel can be implanted back to the host (as represented in Figure 2). By using autologous cells, TE approach combines the advantages of autografts while ruling out the problems associated with conventional prosthetic grafts.

1.5. Scaffolds in tissue engineering

A scaffold can be defined as ‘a porous structure, usually polymeric, which serves as a substrate and guides tissue formation’ (Williams, 1999) or ‘artificial three dimensional frame structure that serves as a mimic of extracellular matrix for cellular adhesion, migration, proliferation and tissue regeneration in three dimension’ (Wen & Zhang 2006). Biodegradable scaffolds enable the gradual replacement of the scaffold material with host tissue thereby avoiding long term immune responses. Major requirements for a tissue engineered scaffold are proper macrostructure, optimum porosity characteristics, suitable degradation properties and appropriate mechanical stability while satisfying biocompatibility criteria (Figure 3). The appropriate porosity characteristics of the scaffold within the structure facilitate the cellular invasion into the scaffold (Matthews *et al*,. 2002). Once the tissue-

engineered construct is implanted, the scaffold should provide the initial mechanical support to withstand the *in vivo* forces. Controlled biodegradability of scaffold material enables the replacement of the scaffold by the growing tissue. Moreover the degradation products must be nontoxic to the surrounding tissues and should be non-immunogenic (Shoichet, 2010).

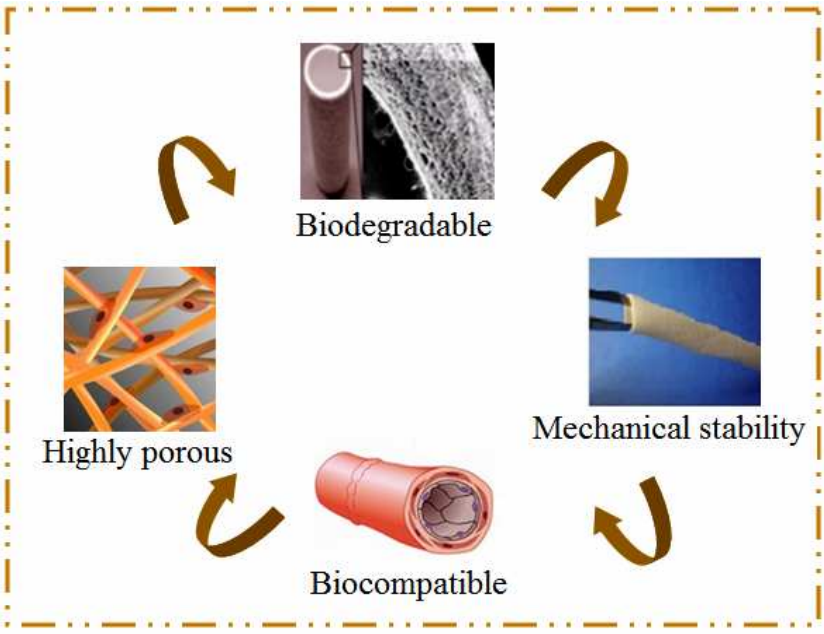

Figure 3: Schematic diagram showing requirements for an ideal scaffold

1.5.1. Relevance of scaffold microstructure in tissue engineering

The most important micro-structural parameters of scaffold are porosity and pore size. While porosity represents total pore volume present within the scaffold, pore size is the average diameter of the pores present in it (Ho & Hutmacher, 2006). High porosity can facilitate uniform cellular in-growth with enhanced diffusion of metabolites into the scaffold (Karande *et al.*, 2005, Taboas *et al.*, 2003), though mechanical properties may deteriorate. It has been reported that cell growth is highly

specific and influenced by scaffold pore size (Yang *et al*., 2001, Lee *et al*., 2008). Pore size is also reported to influence the scaffold mechanical properties and degradation characteristics (Yu *et al*., 2008, Odelius *et al*., 2011). Moreover, the scaffolds should have a well-interconnected porous structure for facilitating the delivery of cells and nutrients.

1.5.2. Scaffold biodegradation and mechanical stability

Biodegradation of the scaffold is a desirable prerequisite in tissue engineering endeavours for facilitating natural tissue formation. Degradation profile of the scaffold may be regulated for successful tissue fabrication by choosing appropriate matrices. Ideally, the rate of scaffold biodegradation and the tissue growth may be correlated as represented in Figure 4.

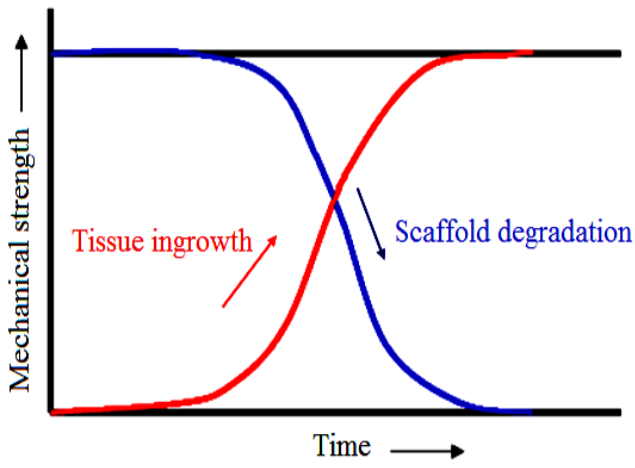

Figure 4: Illustration showing preferable biodegradation rate of TE scaffold

(Reference: Hutmacher, 2000)

The scaffold should provide sufficient mechanical support in the physiological conditions immediately upon implantation. As scaffold degrades, its mechanical strength should be gradually transferred to the growing tissue such that

the integrity of the construct should be maintained *in vivo* (Dong *et al*., 2009). Most of the earlier tissue engineering efforts for blood vessels evaluated only the initial strength of scaffold and did not account for the performance of scaffold when it undergoes degradation. Degradation can alter scaffold porosity and pore size which in turn can affect the mechanical strength of the construct. This may be the reason for failure of most of the tissue engineering constructs.

1.6. Challenges in designing scaffolds for blood vessels

The major challenges in attaining an ideal scaffold for a blood vessel are (i) Designing a tubular scaffold with multilayered macro-structure similar to that of the native blood vessel, (ii) Regulating the pore size and porosity at the individual layers in terms of growth of vascular cells such as endothelial cells, smooth muscle cells and fibroblasts (iii) Attaining the mechanical properties of scaffolds as required for blood vessel applications (iv) Achieving degradation characteristics suitable for long-term implant applications (v) Ability to withstand microbial contamination during *in vitro* culture conditions.

1.7. Biodegradable polymers for fabricating scaffold

While designing the scaffold, there are two options for selecting the polymeric material which may be of natural or synthetic origin. The naturally-derived polymers include proteins of natural extracellular matrices such as collagen, elastin, glycosaminoglycans, alginic acid, chitosan, silk fibroin and fibrin (Chen *et al*., 2002). Since natural polymers are derived from nature, these are associated with good biocompatibility. Besides, structurally, they closely mimic natural cellular

environment, thereby facilitating cell-scaffold interaction. However unstable material availability and batch-to-batch variation in properties of these materials are drawbacks associated with these polymers. In addition, many of these polymers require chemical cross-linking with agents such as glutaraldehyde, whose excess limits may promote cytotoxic effects. Poor mechanical properties and fast biodegradation rates are other disadvantages associated with natural polymeric materials.

Synthetic polymers are another class of materials in tissue engineering. It is mostly aliphatic polyesters such as poly(glycolic acid) or PGA, poly(lactic acid) (PLA), poly(lactic-co-glycolic acid) (PLGA), poly(ε-caprolactone) (PCL) etc. that are frequently employed in tissue engineering strategies. Since these polymers have received US Food and Drug administration (FDA) approval for some implantable devices and sutures, they are used in several biomedical applications (Ma, 2004 and Woodward *et al*., 1985). The relevant properties of these polymers are as mentioned in Table 1.

Polymer	Melting point (^{0}C)	Glass transition temp (^{0}C)	Modulus (GPa)	Elongation (%)	Degradation time (months)
PGA	225-230	35-40	7.0	15-20	6-12
PLLA	173-178	60-65	2.7	5-10	>24
PDLLA	Amorphous	55-60	1.9	3-10	12-16
PCL	58-63	-65 to -68	0.4	300-500	>24

Table 1: Properties of biodegradable aliphatic polyesters

Abbreviations PLLA and PDLLA indicate L and DL isomeric forms of PLA respectively

The major advantages of these types of polymers are their availability from reliable sources, excellent mechanical properties and fine control over degradation and fine tunability of properties by altering the composition. However, they are deficient in appropriate cell binding sites, hence resulting in lowering of cell-material interaction that favors cell adhesion, migration and proliferation.

1.7.1. Poly(ε-caprolactone) (PCL)

PCL is the selected polymer for the current study. It is a semi-crystalline polymer with glass transition temperature of -60^0C and melting temperature of $58\text{-}63^0$C. The repeating molecular structure of PCL consists of five non-polar methylene groups and a single hydrophilic ester group.

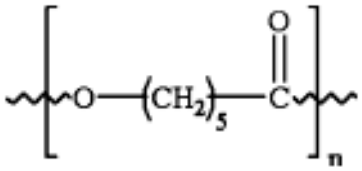

Figure 5: Diagram representing the structure of PCL

Unique properties of PCL are due to its chemical structure. The hydrolytically liable ester group makes the polymer degradable. PCL is not only one of most biocompatible polymers and with ease of fabrication and excellent mechanical properties; it has become a good candidate for tissue engineering applications. The complete resorption of PCL requires more than 2 years (Yang *et al.*, 2001) and the degradation product caproic acid is easily metabolized within the body.

1.8. Strategies for imparting antimicrobial activity to the scaffold

Implant-associated infections are quite severe in tissue engineering strategies particularly during *in vitro* culture periods of cell-seeded construct. It has been reported that the incorporation of appropriate agents such as silver, gold, zinc oxide etc can impart antimicrobial properties to the scaffolds.

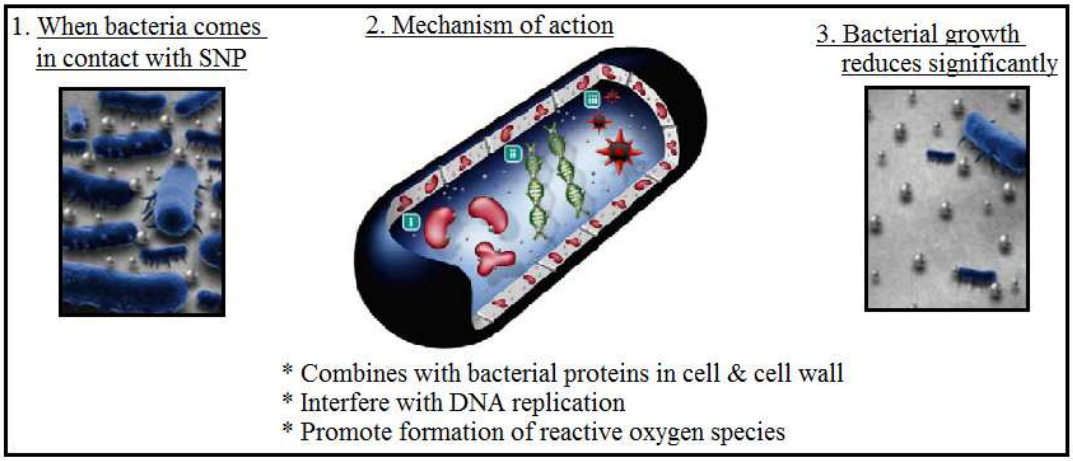

Figure 6: Scheme indicating the mechanism of antibacterial action of SNP

(Reference: www.ecounterre.com)

Recently silver nanoparticles (SNP) have attracted attention in the biomedical field owing to its broad spectrum of antimicrobial activity against a number of bacterial strains at extremely small quantities. The mechanism of antimicrobial properties of SNP is given in the schematic Figure 6. The various approaches that consider the integration of silver nanoparticles into the biomaterials were found to be efficient to prevent biomaterial-associated infections. The efficacy of imparting antimicrobial activity into PLLA (Xu *et al*., 2006), PLGA (Fortunati *et al*., 2011) and PCL (Duan *et al*., 2007) has been reported for several biomedical applications. It was

observed that scaffold properties may be influenced by nanoparticle incorporation especially during the electrospinning process (Duan *et al*., 2007, Xing *et al*., 2010).

1.9. Hypothesis

Native blood vessels are characterized by distinct layers of endothelium and vascular media which is responsible for its inherent non-thrombogenicity and vasoactivity respectively. It is obvious that the growth of endothelial and smooth muscle cells is dependent on the micro-structural characteristics of scaffolds and reported to be highly specific. Moreover, incorporation of a suitable agent during scaffold fabrication can impart antimicrobial activity to the scaffold. Since multilayered constructs can mimic native blood vessel architecture, it is conceptualized that fabrication of a bi-layered antimicrobial scaffold with pore size gradient across the scaffold wall with appropriate physico-mechanical properties may have the potential to support blood vessel tissue engineering. In order to accomplish this, the following steps are conceptualized

(1) Morphology of PCL based scaffolds may be optimized by suitable selection of fabrication parameters during solvent casting and electrospinning

(2) Antimicrobial property may be induced by incorporating suitable agent during the fabrication process

(3) Multilayered scaffold with a pore size gradient across the layers may be fabricated for tissue engineering of small diameter blood vessels while satisfying the mechanical and degradation characteristics

(4) Microstructure of scaffolds may be a determining factor in deciding the final performance of vascular grafts.

1.10. Objectives of the study

In order to prove the hypothesis, following objectives were defined in the present study

1. To standardize the fabrication parameters to obtain appropriate scaffold microstructure and optimum physico-mechanical properties using solvent casting and particulate leaching and electrospinning techniques
2. To evaluate the degradation characteristics of selected solvent cast and electrospun scaffolds
3. To investigate the effect of silver nanoparticle incorporation on properties of selected solvent cast and electrospun scaffolds
4. To evaluate the potential of the scaffold systems to support the growth of primary endothelial cells
5. To design an antimicrobial bi-layered scaffold (BS) with pore size gradient across the scaffold wall
6. To evaluate the physico-mechanical properties of BS scaffold required in comparison with the native blood vessel
7. To demonstrate the antimicrobial activity of the scaffold using appropriate control material

8. To investigate the potential of bi-layered scaffolds for supporting the growth of endothelial cells and smooth muscle cells in a bioreactor system

1.11. Brief overview of the study

Tubular scaffolds having an inner diameter of 4mm were fabricated by solvent casting followed by particulate leaching using poly(ethylene glycol) (PEG) as porogen. The effect of PEG concentration on the physicomechanical properties of the scaffold was studied by varying the PCL-PEG ratio. In addition, effect of PEG molecular weight upon the properties was also studied. Scaffold compositions were optimized on the basis of tubular consistency, wall thickness, porosity characteristics and tensile properties. Growth potential of the scaffolds was evaluated using primary endothelial cells. The selected scaffolds were further screened by subjecting them to *in vitro* degradation up to six months. Scaffold composition was optimized on the basis of better retention in morphological and mechanical properties of scaffold.

PEG-protected silver nanoparticles (SNP) were synthesized and characterized in the lab. In order to impart antimicrobial activity, SNP was added into the optimized solvent cast system. The scaffold microstructure and mechanical properties of SC-SNP scaffolds were evaluated by comparison with those of bare scaffolds and that of native artery. Cyto- and hemocompatibility of SNP-incorporated scaffolds were evaluated and endothelial cell growth was monitored. The wall thickness and inner diameter of the scaffolds were measured in comparison with that of excised sheep artery.

Electrospun scaffold systems were prepared by varying the flow rate during electrospinning. Pore size distribution, tensile properties and variation in tubular wall thickness were studied as a function of flow rate during electrospinning. Electrospinning parameters were optimized to obtain better uniform tubular wall thickness. The structural integrity of the scaffolds was examined after subjecting to degradation up to one year.

Electrospun scaffold properties were evaluated after SNP incorporation. Fiber diameter and pore size of these scaffolds were compared to that of bare scaffolds whereas the mechanical properties were compared with that of native artery. Crystalline properties, surface wettability and surface roughness of the SNP-incorporated scaffolds were also determined. Cyto- and hemocompatibility of scaffolds were studied and endothelial cell growth potential of the scaffolds was investigated.

A bi-layered scaffold (BS) was successfully designed with SC-SNP as the luminal layer which is expected to provide a smooth, antimicrobial and hemocompatible layer and ES as abluminal layer which provides mechanical integrity to the graft. Physico-chemical evaluation showed BS scaffold to possess adequate mechanical integrity for blood vessel tissue engineering. Antimicrobial activity of scaffolds was demonstrated using zone of inhibition assay. Endothelial cells and smooth muscle cells were isolated from rabbit blood and co-culture system was demonstrated on BS scaffold. After 3 days of co-culture, endothelial cells were found to align along the direction of flow and smooth muscle cells were found to be growing on the abluminal fibrous layer.

CHAPTER 2

LITERATURE REVIEW

The major objective of the study is to design and fabricate an antimicrobial bi-layered scaffold with gradient porosity within the scaffold wall to facilitate the growth of vascular cells while satisfying the physico-mechanical properties of blood vessels. To achieve this goal, a thorough knowledge of current progress in this field is required. The following chapter on literature survey elaborates in detail the history of vascular grafts, modification of small diameter prosthetic grafts and various vascular tissue engineering approaches. Scaffold design strategies in vascular tissue engineering that emphasize the importance of microstructure and multilayered macro-structure are also discussed. The influence of scaffold microstructure on cell growth, mechanical properties and degradation characteristics are reviewed in detail. Factors such as scaffold fabrication methodologies, bio-mimetic modification of synthetic scaffolds, development and evaluation of tissue-engineered blood vessels are also discussed. With the aid of published literature, it is possible to derive experimental design strategies for the present study.

2.1. History of vascular grafts

The evolution of vascular grafts was greatly influenced by the progress made in vascular surgery especially in suturing and replacement therapies for diseased vessels. During ancient times, vascular interventions were limited to compressing and cauterizing injured vessels to suppress bleeding. Hallowell and Lambert repaired

a bronchial artery with a suture for the first time in 1759. The first vascular anastamosis or surgical connection of blood vessels was performed in dogs by Nicholas Eck in 1877 (Starzl, 2003). Further Carrel and Gruthrie optimized the vascular anastamosis transplantation technique. Alexis Carrel known as 'Father of vascular surgery,' received Nobel Prize for physiology or medicine in 1912 (Chlupac *et al*., 2009).

For the first time, an autologous vein graft was used for aneurysm repair in 1906. Later, vascular surgery was performed using a sephenous vein graft, thereby initiating a successful era for this type of graft (Lopez & Ginzberg 2008). Human arterial allograft is also reported to have come into use in human vascular reconstructive surgeries (Gross & Hurwitt, 1948). An artificial prosthesis 'Vinyon N' was first implanted for arterial replacement in dogs in 1952 (Voorhees *et al*., 1952). The same graft was employed to treat abdominal aneurysm in humans in 1954, leading to rapid progress in vascular surgery and graft-related research. Later, synthetic prosthetic grafts based on textile fabrics made from Dacron (Deterling & Bhonslay, 1955), PTFE (Soyer *et al*., 1972) and polyurethane (PU) (Lyman *et al*., 1978) were introduced and are now widely employed for repairing large- and medium-diameter grafts.

2.2. Modification of small diameter prosthetic grafts

In spite of the excellent mechanical properties of these prosthetic grafts, its inherent thrombogenicity (Nicolaides, 1985) limits its application in small diameter replacements. Many strategies have been adopted to improve the blood compatibility of these grafts by modifying the graft lumen. Earlier reports have shown that carbon-

coated ePTFE grafts showed decreased platelet adhesion, though the overall patency rates could not be improved (Kapfer *et al*., 2006). Later, immobilization of anticoagulants such as heparin was found to improve the patency of Dacron graft (Devine & Mccollum, 2004), ePTFE and PU grafts (Walpoth *et al*., 1998). Herring *et al* demonstrated that by seeding endothelium on the graft lumen, the patency of Dacron prosthesis in humans could be improved (Herring *et al*., 1978). In order to overcome the issue of de-lamination of EC layer from graft lumen after implantation, preconditioning strategies were employed by subjecting the graft to *in vitro* shear stress (Rademacher *et al*., 2001). Modification methodologies of the graft lumen using EC anchorage enhancing entities such as fibrin (Meinhart *et al*., 2005), collagen (Lu *et al*., 2013) and RGD peptides (Walluscheck *et al*., 1996) were also tried.

2.3. Vascular tissue engineering approaches

The concept of biologically viable, living blood vessels has attracted increasing interest in recent years in the stride towards the development of bioengineered vessels. Construction of vessels is based on the tissue engineering principle with the aid of a biodegradable polymer scaffold. It is expected that bioengineered vessels have the capacity for growth and remodelling according to the host requirements and less chances for thrombosis, infection and rejection (Rezai *et al*., 2004). The various approaches adopted for tissue engineering of blood vessels are also reviewed below.

2.3.1. Based on collagen scaffolds

Weinberg and Bell put forward the idea of living blood vessels and reported that they developed the first tissue-engineered vessel *in vitro* based on collagen gel tubes

(Weinberg & Bell, 1986). These collagen tubes were found to be devoid of adequate mechanical strength and graft modification was done by providing an external Dacron mesh. Bovine SMCs were incorporated into the collagen scaffold during the casting process. Further, ECs and fibroblasts cells were seeded onto the inner and outer graft surfaces, respectively to generate a multilayered construct. The major disadvantage of this model was its inadequate burst strength which could not be improved significantly even after reinforcement with Dacron mesh). Factors such as absence of elastin, longitudinal alignment of SMCs, low densities of SMCs and collagen were identified as the reason for the poor mechanical performance of the model. Later Kanda *et al* constructed an artificial vessel from a non-degradable polyurethane graft and collagen gel embedded with bovine SMCs. ECs were seeded onto the lumen of this graft and subjected to the pulsatile flow. They observed that ECs were aligned parallel to the flow while SMCs were found to have a circumferential alignment after 10 days of culture (Kanda & Matsuda, 1994). Thereafter, a number of experiments were performed with the collagen-based scaffold system. As an alternative strategy, a magnetic field was applied during collagen fibrilogenesis to create a vascular media equivalent where collagen fibrils were circumferentially oriented with SMCs aligned in the same direction (Tranquillo *et al*., 1996).

2.3.2. Cell sheet constructs without the use of scaffold

A novel technique for the production of an artificial blood vessel exclusively from human cells was investigated by L'Heureux *et al* without employing any scaffold (L'Heureux *et al*., 1998). Human umbilical cord SMCs was cultured up to 30 days to

form a cell sheet. It was peeled off from the culture plates and wrapped around the tubular support to form the media. After one week of maturation, cultured fibroblast sheet was once again rolled around to form the outer adventitial layer. The tubular support was removed after 7 weeks of maturation and human umbilical cord ECs were seeded on the lumen of the construct and allowed to grow for one more week. The resultant construct was found to possess a well-ordered three-layered vessel wall that mimicked native blood vessel structure. It was also found to possess burst strength values of ~2594 mmHg. These grafts demonstrated only 50 % patency for 7 days when implanted as an interposition femoral artery graft in mongrel dogs. Relatively high production time was the major drawback of this model.

2.3.3. Based on decellularized matrices

Decellularized matrices can provide ECM components that support cell adhesion together with good mechanical properties. Small intestinal submucosa (SIS) has been widely employed for vascular tissue engineering purposes (Badylak *et al.*, 1999). These have demonstrated high patency rates in canine aorta, carotid and femoral arteries and in superior vena cava (Lantz *et al*, 1990). A 4mm diameter collagen graft derived from SIS and type I collagen exhibited patency 3 months after implantation and remodelled into cellularized vessels (Huynh *et al*., 1999). Endothelial cell seeding was found to be fatal in the performance of these xenografts. EC-seeded decellularized porcine iliac vessels remained patent for 130 days while non-endothelized grafts occluded within 15 days (Kaushal *et al*., 2001). The cellular infiltration into these scaffolds were found be limited due to tight matrix organization. Later, decellularized human umbilical cord arteries remained patent

upto 8 weeks after implantation as abdominal aortic interposition grafts in rats (Gui *et al*., 2009). The main problem associated with this type of graft was the risk of transmission of animal pathogens.

2.3.4. Based on biodegradable scaffolds

Artificial blood vessels can be constructed using biodegradable and biocompatible scaffolds. In the earlier stages, poly(glycolic acid) (PGA) was the most commonly used polymer for the purpose. Niklason *et al* constructed the first synthetic vascular graft based on PGA scaffold. Bovine SMCs were cultured on these scaffolds in a pulsatile condition for 8 weeks and autologous ECs were cultured for 3 days prior to implantation into sephenous vein in swine model. The grafts exhibited enough burst strength before implantation. However, due to its rapid degradation, the graft was unable to withstand hemodynamic pressures (Niklason *et al*., 1999). In a modified approach, PGA/polyglactin scaffolds were implanted into pulmonary arteries in lambs after seeding with SMCs and ECs. After 11 and 24 weeks evaluation, it was observed that tissue-engineered constructs were almost histologically similar to native blood vessel (Shinoka *et al*, 1998). Later, vascular graft composed of PGA non-woven mesh tubes coated with 10 % solution of poly(lactide-co-glycolide) were fabricated and seeded with autologous bone marrow derived mononuclear cells. These grafts were implanted as inferior vena cava interposition grafts in juvenile lambs and after 6 months, explanted grafts showed comparable results in histological evaluation with well-deposited collagen, elastin and proteoglycans (Brennan *et al*., 2008).

The first clinical application of bioengineered vessels based on freeze-dried PLCL reinforced with woven PGA was demonstrated for pulmonary artery reconstruction after seeding with bone marrow cells. These grafts were reported to have 95 % patency for one year without any aneurysm formation. The grafts were designed for pulmonary artery applications but could not withstand arterial pressures (Shin'oka *et al*., 2005). Jeong *et al* constructed a tissue-engineered vessel based on a P(LLA-CL) scaffold cultured with rabbit SMCs under pulsatile flow culture conditions for 6 weeks. The scaffolds were found to support cell proliferation with collagen deposition and cells aligned in the radial direction (Jeong *et al*., 2005). Scaffolds fabricated from P(LLA-CL) were found to possess the tensile strength required for a blood vessel and supported the growth of HUVECs (Uchida *et al*., 2008). Poly(caprolactone) based small diameter nanofibrous scaffolds were fabricated using electrospinning and implanted into rat arterial circulation using ePTFE control grafts. PCL grafts exhibited faster endothelization, neointimal and neovascularisation formation compared to ePTFE grafts (Pektok *et al*., 2008).

2.4. Scaffold design in vascular tissue engineering

2.4.1. Design of scaffold microstructure

Scaffold microstructure is an important parameter which can decide the fate of the tissue-engineered construct. Porosity and pore size are the main architectural parameters of scaffolds (Rnjak-Kovacina & Weiss, 2011). These parameters can significantly influence cellular growth (Lee *et al*., 2008) and other scaffold properties such as mechanical strength (Yu *et al*., 2008) and degradation characteristics (Odelius *et al*., 2011).

2.4.1.1. Effect on cellular growth: Cells are inherently sensitive to their micro-environment. Highly defined and specific micro-structure is essential for normal phenotype and correct tissue development and its function (Stevens & George, 2005). Scaffold porosity and pore size have been found to influence cell attachment, proliferation, differentiation and ECM deposition (Zeltinger *et al*., 2001). Earlier reports suggested that pore size is highly specific for all the cell types and varies within 5-500 µm range (Yang *et al*., 2002, Zeltinger *et al*., 2001). PLA scaffolds have been fabricated by solid freeform fabrication and the effect of scaffold pore size and pore volume on the behaviour of different cell types were studied by Zeltinger *et al.* Vascular endothelial cell growth and proliferation was favoured on scaffolds with < 38 µm pore size, while smooth muscle cell growth was favoured on scaffolds with 38-150 µm and fibroblast cell infiltration was found better on 68-150 µm pore-sized scaffolds. A pore volume of nearly 90 % was found to enhance cellular infiltration into the scaffolds (Zeltinger *et al*., 2001). The effect of pore size on mature elastin deposition was studied by Lee *et al*. Poly(glycerol sebacate) (PGS) scaffolds with different pore sizes were fabricated using the solvent casting process and cultured with baboon adult primary SMCs in a pulsatile flow bioreactor for 3 weeks. Scaffolds with 25-32 µm were found to support cell organization and elastin synthesis when compared to scaffolds with pore sizes 45-53 µm and 75 to 90 µm (Lee *et al*., 2011).

2.4.1.2. Impact on scaffold mechanical properties: Micro architectural parameters can influence the mechanical performance of the construct. The effect of pore size and porosity on the mechanical properties of poly(caprolactone)-hydroxyapatite

scaffolds were studied by Yu *et al*. Scaffold pore size was altered by using porogen sodium chloride (NaCl) having different sizes such as 212-355 µm, 355-600 µm and porosity was varied by changing NaCl concentration (0.25 to 4 wt/wt%) in the polymer matrix. Both tensile strength and young's modulus of scaffolds were found to reduce with increase in pore size and porosity of scaffolds (Yu *et al*., 2008). The dependence of mechanical properties of electrospun scaffolds on fiber diameter and packing density was studied by Soliman *et al*. While fiber diameter was altered by changing polymer concentration, packing density of electrospun mats was changed by varying the collector-to-needle distance or by operating with an auxiliary ring collector. Scaffolds composed of microfibers were fabricated at high fiber density (M-HD) and at low fiber density (M-LD). Nanofiber scaffolds were also prepared at high fiber density (N-HD) and at low fiber density (N-LD). The trend in tensile strength and modulus was found similar and microfibers exhibited better properties than nanofibers at high or low density conditions. Elasticity was found to be better for nanofibers at both conditions compared to the corresponding microfiber meshes (Soliman *et al*., 2011).

2.4.1.3. Influence on scaffold degradation characteristics: In addition to chemical nature, it is reported that architectural parameters of the scaffold could also influence the degradation rate. The effect of porosity and pore size on degradation properties of PLGA scaffolds was studied by Wu & Ding. Scaffolds with varying porosities of 80 to 95 % and pore sizes 50 to 450 µm were fabricated using compression moulding followed by particulate leaching. It was found that scaffolds with higher porosity or small pore size degraded more slowly compared to scaffolds with low porosity and

high pore size. This is because scaffolds with lower porosity and smaller pores depress the diffusion of degradation products which cause autocatalytic effect leading to an enhanced degradation rate (Wu & Ding, 2005). The effect of pore size on the degradation profile of polylactide scaffolds was studied by Odelius *et al*. The scaffolds with smaller pore size were found to slow down the rate of hydrolysis. Scaffolds with larger pore size and solid films exhibited much higher degradation rate due to autocatalysis induced by the trapped degradation products. In smaller pore sized scaffolds, the size of the pores was found to decrease during the degradation with subsequent formation of a solid surface on the top of the scaffold (Odelius *et al*., 2011). Studies also reported that high surface area tends to accelerate the degradation rate of nanofibrous poly(L-lactic acid) foams (Chen & Ma, 2006). Chitosan fiber meshes demonstrated an enhanced degradation rate with increase in scaffold porosity and reduced fiber diameter (Cunha-Reis *et al*., 2007).

2.4.2. Relevance of multilayered scaffold design

The regeneration of multilayered tissues such as skin, bone, vascular grafts, tracheal splints, heart tissue etc. requires good organization of various cell types (Murphy & Atala, 2014). A new trend is emerging in tissue engineering where different biomaterials and fabrication technologies are combined to provide the desired scaffold architecture. Scaffolds which possess two or more pore size distribution is found to facilitate the growth of multiple cell types leading to better formation of multiple tissue interfaces (Karageorgiou & Kaplan, 2005). Importance of gradient porosity characteristics have been studied earlier in cartilage (Woodfield *et al*., 2005) and bone (Schwarz & Epple, 1998) tissue engineering. A number of multilayered

scaffold designs which were evaluated earlier for blood vessels are reviewed in detail below.

2.4.2.1. Tri-layered scaffold construction: Zhang *et al* constructed a tri-layered scaffold composed of inner and outer layers as porous poly(lactic-co-glycolic acid) and middle compact polyurethane layer using solvent casting, spraying and solvent casting respectively (Zhang *et al*., 2008). The overall pore size present within the scaffolds ranged from 30-74 µm, but there is no account on pore size present on individual layers. The thickness of the middle PU layer was found to influence the mechanical properties of scaffold, which was optimized to obtain adequate burst strength, suture retention strength and compliance for blood vessel tissue engineering. After culturing with bone marrow stromal cells (bMSCs) for 7 days, these scaffolds were implanted in canine abdominal aorta and found to be patented after 3 months. Han *et al* fabricated a tri-layered scaffold composed of PCL/gelatin luminal layer, PLGA/gelatin-VEGF middle layer and PCL/gelatin outer layer using electrospinning (ES). Mechanical properties such as tensile strength, elasticity, burst strength and suture retention strength of the electrospun scaffold was found to be better than that of artery and vein. Vascular endothelial and smooth muscle cells were seeded onto the inner and outer surfaces of the scaffold and cultured up to 6 days. The release of VEGF and PGF which enhances endothelial and smooth muscle cell proliferation respectively from the scaffold was demonstrated. These grafts exhibited 8 weeks of patency when implanted in rabbit carotid artery (Han *et al*., 2013).

2.4.2.2. Bi-layered scaffold construction: Williamson *et al* constructed a composite bi-layered scaffold where wet spun polycaprolactone and electrospun polyurethane formed the luminal and abluminal layers respectively. The luminal layer exhibited oriented PCL fibers with 1 to 5 µm gap between them and outer layer was found to be porous with 10-30 µm pore size. It was demonstrated that human umbilical cord vein endothelial cells (HUVEC) formed a monolayer on the PCL layer and SMCs proliferated well on the PU layer after 7 days of culture (Williamson *et al*., 2006). A bi-layered scaffold based on elastomeric poly(ethylene urethane ether urea) (PEUU) scaffold was designed and fabricated by combining thermal-induced phase separation (TIPS) followed by electrospinning. Pores of average size of 51 ± 3 µm and 123 ± 3.2 µm were found to be present at the inner TIPS and outer electrospun layers respectively. These scaffolds were found to possess the tensile strength, suture retention strength and compliance required for blood vessels. Rotational seeding methodology was found to be highly efficient to get high cellular density on the scaffold after seeding with adult stem cells (Soletti *et al*., 2010). Dual-layered poly(lactide-co-caprolactone) (PLCL) scaffolds were designed using electrospinning (Shin *et al*., 2014). By varying the concentration and flow rate, a construct composed of nano-fibrous and micro-fibrous layers with 700 nm and 5 µm fiber diameters respectively was fabricated. After modifying the mat with gelatin, it was found that the growth of endothelial and smooth muscle cells showed significant differences. While EC growth was facilitated on the nanofibrous layer, SMC growth was found to be better in the micro-fibrous layer. Reports suggested that most of the tissue engineering strategies which adopted multilayered scaffolds have not addressed

porosity characteristics in terms of cellular, mechanical and degradation characteristics (Table 2).

Previous works	Scaffold systems	Fabrication method	Pore size	Mechanical properties	Degradation
Zhang *et al* (2008)	Tri-layered (PLGA→ PU→ PLGA)	SCPL→ spraying → SCPL	30-74 µm	Acceptable	No data available
Han *et al* (2013)	Tri-layered (PELCL, PDGF, gelatin → PLGA, VEGF, gelatin→ PCL, gelatin	ES	No data available	Acceptable	No data available
Soletti *et al* (2010)	Bi-layered (PEUU→ PEUU)	TIPS→ ES	No data available	Acceptable	Acceptable
Wang *et al* (2012)	Bi-layered (Gelatin with heparin→ PU)	ES	No data available	No data available	No data available

Table 2: Multilayered scaffold designs adopted earlier for blood vessels

2.5. Scaffold fabrication methodologies

Many techniques have been developed for the fabrication of tissue engineered scaffolds. The conventional methods of scaffold fabrication include solvent casting and particulate leaching (Suh *et al*., 2002), phase separation (Tu *et al*., 2003), gas foaming (Yoon & Park, 2001), melt moulding (Oh *et al*., 2006), fiber bonding (Mikos *et al*., 1993) and textile methods such as electrospinning (Hasan *et al*., 2014). Advanced methods based on computer-aided designing (CAD) or computer aided modelling (CAM) such as three-dimensional printing (Leukers *et al*., 2005), stereolithography (Melchels *et al*., 2009), fused deposition modelling (Zein et *al*., 2002), selective laser sintering (Williams *et al*., 2005) can also be employed. Among

these techniques, solvent casting followed by particulate leaching and electrospinning can be employed to regulate the pore size and porosity. Solvent casting technique can provide a smooth surface which may enhance hemocompatibility, though these scaffolds tend to possess limited thickness. Electrospun scaffolds can mimic the morphology of extracellular matrix components such as collagen and elastin, but limited blood compatibility due to fibrous morphology may result. By integrating SCPL and electrospinning methodologies, the limitations of these individual techniques is expected to be overcome by fabricating multilayered scaffolds with desired properties.

2.5.1. Solvent casting and particulate leaching (SCPL)

This is an easy, simple and inexpensive method of scaffold fabrication. In the SCPL methodology, polymer and pore-forming material called porogen can be mixed in a suitable solvent and cast into the desired shape. The major advantage of SCPL technique is the capability to control the pore size and porosity of scaffolds by varying porogen size and polymer/porogen ratio respectively. Further, such scaffolds enable understanding of the effect of microstructure on other scaffold properties and cell-scaffold interaction (Rogers *et al*., 2013, Lee *et al*., 2011). Sodium chloride (NaCl) (Liao *et al*., 2002), gelatin (Suh *et al*., 2002) and paraffin (Zhang *et al*., 2005) have been commonly used as porogens for fabricating tissue engineering scaffolds via SCPL. The major drawback associated with sodium chloride being used as a porogen is its incomplete leaching from a polymeric matrix which drastically reduces pore interconnectivity. Moreover, its immiscibility with hydrophobic polymer systems may facilitate anisotropy in pore distribution along with formation of a

nonporous surface skinny layer. More recently, poly(ethylene glycol) (PEG) has been used as porogen in poly(caprolactone) scaffolds for blood vessel tissue engineering (Pankajakshan *et al.*, 2008).

2.5.2. Electrospinning

This is becoming a popular technique for fabrication of tissue-engineered scaffolds since highly porous fibrous matrices can imitate native ECM components more closely and high surface area to volume ratio facilitates better cell-scaffold interaction (Ma *et al*., 2005). Electrospinning process can generate high porous fibrous matrices whose porosity characteristics can be altered by adjusting fiber diameter and alignments. In the electrospinning process, a stream of polymer solution is injected through a needle using the syringe pump. The needle is connected to a high voltage power supply which can generate voltages between 1-30kV. When the electrostatic charge becomes greater than the surface tension of polymer drop at the needle, the droplet is deformed into a conical-shaped structure called Taylor cone, which becomes unstable beyond a critical charge density. Fibers are ejected from the tip of the Taylor cone and accelerated to the collector. Fibrous mats consisting of nano to micrometer range fibers can be generated through this technique. The possibility of altering the fiber morphology and diameter by regulating solution and processing parameters allow the use of electrospinning for a wide variety of tissue engineering applications (Sill & Recum, 2008). Depending upon the cells involved, the fibrous structure can be designed to yield optimum pore size along with the required mechanical properties (Pham *et al*., 2006). In addition to that, integration of cells (Stankus *et al*., 2006), growth factors (Sahoo *et al*., 2010)

and drugs (Innocente *et al*., 2009) into the scaffolds is also possible via electrospinning.

2.6. Bio-mimetic modification of synthetic scaffolds

A major limitation of synthetic polymers is the lack of native cell binding sites which leads to poor cell-scaffold interaction. Synthetic scaffolds have been modified using specific biological molecules for facilitating cell adhesion and differentiation potential. It was reported that conjugating with cell-adhesive ligands like a tripeptide such as arginine-glycine-aspartic acid (RGD) could improve the cell growth on synthetic matrices (Ruoslahti *et al*., 1987). Another strategy is to combine synthetic polymers with natural polymers which can facilitate cell growth along with improvement in the biocompatibility of the synthetic scaffold. It has also been reported that collagen (He *et al*., 2005), elastin, gelatin (Han *et al*., 2011) and fibrin (Koch *et al*., 2010) can be incorporated into blood vessel tissue engineered scaffolds.

2.7. Cell sources for tissue engineered blood vessel

Cells are one of the major components of tissue-engineered blood vessel. Blood vessel functionality can be achieved only with a non-thrombogenic inner layer composed of endothelial cells (ECs) and vaso-active media comprised of smooth muscle cells (SMCs). Earlier attempts for endothelial cell seeded grafts were based on autologous cell sources (Mansfield *et al*., 1975). Since these are isolated from the patients, adverse immune responses can be avoided. Alternate options are allogenic and xenogenic cell sources. Both these cell types can cause immune problems while xenogenic cells are also associated with potential risk of transferring animal

pathogens to humans. Researchers have been focussing on the possibility of using stem cells as potential cells for tissue engineering purposes. These cells have the ability to differentiate into specialized cell types. Stem cells can be isolated from a number of sources; embryonic tissue, adipose tissue, bone marrow and peripheral blood and can be differentiated into different vascular cells (Pankajakshan & Agrawal, 2010). The identification of endothelial progenitor cells in peripheral blood was reported earlier (Asahara *et al*., 1997). Later, smooth muscle progenitor cells were also identified and isolated from peripheral blood (Simper *et al*., 2002). Donor site morbidity could be minimized for this kind of cell collection.

2.8. Development of a tissue-engineered blood vessel

The most deciding step towards constructing a successful small-diameter vascular graft relies on designing a scaffold with optimum physico-mechanical properties. Scaffold microstructure, mechanical properties, degradation characteristics, antimicrobial aspects and other physico-chemical properties should be properly evaluated. Since regeneration of vascular tissue can be significantly affected by *in vivo* physiological environment, appropriate *in vitro* culture strategies should be primarily considered for developing a tissue-engineered blood vessel.

2.8.1. Evaluation of scaffold

2.8.1.1. Scaffold micro-architecture: Scaffold microstructure plays a crucial role in the performance of the vascular graft which should be characterized and regulated carefully. Scanning electron microscopy (SEM) can be used for qualitative analysis of surface topography of scaffolds (Gaudio *et al*., 2009). With the aid of software

like Image J, pore size and electrospun fiber diameter etc can be quantified. Mercury intrusion porosimetry can be employed to quantify porosity characteristics like pore size distribution, total pore volume and surface area of scaffolds (Giesche, 2006). However, it cannot account for pore interconnectivity and there is chance for erroneous measurements due to high pressure mercury intrusion which is not suitable for compressible samples and nanofibrous meshes. In the case of liquid extrusion also, pore size distribution, pore volume and permeability of scaffolds can be measured. However, the liquid (ethanol) can intrude into the bulk of polymer which may result in overestimation of pore volume (Jena & Gupta, 2003). Micro-computed Tomography (Micro-CT) is a non-destructive, powerful alternate tool for morphological evaluation of scaffolds (Lin *et al*., 2003). It can provide precise quantitative and qualitative information of three-dimensional (3D) morphometric parameters of scaffolds such as pore volume, pore size distribution, average pore size, pore interconnectivity, density distribution and wall thickness distribution. The gravimetric method also can be used to quantify the pore volume present within the scaffolds (Pham *et al*., 2006).

2.8.1.2. Mechanical properties: The scaffold should provide the initial mechanical integrity required for the graft immediately after the implantation. The mechanical properties such as tensile strength, elasticity, burst strength, suture retention strength and compliance are critical in proper functioning of the graft (Konig *et al*., 2009). The maximum stress and strain that the scaffold can withstand when stretched before failure are denoted by its strength and elasticity. Tensile properties can be measured using a dynamic mechanical analyzer (Nerem *et al*., 1998) or universal testing

machine (UTM). Burst strength or burst pressure is the maximum pressure that the vascular conduit can be subjected to before an acute leak develops and the conduit fails (Sarkar *et al*., 2006). The term compliance encompasses the changing mechanical properties of the graft depending upon the hemodynamic force experienced within it (Sarkar *et al*., 2006), which can be analyzed in static or dynamic states using a video motion analyzer (Nerem *et al*., 1998). Mechanical properties for native blood vessels are summarised in Table 3.

Mechanical properties	**Vessel type**		**References**
	Human sephenous vein	**Human artery**	
Tensile strength (MPa)	--	1-2	(Mohan *et al*., 1982)
Elasticity (%)	--	45-99	(Xu *et al*., 2004b)
Modulus (MPa)	--	---	
Burst strength (mmHg)	1680-2273	2031-4225	(L'Heureux *et al.*, 2006)
Suture retention	196 ± 2	200 ± 119	
Compliance (%)	0.7-1.5	4.5-6.2	

Table 3: Mechanical properties of native blood vessels

2.8.1.3. Degradation characteristics**:** For blood vessel tissue engineering, scaffold material should possess stable degradation characteristics suitable for long-term implantable applications. Degradation of scaffolds has been characterized by weight loss, deterioration of polymer molecular weight and mechanical properties. Degradation studies can be conducted as a real-time test or accelerated conditions depending upon the time needed for the scaffold material to be degraded considerably (Lam *et al*., 2008). As a result of degradation, the mass of the scaffold decreases, which can be measured gravimetrically. Molecular weight loss can be

calculated using Gel permeation chromatography (GPC) and mechanical properties can also be measured (Lam *et al*., 2009) as described in section 2.2.1.2.

2.8.1.4. Efficacy studies of antimicrobial activity in scaffold: While incorporating the nanoparticles into the scaffold, its distribution within the polymer matrix may affect its release profile. The presence of nanoparticles can be estimated using transmission electron microscopy and electron dispersive spectroscopy (EDS) (Yu *et al*., 2012) and their release profile can be studied using inductively plasma optical emission spectroscopy (ICP/OES) (Xing *et al*., 2010). The antimicrobial activity of the scaffolds can be studied using relevant bacterial strains and evaluated by zone of inhibition assay (ZIA) (Madhavan *et al*., 2011). Usually, different strains such as *Staphylococcus aureus, Escherichia Coli, Staphylococcus epidermis* etc. are employed for evaluation.

2.8.1.5. Characterization of other scaffold properties: Scaffold properties such as wetting characteristics, roughness parameters etc can influence both cellular growth and hemocompatibility of the vessel (Xu *et al*., 2004a, Gorbet & Sefton, 2004). Surface wettability can be measured using goniometry (Yang *et al*., 2002) and surface roughness using atomic force microscopy (Siedlecki & Marchant, 1998). The fabrication process can affect the polymer crystallinity which may be evaluated using X-ray diffraction (XRD) and Differential Scanning Calorimetric (DSC) methods. Since the incorporated nanoparticles can evoke toxicity problems, cytocompatibility of scaffolds should be estimated which can be done using direct contact assay and MTT assay. Vascular constructs are also expected to possess appropriate blood compatibility which can be measured by hemolysis assay (Thomas & Nair, 2011).

2.8.2. Culture conditions of vascular construct

The blood vessel is always subjected to a dynamic mechanical environment. Reports suggest that vascular tissue organization and its mechanical properties are dependent on mechanical stimulation during *in vitro* culture (Seliktar *et al*., 2003). With the aid of a bioreactor, *in vivo* dynamic conditions can be mimicked to the engineered tissue which should be set up in a high sterile environment. A bioreactor can be defined as any apparatus that attempts to mimic and reproduce physiological conditions in order to maintain and encourage cell culture for tissue generation (Bilodeau & Mantovani, 2006). Cell culture parameters such as temperature, pH, biochemical gradients and mechanical stresses can be continuously monitored. It was reported earlier that the phenotype of endothelial and smooth muscle cells, their alignment in longitudinal and circumferential directions, respectively and deposition of ECM components such as collagen and elastin can be regulated by the influence of bioreactor compared to static culture conditions (Williams & Wick 2004). Perfusion bioreactors have been frequently employed for the culture of vascular grafts (Jeong *et al*., 2005).

To summarize, significant progress has been made in vascular research towards creating a successful small-diameter vascular graft. The development of a functional scaffold with required microstructure, optimum mechanical and degradation properties still remains as a challenging task in vascular tissue engineering. In this study, a bi-layered antimicrobial scaffold with appropriate gradient porosity and optimized properties is expected to serve the purpose and efforts are being taken to achieve this.

CHAPTER 3

MATERIALS AND METHODS

In this study, efforts were made to develop an appropriate scaffold for tissue engineered small diameter blood vessels. Methods adopted for scaffold fabrication were SCPL and electrospinning. Finally the bi-layered scaffold (BS) was developed by combining both techniques. Silver nanoparticles were synthesized and incorporated into the scaffold for imparting antimicrobial activity. All experiments related to scaffold fabrication are described in section 3.1. The physico-mechanical properties of the scaffold systems are evaluated and detailed in section 3.2. The cyto-compatibility experiments are described in section 3.3.

3.1. Fabrication of scaffold for blood vessel tissue engineering

3.1.1 Commercial reagents

Poly(ε-caprolactone) (M_n = 42,500 & 80,000) and Poly(ethylene glycol) (M_n = 3,400 & 8,000) were purchased from Sigma Aldrich, USA. Silver nitrate (AR grade), Poly(ethylene glycol) (M_n = 200) and Dichloromethane (DCM, HPLC grade) were obtained from Merck, India.

3.1.2. Fabrication of scaffolds by Solvent Casting- Particulate Leaching [SCPL]

Different polymer-porogen compositions were prepared for solvent casting. The combination ratios of PCL and PEG in the dissolved mixtures were varied as

depicted in Table 4. Uniform dispersion of these mixtures was facilitated by magnetic stirring.

Sample Code	Polymer	Porogen	*PEG loading (%)	PCL-PEG ratio
SC1	PCL42500	PEG8000	25	4:1
SC2	PCL42500	PEG8000	50	4:2
SC3	PCL42500	PEG8000	75	4:3
SC4	PCL42500	PEG8000	100	4:4
SC4	PCL42500	PEG3400	25	4:1
SC5	PCL42500	PEG3400	50	4:2
SC6	PCL42500	PEG3400	75	4:3
S24	PCL42500	PEG3400	100	4:4

Table 4: Composition of different solvent cast PCL scaffolds

*Concentration of PCL is kept constant (8.5 wt %) in all compositions and PEG is loaded in 25, 50, 75 and 100% of PCL taken.

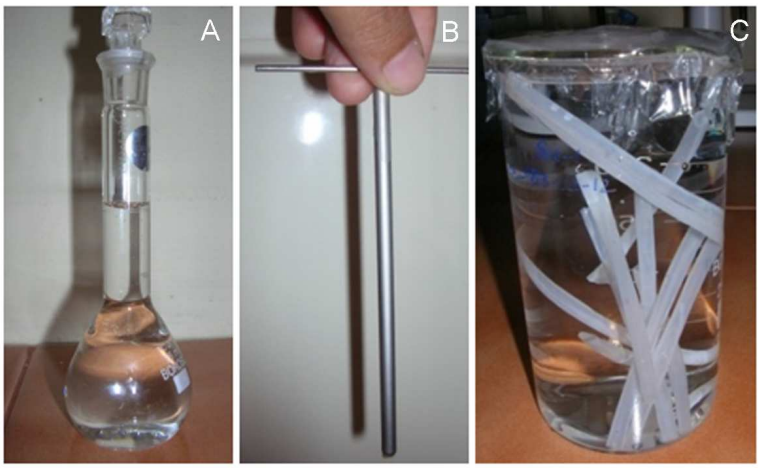

Figure 7: Solvent casting set up of tubular scaffolds: A, PCL-PEG solution; **B,** Cast on to mandrels and C**,** leaching of porogen from scaffolds

Steps involved in SCPL fabrication of tubular scaffolds were PCL-PEG solution preparation, casting process and leaching of porogen PEG as represented in Figure 7. Tubular scaffolds were cast on stainless steel (SS) mandrels having a diameter of 4mm and a length of 100 mm followed by particulate leaching. The conduits were carefully removed from the mandrels and stored further in deionized water (DI/W) for 72 h with intermittent change of DI/W to facilitate leaching of porogens. On completion of the leaching process, scaffolds were washed repeatedly and lyophilized in a freeze drier (Alpha 1-4 LD, Christ, Germany). Wall thicknesses of these scaffolds were measured using a micrometer.

3.1.3. Fabrication of scaffolds by electrospinning technique

The concentration of PCL (M_n = 80,000) in dichloromethane was varied from 10, 12, 14, 16, 18, 19 to 20 wt % and the optimum concentration (19 wt %) at which uniform fibers were formed without any bead formation was identified. The selected PCL solution (19 wt%) was then subjected to electrospinning using the equipment HO-NEU-02 (Holmarc mechanotronics Pvt.Ltd, India) as shown in Figure 8.

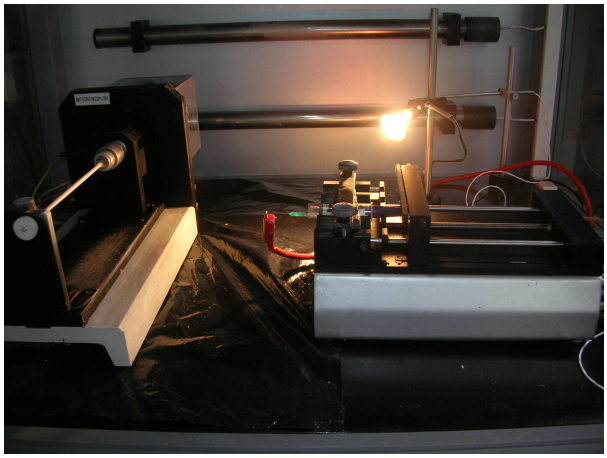

Figure 8: Electrospinning set up for the fabrication of tubular scaffold

Using a voltage source (Gamma high voltage research, USA), the polymer solution was ejected through a 10 ml syringe with 21 G needle. Fiber mats were fabricated by varying the flow rate from 1 to 5 ml/hr while applying 14-21 kV voltage and maintaining the collector-to-needle distance at 15-20 cm. The ejected fibers were collected on a mandrel having a diameter of 4 mm which was kept at a rotating speed of 1000 rpm. The scaffolds were carefully separated from the mandrels and analyzed.

3.1.4. Synthesis and characterization of silver nanoparticle

Poly(ethylene glycol) protected SNP solution was synthesized as shown in Figure 9. About 3.88 g of PEG 3400 was dissolved in PEG 200 (10ml) at 80^{o} C with stirring. After dissolution, 0.1 g silver nitrate was added in small quantities at 40-43^{o}C with mild stirring which was continued for 1 h. A clear brown colour indicated completion of reaction. Synthesized SNP was characterized by Transmission electron microscopy (TEM, Hitachi H-7650, Japan), UV-Visible spectroscopy (UV-1800, Shimadzu, Japan) and X-ray diffraction (XRD, SEIMENS D-5005, Germany).

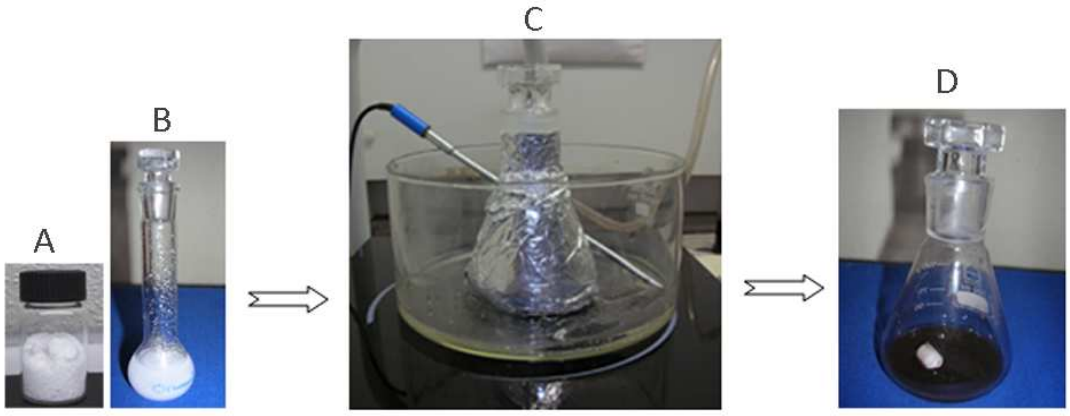

Figure 9: Diagram showing synthesis of SNP: A, silver nitrate; **B,** PEG solution prepared by mixing PEG-3400 and 200; **C,** synthesis set up of SNP solution and **D,** synthesized SNP solution

3.1.5. Fabrication of SNP incorporated SC and ES scaffolds

Fabrication of SNP-incorporated solvent cast and electrospun scaffolds was carried out by adding SNP solution into PCL-PEG and PCL solutions in such a way that each system contained silver nanoparticles amounting to 0.1 % of the total polymer content. The corresponding SC-SNP and ES-SNP solutions were subjected to solvent casting (as detailed in section 3.1.2) and electrospinning (as detailed in section 3.1.3). The overall scheme for the fabrication of SNP-incorporated scaffolds is represented in Figure 10. The scaffolds were carefully separated from the mandrels and lyophilized.

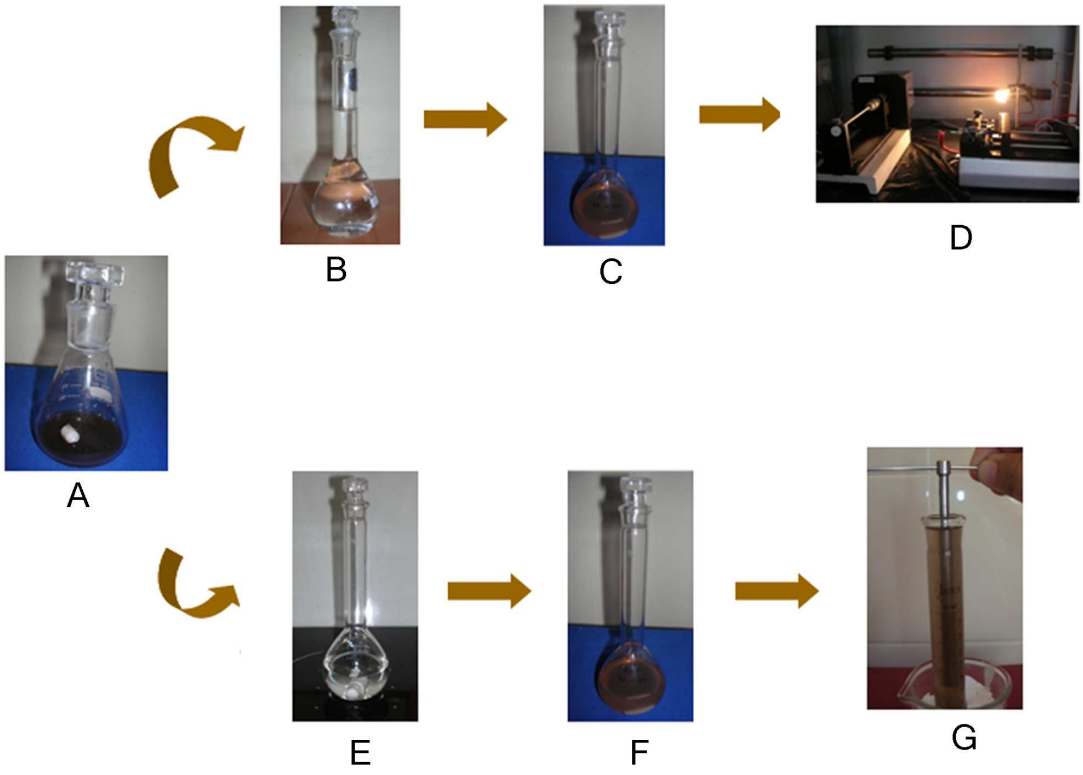

Figure 10: Scheme illustrating the fabrication of SNP incorporated scaffolds: A-D represents electrospinning fabrication and **A & E-G** represents solvent casting; **A,** synthesized SNP; **B,** PCL solution; **C,** SNP incorporated PCL solution; **D,** electrospinning set up; **E,** PCL-PEG solution; **F,** SNP incorporated PCL-PEG solution and **G,** solvent casting

3.1.6. Design of bi-layered scaffold by combining SCPL and electrospinning

Bi-layered scaffolds having outer diameter of 4 mm and length of 70 mm were fabricated by combining SCPL and electrospinning methodologies as shown in Figure 11. Initially tubular scaffolds were solvent cast from the SC-SNP solution and lyophilized (as described in section 3.1.2). These were inserted into electrospinning mandrels (Figure 11B) and fibers were collected on them (as described in section 3.1.3). During the initial deposition of PCL fibers, a mild heat treatment was applied on the top surface of the solvent cast scaffolds using a hair dryer for improving inter layer adhesion between the two layers. Electrospinning was carried out at 3 ml/hr flow rate at a voltage of 13 kV with collector needle distance of 20 cm. All other electrospinning parameters were kept as such as described in section 3.1.3.

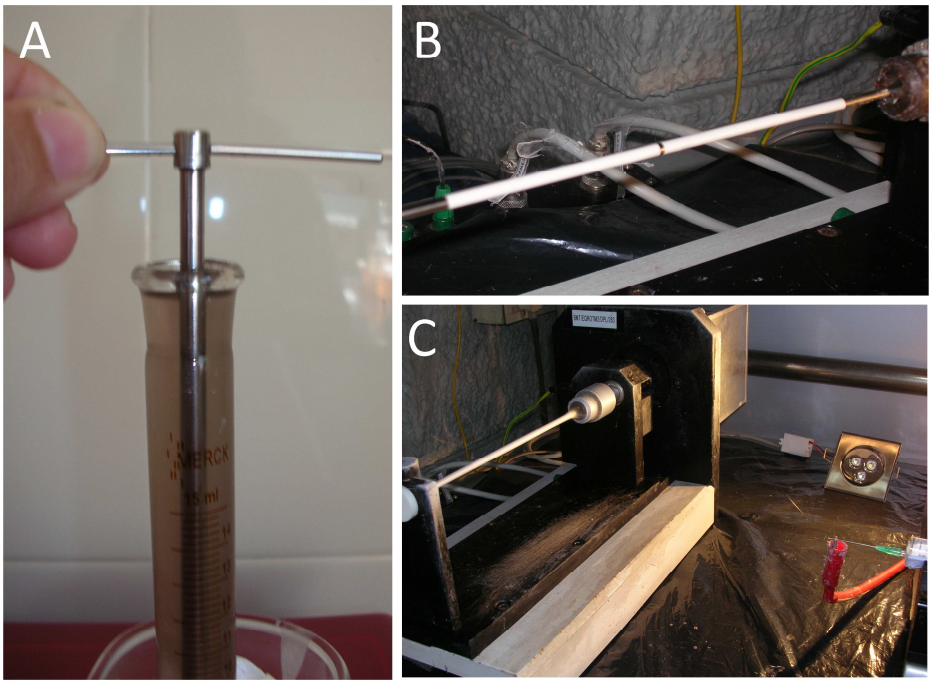

Figure 11: Various steps involved in fabrication of bi-layered scaffolds: A, fabrication of solvent cast SC-SNP scaffold; **B,** insertion into mandrel and **C,** electrospinning on to SC-SNP scaffold to generate the bi-layered scaffold

3.2. Characterization and evaluation of scaffolds

3.2.1. Surface analysis

The surface topography of the scaffolds was examined using a scanning electron microscope (SEM, Hitachi S2400 Japan). The scaffolds were fixed on aluminium stubs, sputter coated with gold and scanned at a voltage of 15 kV. In the case of electrospun scaffolds, the fiber diameter distribution was quantitatively analyzed from scanning electron micrographs using Image J software.

3.2.2. Porosity analysis

Scaffolds were analyzed using a micro-computed tomography (micro-CT, Scanco µCT 40, Switzerland) equipped with a charge-coupled device (CCD) detector (Figure 12). Samples were scanned at 12 µm voxel resolution using X-rays having energy 45keV and 177mA intensity. The isotropic slice data obtained by the system was reconstructed to about 300 to 400 two dimensional (2D) images. The 2D slice images were then compiled and analyzed to obtain the three dimensional (3D) images. The images were analyzed using an in-built software (Scanco) for estimating pore characteristics such as pore size and pore volume of each scaffold. Parameters such as scaffold wall thickness and inner diameter were also analyzed.

Dimensional parameters of sheep artery (collected after IAEC approval, B1062008 V) such as inner and outer diameters and wall thickness were also analyzed using micro-CT by scanning at experimental conditions similar to that of scaffolds.

Figure 12: Micro-CT analysis of scaffold: A, micro-CT equipment and **B,** scout view of sample with container

3.2.3. Gravimetric Analysis

An alternate method adopted to study porosity was the gravimetric technique. Knowing the density of PCL (ρ_{PCL}= 1.145g/ml), pore volume of each scaffold was calculated using this method. Scaffold discs of 8 mm diameter were prepared and scaffold density ($\rho_{scaffold}$) was calculated from mass and volume of discs (Pham *et al.*, 2006). Porosity was estimated using the equation,

$$\text{Porosity} = 1 - (\rho_{scaffold} / \rho_{PCL}).$$

3.2.4. Distribution and release profile of SNPs

Distribution of SNPs within the electrospun mat was studied using Energy Dispersive Spectroscopy (EDS, Oxford Instruments, Swift Ed, and Japan) and surface distribution of SNPs on spun fibers was studied by TEM (Hitachi H-7650, Japan). The release of SNPs from PCL scaffold matrix (diameter- 4mm, length-

60mm) was monitored in DI water at 1, 2, 3, 4, and 5 days using inductively coupled plasma optical emission spectroscopy (ICP/OES, Perkin-Elmer, 5300DV, USA).

3.2.5. Antimicrobial activity testing

Susceptibility of bacterial strains to SNPs was evaluated by Zone of Inhibition Assay (ZIA). Scaffolds with and without SNPs were incubated in PBS at 37^{o} C for 3 days. The eluted medium was collected, 100 ml was blotted on to absorbent discs and antimicrobial activity was tested against Gram-positive (S. aureus ATCC 25923) and Gram-negative (E. coli ATCC 25922) bacteria using gentamicin disc (10 mg) as the positive control. The samples were placed on the agar plates cultured with microbes for 24 h at 37^{o} C and zone of inhibition was evaluated.

3.2.6. Analysis of scaffold crystallinity

Scaffolds were scanned using differential scanning calorimetry (DSC, TA instruments, DSC-Q100, USA) as per procedure stipulated in ASTM D3418-08. Thermograms were recorded (-90 to 100^{o} C) at a heating rate of 10^{o} C/min in nitrogen atmosphere. Considering the enthalpy of melting (H_{ft}) of 100 % crystalline PCL as 139.5 J/g (Eldsater *et al*., 2000) and knowing actual heat of fusion (H_{fa}) of the scaffold, crystallinity of scaffolds was calculated (Barbanti *et al*., 2004) using the equation,

$$\text{Degree of crystallinity (\%)} = (H_{fa}/H_{ft}) \times 100.$$

Scaffold crystallinity was also estimated by X-ray diffraction (XRD, SEIMENS D-5005, Germany) using the powder diffraction method.

3.2.7. Contact angle studies

The surface wettability of solvent cast scaffold was determined by sessile drop method using a video-assisted contact angle measuring device (DataPhysics OCA15 plus, Germany) and imaging software (SCA20 software, Germany). Within 10 seconds of the introduction of the DI/W droplets, the contact angle formed between the sessile droplets and the scaffolds were measured. The contact angle is expressed as average of four independent measurements taken at different sites on each scaffold.

3.2.8. Surface roughness analysis

The scaffolds were scanned using atomic force microscopy (AFM, Nanosurf Easyscan 2, Switzerland). Images of each sample were captured in the ambient air at 15–20 % humidity at a tapping frequency of approximately 300 kHz and with a scan view of 50 x 50 µm. Surface roughness (nm) in each of three random fields of scaffolds was obtained which was averaged and recorded.

3.2.9. Mechanical testing

3.2.9.1. Tensile testing: The tensile stress at maximum load of tubular scaffolds (4mm diameter x 40 mm gauge length) was determined using a Universal Testing Machine (UTM, Instron 3365, UK) as shown in Figure 13A. Outer diameter and wall thickness of each scaffold were measured. The test was conducted uniaxially at crosshead speed of 50 mm/min using a 10 N load cell. Maximum load (N) is obtained from the load-extension curve and knowing the sample cross-sectional area, tensile strength of scaffolds was calculated.

3.2.9.2. Suture retention strength testing: The suture retention strength of scaffolds was also determined using tensiometry (Roh *et al*., 2008) as shown in Figure 13B. Tubular scaffolds were cut into 0.5 cm x 2 cm strips and suture retention strength was measured by placing a 5-0 suture approximately 1 mm from the end of scaffold. The suture was clamped into the upper grip with scaffold immobilized in the lower grip. The force needed to displace the suture from scaffold was measured uniaxially using a crosshead speed of 10 mm/min.

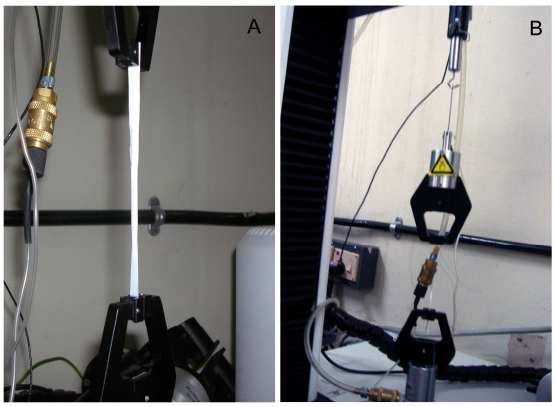

Figure 13: Mechanical testing of scaffolds: A, Tensile testing and **B,** suture retention testing

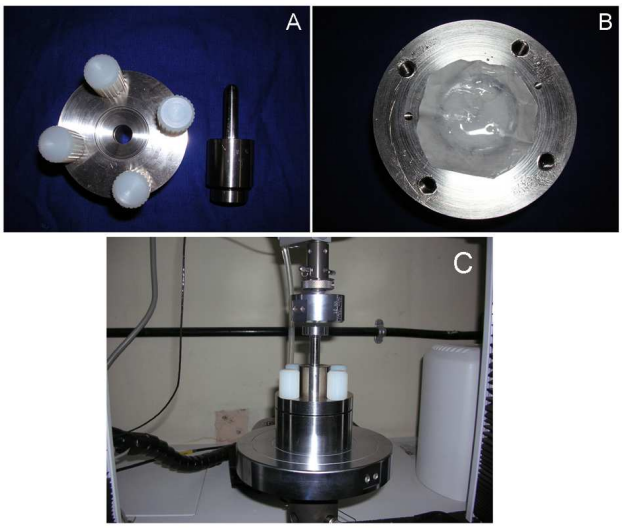

Figure 14: Burst strength testing of scaffolds: A, Sample holder with traversing probe; **B,** Scaffold on the holder and **C,** Sample holder with traversing probe on UTM

3.2.9.3. Burst strength testing: The sample to be tested was clamped over an orifice by means of a flat annular clamp ring [Figures 14A-B], and a cylindrical probe with a hemispherical head was traversed through the specimen until it ruptured as represented in Figure 14C. The applied load was measured continuously during the procedure using tensiometry. By knowing the maximum force 'F', thickness of sample 't' and diameter of probe 'd', burst strength could be calculated using the equation, Burst strength = 2Ft/d.

3.2.10. Determination of degradation profile of scaffolds

The degradation properties of scaffolds were studied as per the procedure stipulated in ISO 10993-13. Each scaffold (4 mm diameter x 70 mm length) was initially weighed (W_0), washed with 70 % alcohol and stored separately in 45 ml PBS (pH =7.4) and incubated at 37^o C upto one year.

3.3.10.1. Gravimetric weight loss: At the completion of degradation period of one year, the samples were taken out, rinsed with deionized water, lyophilized, weighed (W_f) and weight loss was determined. The percentage weight loss was estimated using the equation,

$$\text{Gravimetric weight loss (\%)} = (W_0 - W_f)/ W_0 \times 100.$$

3.3.10.2. Analysis of MW as an indicator of degradation: Molecular weights of scaffolds before (M_0) and after degradation (M_f) were determined using gel permeation chromatography (GPC, Shimadzu Prominence, LC-20, Japan) equipped with a refractive index (RI) detector. Twenty micro-litres of 0.5% solution of scaffolds in chloroform was injected, chloroform was used as the mobile phase at a

flow rate of 2ml/minute for each analysis. Average molecular weights were determined from GPC chromatograms. The percentage loss in MW was calculated using the equation,

$$\text{Loss in MW (\%)} = (M_0 - M_f)/ M_0 \times 100.$$

3.3.10.3. Analysis of mechanical strength after degradation: The tensile strength of PCL scaffolds before and after degradation was measured using the same methodology adopted for non-degraded scaffolds as given in section 3.2.7.1.

3.2.11. *In vitro* Cytocompatibility evaluation

3.2.11.1. Direct contact assay: Cytotoxicity test was evaluated using direct contact method as per ISO 10993-5 procedure. The ETO sterilized samples along with negative control high-density polyethylene (HDPE) and positive control polyvinyl chloride (PVC disc) in triplicate were kept on top of the confluent layer of L929 mouse fibroblast cells. The cells were incubated with the samples at 37 ± 2^{o} C for 24 ± 2 h and cell culture was examined under phase contrast optical microscope for cellular response around test and control samples. The morphology of cells was examined and compared to negative and positive controls.

3.2.11.2. MTT assay: Test samples were incubated with 1ml of culture medium containing serum at 37 ± 1^{o} C for 24 ± 2 h. After 24 h, the extract was diluted with culture medium to get 100 %, 50 %, 25 % and 12.5 % dilution. Cells cultured on normal medium were considered as experimental control. Equal volumes of various dilutions of test samples along with extract of negative control (Ultra High Molecular Weight Polyethylene) and positive control (13mg/ml phenol diluted with culture

medium containing serum) were placed on sub-confluent monolayers of L929 cells. After incubating at 37 ± 1^{o} C for 24 ± 2 h, the extract and control medium were replaced with 50 µl of MTT solution and were incubated at 37 ± 2^{o} C for 2 h. After discarding MTT solution, 100 µl of isopropanol was added to all the wells. Purple colouring developed due to formation of formazan was quantified by measuring absorbance at 570 nm using a spectrophotometer (Powerwave XS, Biotek, USA). The data obtained for test samples, negative and positive controls were compared with experimental control.

***3.2.11.3. Hemolysis studies*:** The effect of contact of scaffold material with blood was examined using percentage hemolysis assay, which was performed according to ISO 10993-4 procedure. Human blood was collected (IEC Approved, ECR/189/INST/KL/2013) into the tube containing anticoagulant acid citrate dextrose (ACD). The test materials (4mm diameter disc) were placed in the culture plates and agitated with phosphate buffered saline (PBS). To each plate, 1.5 ml blood was added and a 0.5 ml sample was collected immediately for analysis. The remaining 1 ml was exposed to the scaffold for 30 minutes under agitation at 75 ± 5 rpm using an Environ shaker (Lab-line instruments Inc, USA) at 35 ± 2^{o} C. Empty culture dishes exposed to blood were taken as reference. The total hemoglobin in the initial samples was measured using an automatic hematology analyzer (Sysmex- K4500, Sysmex Corporation, Japan). Platelet-poor plasma was prepared from blood exposed for 30 minutes. Free hemoglobin (Hb) liberated into the plasma after exposure was measured for each sample using a Diode array spectrophotometer (HP 8453, Hewlett Packard, Germany) and the percentage hemolysis calculated using the equation,

% Hemolysis = (Free Hb/Total Hb) x 100.

3.3. Cell culture experiments

3.3.1. Materials employed

3.3.1.1. Commercial reagents: Gelatin, Histopaque 1077, ascorbic acid, L-glutamine, heparin, 4',6-diamidino-2-phenylindole (DAPI), TritonX-100 (Sigma Aldrich, USA), MCDB 131 culture medium (Pan Biotech, Germany), trypsin-EDTA, antibiotic-antimycotic, foetal bovine serum (FBS) (Gibco BRL, USA), phalloidin conjugated with Texas Red (Molecular probes, USA), May-Grunwald (Himedia Laboratories Pvt. Ltd, India) and Giesma (Nice Chemicals Pvt. Ltd, India) for preparing May-Grunwald-Giemsa (MGG) were obtained from sources indicated in the brackets.

3.3.1.2. Reagents prepared in-house: Angiogenic growth factor (AGF) was prepared from bovine hypothalamus according to an established method (Maciag *et al*., 1979). Platelet-derived growth factor (PGF) was also prepared as described earlier (Resmi & Krishnan, 2002). Lyophilized powder consisting of fibrinogen and fibronectin (cryoprecipitate from screened and pooled human plasma) and thrombin (purified human thrombin from fibrinogen depleted plasma by diethylaminoethyl (DEAE) cellulose ion exchange chromatography for clinical use obtained in lyophilized form as ~250 IU per vial) were also used.

3.3.2. Preparation of cell culture media

Two specific culture media were prepared and cells were cultured as per reported procedure (Sreerekha *et al.,* 2006) for differentiating endothelial and smooth muscle progenitor cells (EPC and SMPC) into EC and SMC.

3.3.2.1. Endothelial cell specific medium: The EPC culture medium consisted of MCDB 131 culture media supplemented with FBS (10 %), L-glutamine (10 mM/L), ascorbic acid (0.3 mM/L), heparin sulphate (10 IU/ml), AGF (50 µg/ml) and antibiotic-antimycotic (10 µg/ml) mixture. The culture medium was mixed well and filtered through a syringe filter and stored at 4^{o} C.

***3.3.2.2. Smooth muscle cell specific medium*:** The SMPC culture medium consisted of MCDB 131 culture media supplemented with FBS (2 %), L-glutamine (10 mM/L), ascorbic acid (0.3 mM/L), PGF (4 µg/ml) and antibiotic-antimycotic (10 µg/ml) agent. The culture medium was mixed well and filtered through a syringe filter and stored at 4^{o} C.

3.3.3. Isolation of cells from blood

Peripheral blood mononuclear cells (PBMNCs) were isolated from rabbit (IAEC approved, SCT/IAEC-067/AUGUST/2013/81) and sheep blood (IAEC approved, B1062008 V) to culture and differentiate into endothelial and smooth muscle cells for vascular tissue engineering applications.

3.3.3.1. Isolation of sheep PBMNCs: Sheep blood was collected; PBMNC was isolated and cultured with minor modification of reported methods (Asahara *et al.,* 1997, Sreerekha *et al.,* 2006). Fifty ml blood was collected aseptically from

experimental animals into heparinized tubes. Red blood cells (RBCs) were settled by centrifugation (Hareus, Germany) at 1200*g* for 1 h in a 50 ml tube. Superficial plasma was discarded and PBMNCs at the interface were collected, diluted and mixed well with equal volumes of Hank's Balanced Salt Solution (HBSS) to make up the volume to 8 ml. These were layered over 6 ml Histopaque-1077 and centrifuged at 400*g* for 30 minutes at 25^{o} C. The layer containing PBMNCs was carefully separated from the plasma-Histopaque interface and washed with HBSS by centrifugation at 150*g* at 4^{o} C for 10 minutes. The washed PBMNCs were suspended in MCDB 131 media.

3.3.3.2. Isolation of rabbit PBMNCs: Rabbit blood (15ml) was collected and PBMNCs were isolated using Histopaque gradient centrifugation as described above with slight modification. Rabbit blood was centrifuged at 1200*g* (Hareus Stratos, Germany) for 30 minutes. Superficial plasma was discarded; leukocytes settled at the interface were collected and PBMNC obtained (as described in section 3.3.3.1).

3.3.4. Culture and differentiation of PBMNCs on cell specific matrix

The PBMNCs isolated from sheep or rabbit blood were processed for obtaining endothelial and smooth muscle cells using cell-specific matrix and medium.

3.3.4.1. Preparation of EPC specific matrix: Culture dishes were coated with the fibrin-based matrix according to established procedure (Sreerekha *et al*., 2006). The modified fibrinogen composite consisting of fibrinogen (2 mg/ml), gelatin (0.2%) and AGF (50 µg/ml) was used. To obtain the composite coated surface, culture dishes were incubated with thrombin (5 IU/ml) for 30 min at 37^{o} C. After incubation, excess thrombin solution was removed and fibrin composite added to the surface

(8µl/cm^2). Fibrin was allowed to polymerize at 37^o C for 30 minutes, frozen at -70^o C for at least 2 h lyophilized (Edwards, Modulyo 4K, UK) and stored at 4° C till use.

3.3.4.2. Preparation of SMPC specific matrix: The culture surfaces were incubated with 5 IU/ml thrombin for 30 minutes. The thrombin solution was aspirated out and surfaces were brought to near dry state. The cocktail consisting of fibrinogen (2 mg/ml), gelatin (0.2%) and PGF (40 µg/ml) was layered over thrombin-adsorbed surfaces (8 µl/cm^2), incubated at 37^o C for 30 minutes, freeze dried and stored at 4^o C until use.

3.3.4.3. Culture of PBMNCs to obtain endothelial cells: Peripheral blood mononuclear cells were isolated from sheep or rabbit blood (as detailed in section 3.3.3). The cells suspended in EPC medium were seeded onto the uncoated tissue culture dishes. After 1 h, floating cells were removed; non-adherent but settled cells were flushed out and seeded on to the EPC specific matrix. These were cultured in a humidified incubator under 5 % CO_2 at 37^o C during which fresh medium was supplemented at a 24 h interval for 3 days and subsequently on every alternate day.

3.3.4.4. Culture of PBMNCs to obtain smooth muscle cells: Peripheral blood mono nuclear cells were isolated from sheep or rabbit blood as described in section 3.3.3. The cells suspended in EPC medium were seeded onto uncoated tissue culture dishes. After 1 h, floating cells were removed; non-adherent but settled cells were flushed out and seeded on to EPC specific matrix. These were cultured in a humidified incubator under 5 % CO_2 at 37^o C during which fresh medium was supplemented at a 24 h interval for 3 days and subsequently on every alternate day.

3.3.5. Bio-mimetic fibrin coating on scaffolds

The scaffolds were coated with a bio-mimetic matrix as per reported procedure (Pankajakshan *et al* 2007) with a modified matrix composition. The bio-mimetic matrix was prepared by mixing fibrinogen (2 mg/ml) solution in sterile water with gelatin (0.2 %). Initially scaffold surfaces were saturated with thrombin solution (5 IU/ml) in sterile water for 30 minutes at 37^{o} C. The tubular scaffold was taken out of thrombin and dipped in the fibrinogen composite solution for ~2 s and then allowed to clot for 30 minutes at 37^{o} C. The coated scaffolds were lyophilized in a freeze dryer (Modulyo 4K, Edwards, UK) and stored at 4 to 6^{o} C.

3.3.6. Cell culture on scaffolds

3.3.6.1. Static culture of endothelial cells on scaffolds: The cells were harvested at the second passage and seeded with $1x10^{6}$ cells/cm^{2} density in the lumen of the fibrin-coated scaffolds. The scaffolds were immersed in EC specific culture medium and allowed to grow for 3 to 5 days under static culture conditions.

3.3.6.2. ***Dynamic culture of EC and SMC on bi-layered scaffold:*** Differentiated ECs and SMCs between 2-3 passages were harvested from the respective culture plates. ECs were seeded onto the luminal surface of the scaffold at a density of 1×10^{6} cells/cm^{2} and SMCs onto the abluminal surface at a density of 3×10^{5} cells/cm^{2} (Mathews *et al*., 2012). After overnight incubation, unattached cells were removed and the scaffolds were immersed in the fresh culture medium. The scaffolds were then connected to a two-channel bioreactor system and shear stress was gradually increased up to 1 dyne/cm^{2} over a period of 24 h and the entire assembly was kept at

37^{o} C under 5 % CO_2. The same medium was used for both channels (EC and SMC compartments) and fresh medium was supplied at 48 h intervals for the culture.

Figure 15: Two channel bioreactor set up for culture of EC and SMC on scaffold

3.3.7. Analysis of cell adhesion and proliferation on scaffolds

For determining EC spreading and growth on scaffolds, the cell grown scaffolds were slit open. Cells were washed three times with phosphate-buffered saline (PBS; pH 7.4) and fixed using 3.7 % formaldehyde in PBS. The fixed cells were permeated using 0.1 % Triton-100. After three repeated washes with PBS, the cells were stained with Texas Red Phalloidin for actin filaments and DAPI for nuclei as per manufacturer's instructions. The cells were subsequently washed and viewed under a fluorescence microscope (Leica DM IRB, Germany) and imaged using a LAS image processing system (Leica, Germany). Cell proliferation on scaffolds was analyzed using environmental scanning electron microscopy (ESEM, Quanta 200, FEI, Netherlands). EC and SMC growth on the scaffolds after 3 days of culture were analyzed using the MGG staining method.

3.3.8. Statistical analysis

Three to six measurements were done for each analysis and quantitative data are presented as average ± standard deviation. ANOVA single factor was taken for comparison purposes in which $p < 0.05$ was used as the criterion for significant difference. The number of tests for each parameter is indicated in the respective figure legends.

CHAPTER 4

RESULTS

Chapter 4 contains the results obtained in the current study. It is divided into five subsections. The first section details the optimization of scaffold properties fabricated using SCPL method. The second section includes the evaluation of solvent cast scaffold properties after SNP incorporation. The third section represents the optimization of electrospun scaffold properties. The fourth section explains the properties of electrospun scaffold after SNP incorporation. The fifth section details the outcome of the design strategy adopted for developing an antimicrobial, bi-layered and porous scaffold whose properties have been evaluated for tissue-engineered small diameter blood vessels.

4.1. Optimization of properties of scaffolds fabricated using SCPL

The major objectives of this section are to evaluate the effect of PEG concentration and molecular weight (porogen size) on the properties of tubular scaffolds and on the degradation rate of selected scaffolds.

4.1.1. Effect of porogen concentration on tubular scaffold properties

4.1.1.1. Scaffold macrostructure

Tubular scaffolds with varying pore size and porosity were fabricated successfully (Figure 16). Scaffold wall thickness was found to increase with PEG content and was found to vary from 27.5 ± 6.2 to 80.3 ± 5.0 µm (Table 5). Macroscopic examination

showed better tubular consistency [Figures 16A&B-Inset] and qualitative 3D images obtained from µ-CT showed more uniformity in the scaffold wall [Figures 17A-D & 18A-D] for both SC4 and SC8 scaffolds when PCL and PEG content were maintained equal.

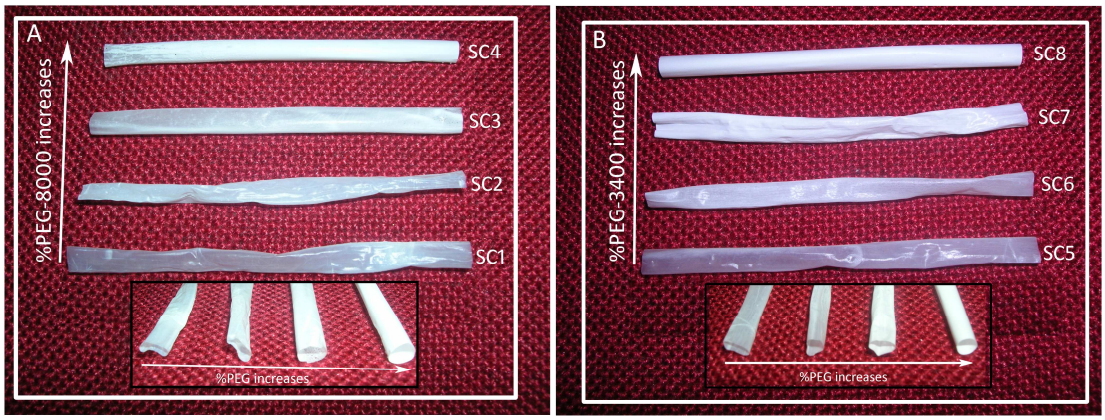

Figure 16: Macroscopic view of solvent cast scaffolds: A, scaffolds containing PEG8000 and **B,** scaffold containing PEG3400. Inset shows cross sectional view of scaffolds

Scaffold ID	Wall thickness (µm)	Crystallinity (%)	Contact angle (θ)
SC1	32.7 ± 5.0	58.06	72 ± 1.5
SC2	35.0 ± 6.6	61.94	74 ± 1.8
SC3	42.6 ± 9.5	67.24	76 ± 2.0
SC4	70.0 ± 4.0	61.94	71 ± 1.5
SC5	27.5 ± 6.2	58.09	62 ± 1.9
SC6	30.7 ± 6.7	60.53	66 ± 2.0
SC7	50.1 ± 10	67.78	67 ± 1.0
SC8	80.3 ± 2.0	51.72	58 ± 2.1

Table 5: Wall thickness, crystallinity and contact angle values of fabricated scaffold

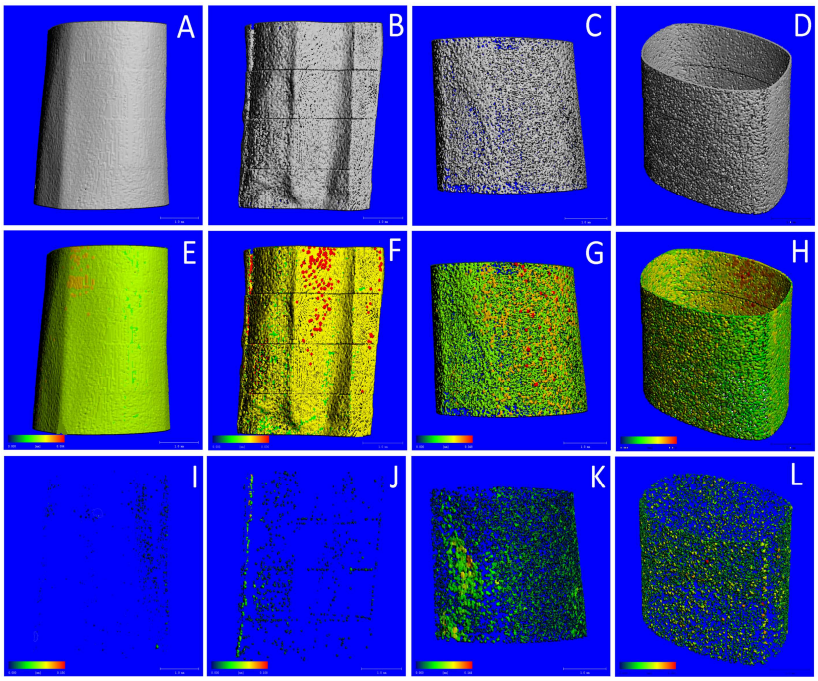

Figure 17: Micro-CT images of PCL scaffolds with PEG8000: A–D represents 3D images; **E–H** represents thickness distribution; **I–L** represents pore size distribution; **A, E & I** are SC1 scaffolds; **B, F & J** are SC2 scaffolds; **C, G & K** are SC3 scaffolds and **D, H & L** are SC4 scaffolds

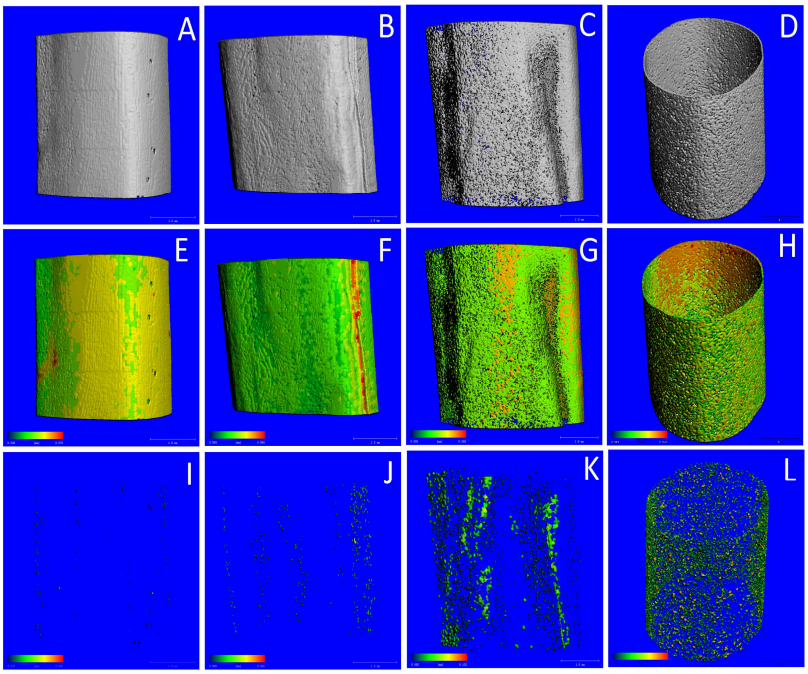

Figure 18: Micro-CT images of PCL scaffolds with PEG3400: A–D represents 3D images; **E–H** represents thickness distribution; **I–L** represents pore size distribution; **A, E & I** are SC5 scaffolds; **B, F & J** are SC6 scaffolds; **C, G & K** are SC7 scaffolds and **D, H & L** are SC8 scaffolds

4.1.1.2. Analysis of porosity characteristics

Scanning electron microscopic images revealed spherical pores within PCL matrix and increase in porosity with rise in PEG content [Figures 19&20]. Uniform scaffold pore size resulted [Figures 19A-B & 20A-B] in PCL100: PEG25 (4:1) and PCL100: PEG50 (4:2) systems. Further loading (4:3 & 4:4 systems) of PEG was found to result in considerable enhancement in the porosity [Figures 19C-D&20C-D]. Inverted images obtained using µ-CT also demonstrated enhancement of the porosity with increasing PEG content in PCL matrix resulting in uniform pore size distribution when PCL- PEG content was kept equal [Figures 17 I-L & 18 I-L].

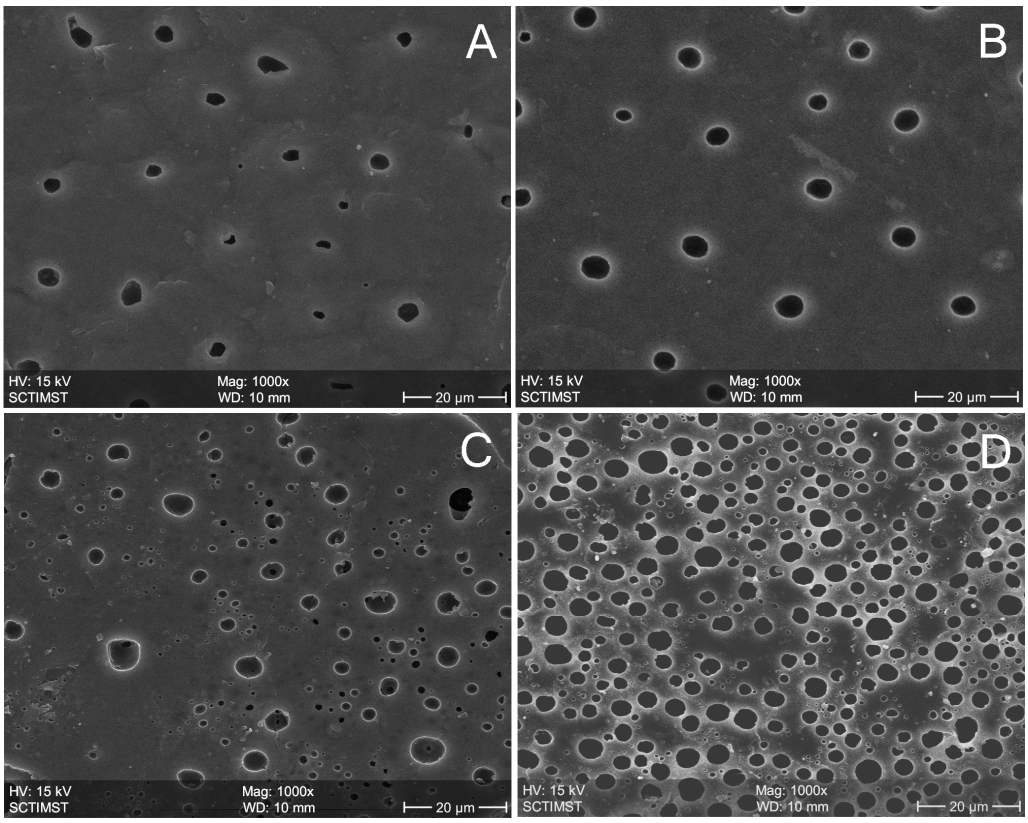

Figure 19: Surface morphology of scaffolds fabricated using PEG8000: A, SC1; **B**, SC2; **C**. SC3 and **D**, SC4 scaffolds

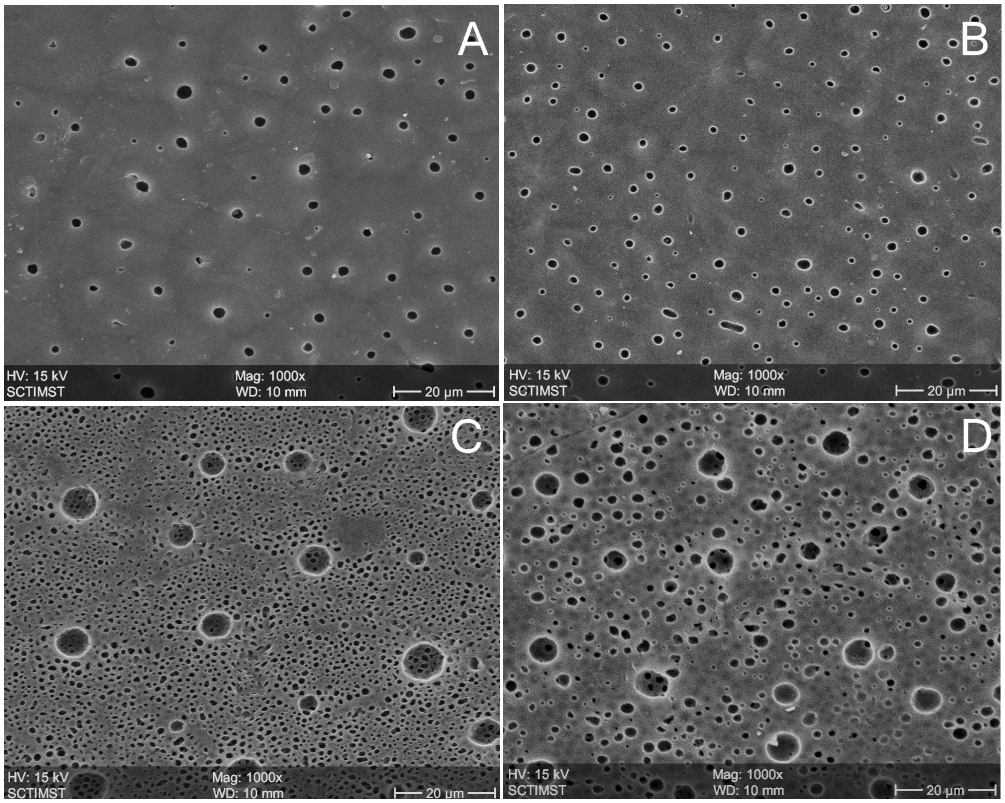

Figure 20: Surface morphology of scaffolds fabricated using PEG3400: A, SC5; **B,** SC6; **C,** SC7 and **D,** SC8 scaffolds

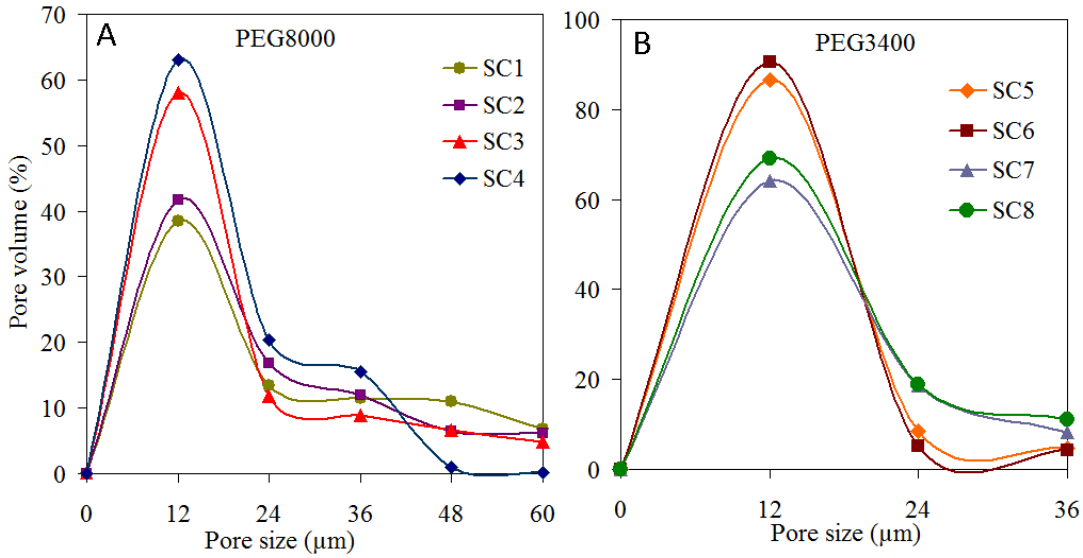

Figure 21: Representative histogram showing pore size distribution: A, scaffolds with PEG8000 and **B,** scaffolds with PEG3400; scaffolds were evaluated in triplicates and results are expressed as mean ± standard deviation (SD)

Quantitative analysis of scaffold pore size showed majority of the pores to be < 24 µm in size [Figure 21]. In scaffolds containing PEG8000, pores in the range of 24-60 µm were predominant whereas those containing PEG3400 showed majority of pores within 24-36 µm range. Porosity was found to increase with PEG content and highest porosity observed was 81.8 ± 1.6% and 77.2 ± 2.1% for SC4 and SC8 scaffolds respectively [Figure 22].

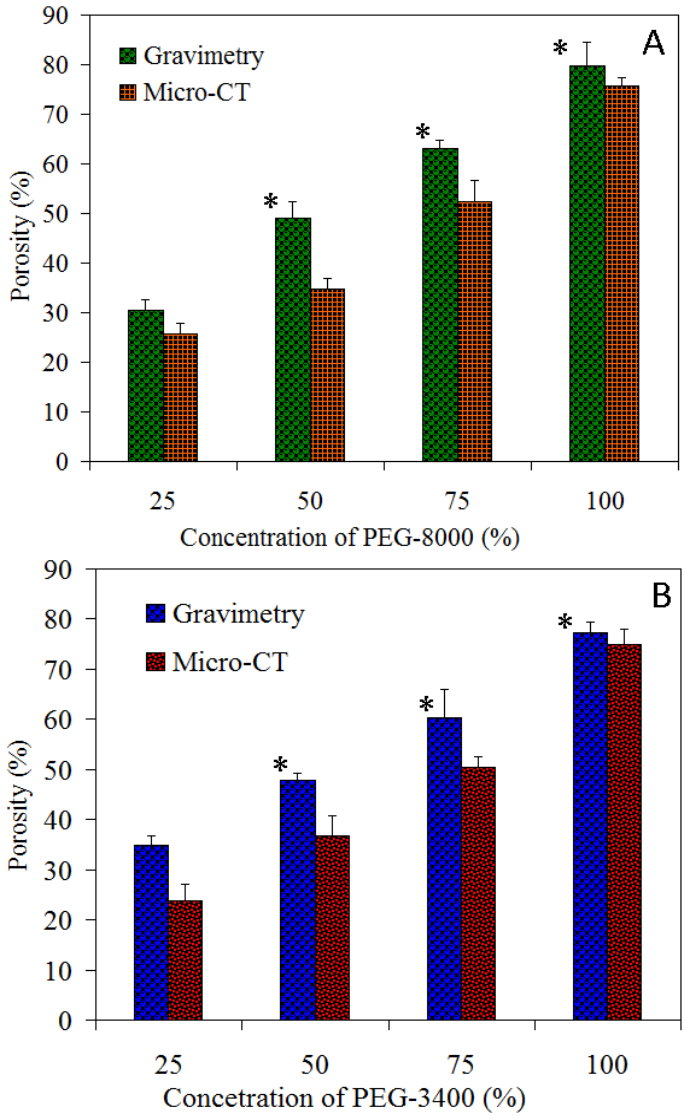

Figure 22: Quantification of pore volume within samples: A, scaffolds with PEG8000 and **B,** scaffolds with PEG3400; Data from six experiments are given as mean ± SD and * indicates $p < 0.05$

4.1.1.3. Hydrophilic and crystalline properties

Contact angle measurements demonstrated the hydrophilic nature of the scaffold surface ($\theta < 90$). Hydrophilicity did not vary significantly with PEG concentration. However, greater surface wettability was observed for all scaffold systems containing PEG3400 compared to PEG8000 system (Table 5). DSC analysis showed the crystalline nature of PCL to be affected by solvent casting process and crystallinity dominated for scaffolds containing 50% and 75% PEG (Table 5).

4.1.1.4. Mechanical strength evaluation

The variation of tensile strength (TS) of scaffolds with PEG content is shown in Figure 23. TS was found to vary from ~8 to 12 MPa; Scaffolds SC1 (11.62 ± 1.36 MPa) and SC5 (12.75 ± 1.45 MPa) showed the highest TS values whereas SC4 (7.28 ± 0.57 MPa) and SC8 (8.22 ± 0.87 MPa) showed low values.

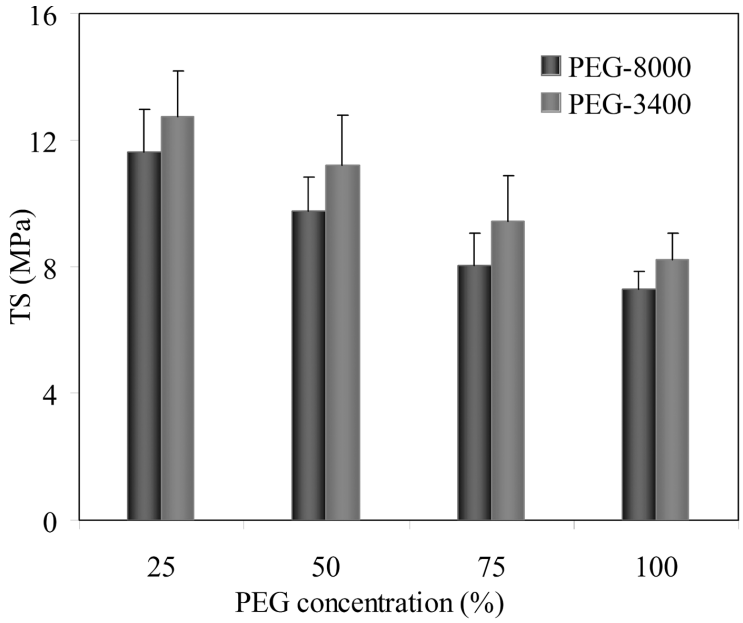

Figure 23: Variation of tensile strength of scaffolds with porogen parameters; six to eight scaffolds were evaluated and values are expressed as mean ± SD values

4.1.1.5. Endothelial cell growth on scaffolds

Microscopic examination of cell grown scaffold revealed good endothelial cell growth. Well spread actin filaments of endothelial cells were observed on both SC4 and SC8 scaffolds after 3 days of culture [Figures 24A&D]. DAPI counterstained cell nuclei are shown in Figures 24B & E. Figures 24C & F represents merged images showing both actin and cell nuclei.

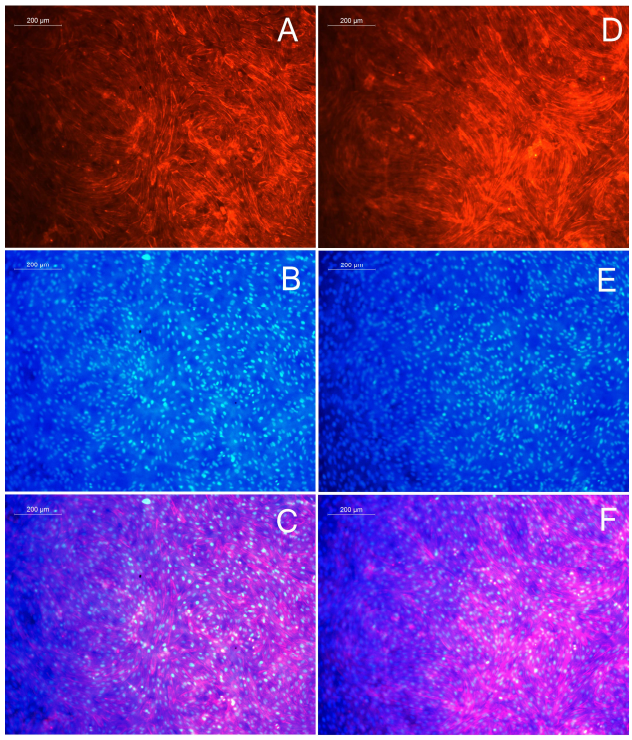

Figure 24: Fluorescent micrographs showing endothelial cell cultured scaffolds for 3 days: A & D are actin stained; **B & E** are nuclei stained and **C & F** are merged images; **A–C** represents SC4 and **D–F** represents SC8 scaffold (scale bar = 200 µm)

4.1.2. The influence of PEG molecular weight on scaffold degradation

4.1.2.1. Macro structure and structural integrity

Macroscopic observation showed a distinct difference in the surface morphology of SC4 and SC8 scaffolds before degradation (0d) and after degradation (6m) as

represented in Figure 25. Surface deformation was observed throughout the length of SC4 whereas SC8 had smooth abluminal and luminal surfaces after the degradation. The structural integrity of both scaffolds after six months degradation is shown as qualitative tracings obtained from micro-CT (Figures 26 & 27).

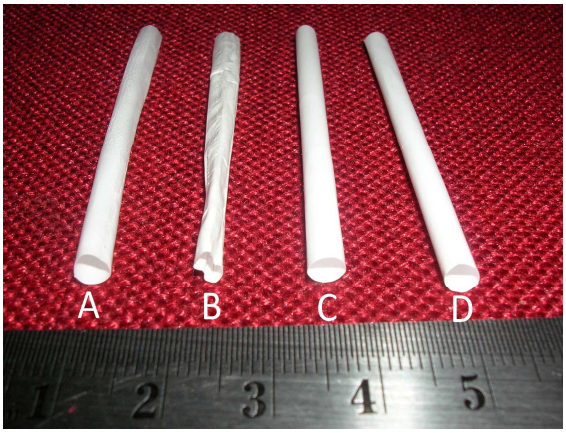

Figure 25: PCL scaffold fabricated via SCPL method before and after degradation: A, SC4(0d); **B,** SC4(6m); **C,** SC8(0d) and **D,** SC8(6m)

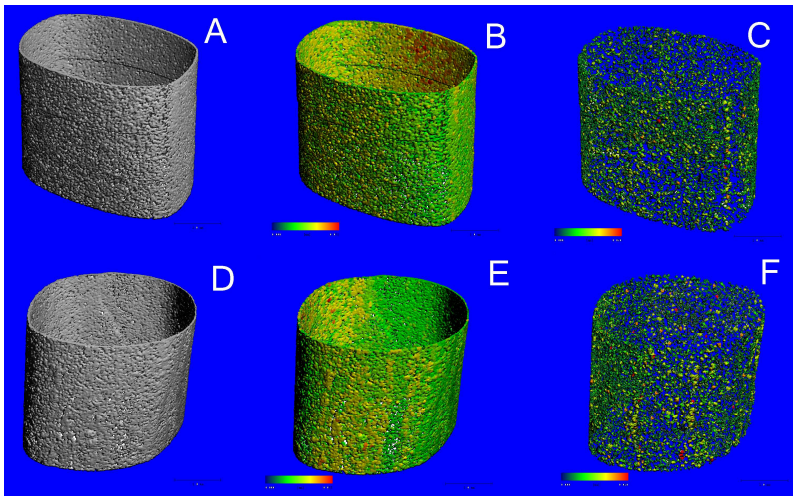

Figure 26: Micro-CT images of SC4 scaffold before and after degradation: A–C represents 0d and **D–F** represents 6m degraded scaffolds; **A & D** are three dimensional images, **B & E** are colour coded images showing the density distribution and **C & F** are inverted images showing porosity distribution within the scaffold

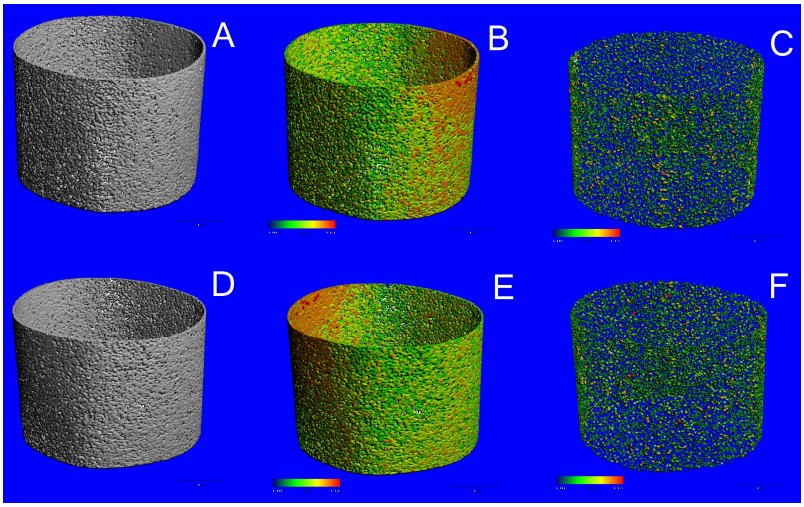

Figure 27: Micro-CT images of SC8 scaffold before and after degradation: A–C represents 0d and **D–F** represents 6m degraded scaffolds; **A & D** are three dimensional images **B & E** are colour coded images showing the density distribution and **C & F** are inverted images showing porosity distribution within the scaffold

4.1.2.2. Porosity characteristics

SEM micrographs of SC4 containing PEG8000 and SC8 with PEG3400 showed spherical pore morphologies [Figures 28A&C]. Uniform pore distribution was observed in both cases though pocket like surface deformations were observed on SC8 scaffold. After degradation, a shift in the pore size as well as wall thickness distribution was observed for both SC4 and SC8 scaffolds [Figures 29 & 30]. While SC8 exhibited narrower pore size distribution, SC4 showed broader distribution after six months of degradation. In the case of SC4 scaffold, the pore size curve become bimodal after degradation, with increase in the percentage of the larger pores (~10 % increase in 24-48 μm pores and only ~9 % increase for those < 12 μm). On the other hand, SC8 scaffold did not exhibit this behaviour, where degradation was found to increase pores of < 24 μm by about 20 % without much increase in higher pore sizes where the curve remained narrower than SC4 after 6 months degradation.

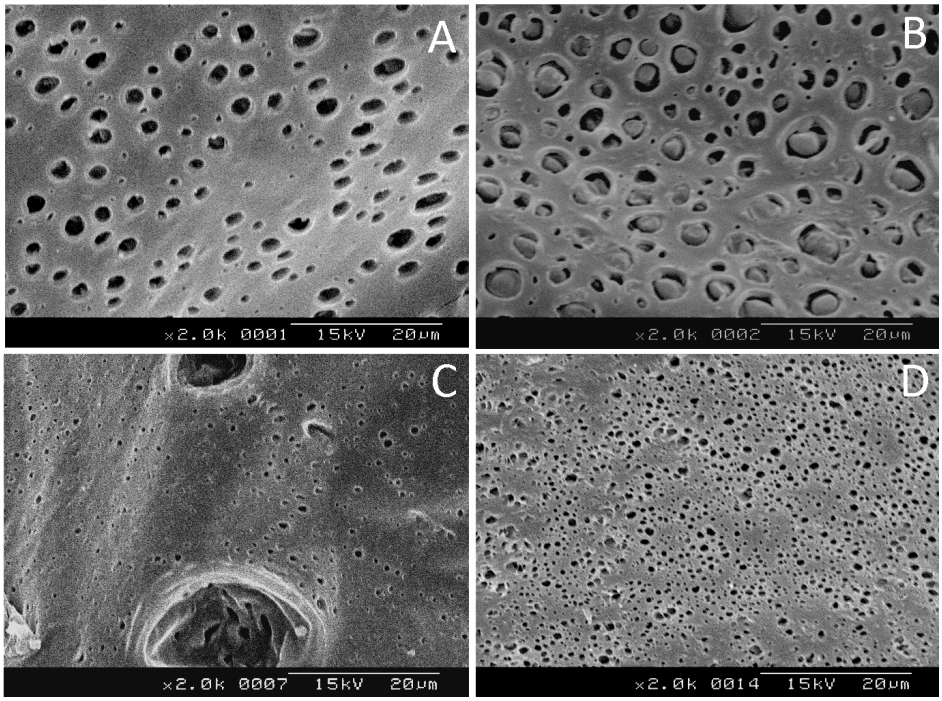

Figure 28: SEM images of PCL scaffolds before and after degradation: A, SC4(0d); **B,** SC4(6m); **C,** SC8(0d) and **D,** SC8(6m)

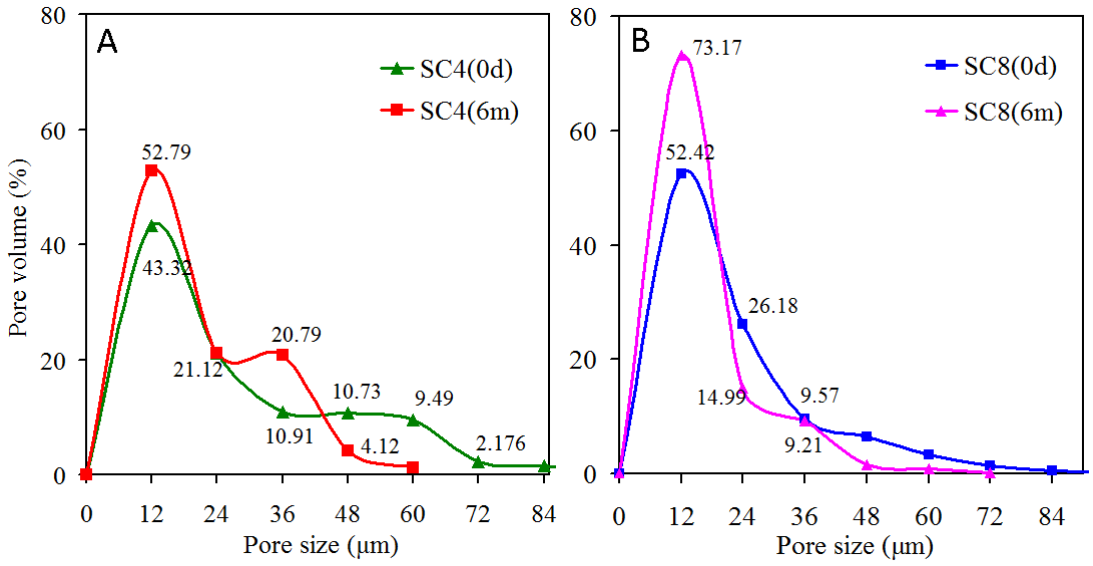

Figure 29: Histogram showing the shift in pore size distribution after degradation: A, SC4 and **B,** SC8 scaffolds before and after 6 months degradation; triplicate scaffolds were evaluated and results are expressed as mean ± SD

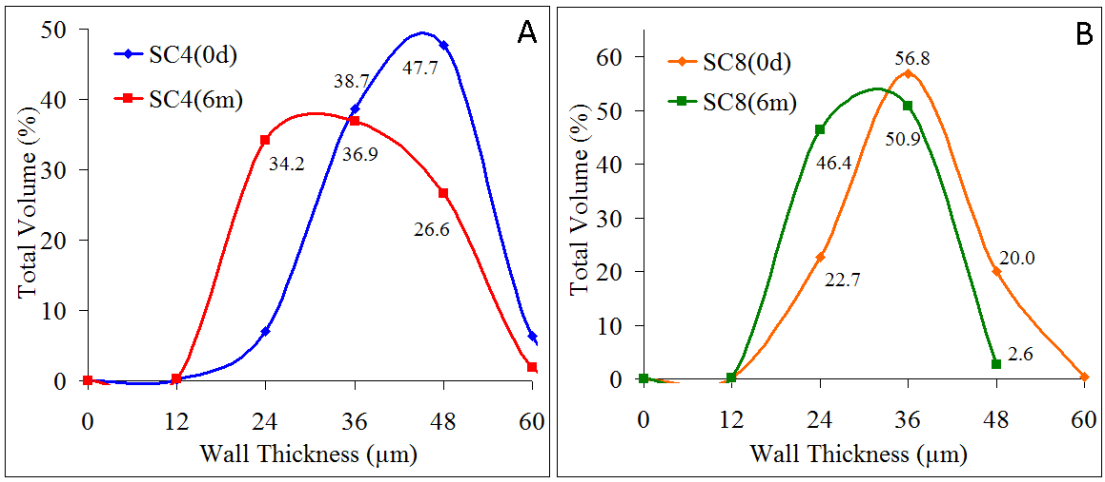

Figure 30: Histogram showing the shift in scaffold wall thickness distribution after degradation: A, SC4 and **B,** SC8 scaffolds; triplicates were evaluated and results are expressed as mean ± SD

4.1.2.3. In vitro degradation properties

The initial tensile strength (0d) values for SC4 and SC8 scaffolds were found to be 7.28 ± 0.57 MPa and 8.22 ± 0.82 MPa respectively [Figure 31A]. Degradation studies revealed ~20 % reduction of tensile strength for SC4 (5.76 MPa) after 6 months of storage in PBS and about ~6 % for SC8 (7.71 MPa). The initial suture retention strengths for SC4 and SC8 were found to be 0.73 ± 0.67 N and 0.79 ± 0.60 N respectively [Figure 31B] which decreased by ~22 % for SC4 and ~20 % for SC8 after degradation for 6 months.

While gravimetric analysis showed weight loss for both scaffolds (< 5%) after *in vitro* degradation [Figure 32A], molecular weight reduction of ~18 % in the case of SC4 and ~16 % in the case of SC8 was observed after 6 months [Figure 32B] storage in PBS.

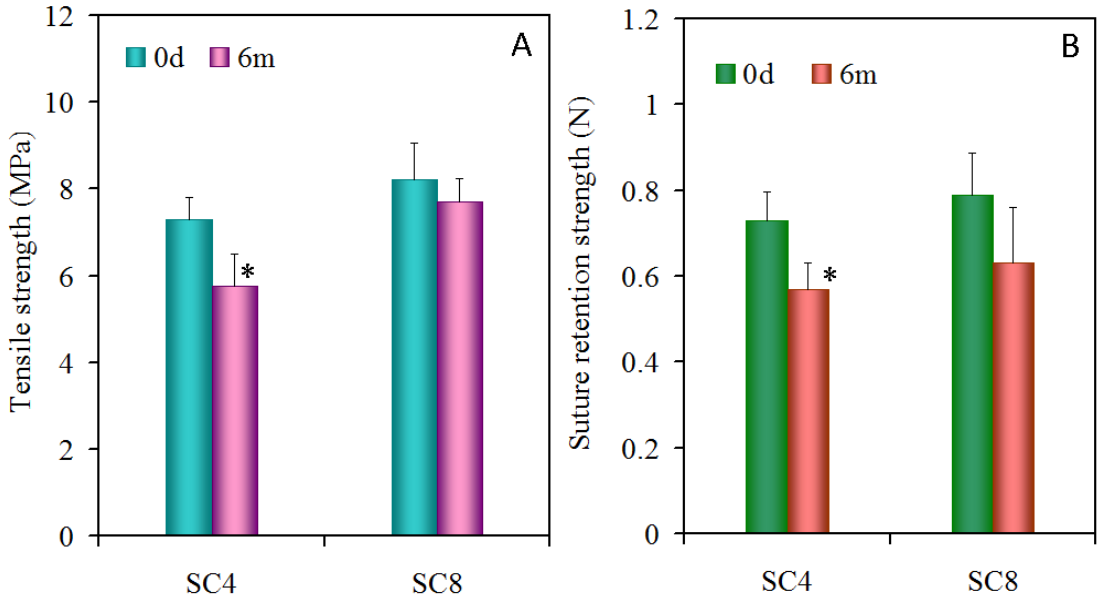

Figure 31: Tensile strength of PCL scaffolds before and after degradation: A, tensile strength and **B,** suture retention strength; six to eight scaffolds were subjected to testing; the results are expressed as mean ± SD values; * indicates that reduction in properties is statistically significant

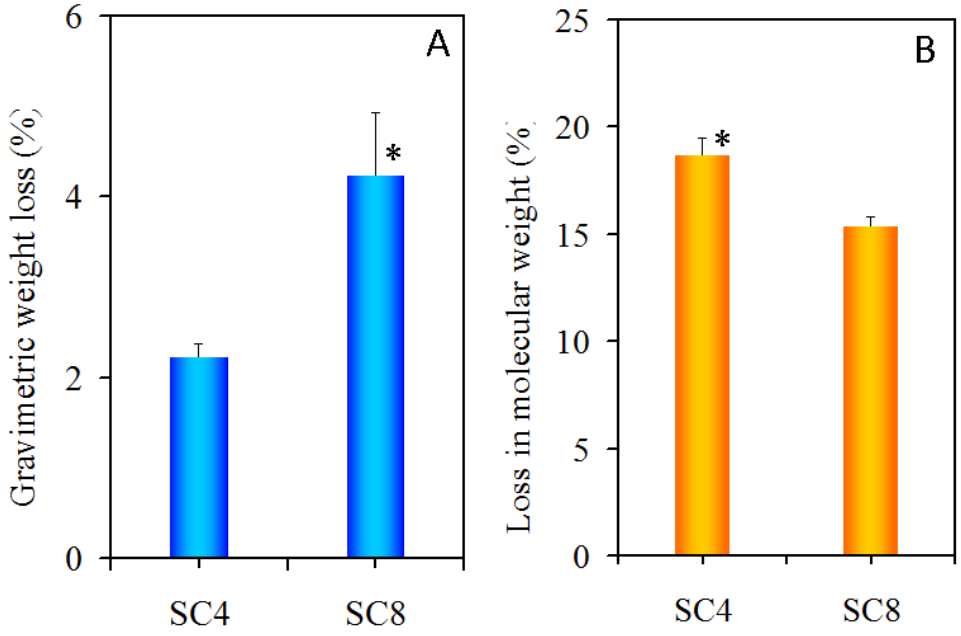

Figure 32: Summary of data obtained after degradation study of the scaffolds: A, loss of weight and **B,** GPC analysis showing molecular weight loss; for gravimetric analysis and GPC analysis, eight and three scaffolds respectively were tested and the results are expressed as mean ± SD values; * indicates statistically significant change in properties

4.2. Evaluation of SC scaffold properties after SNP incorporation

4.2.1. Characterization of SNP

Silver nanoparticles were synthesized and protected from aggregation using poly(ethylene glycol) (Madhavan *et al*., 2011). Transmission electron micrographs showed spherical particles with <20 nm size [Figure 33A]. UV-VIS spectra analysis revealed a characteristic peak corresponding to 410-440 nm range [Figure 33B]. XRD analysis of SNP solution clearly showed the peaks corresponding to silver and PEG [Figure 24C]; peaks at 2θ values of 19.25, 23.10, 25.81, 32.48 and 36.02 corresponding to PEG and 40.2 and 42.72 corresponding (111) and (200) crystalline planes of silver were found.

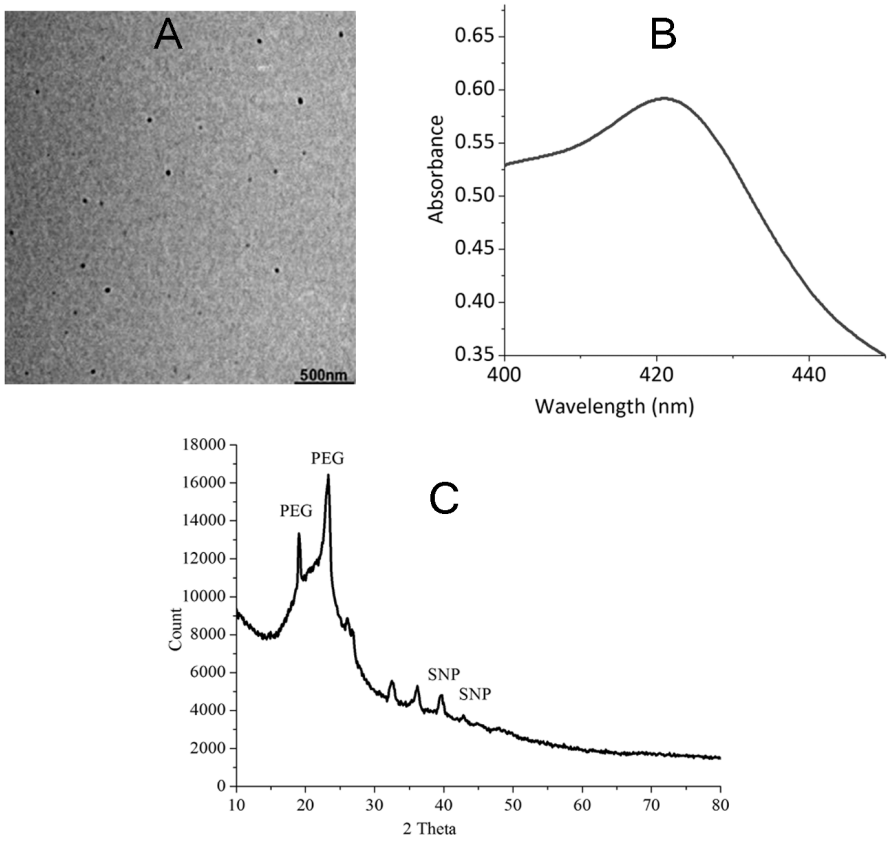

Figure 33: Characteristics of SNP: A, TEM image; **B,** UV-VIS spectra and **C,** XRD spectra

4.2.2. Macroscopic evaluation

Figure 34A illustrates the macroscopic view of SNP incorporated scaffold (SC-SNP) in comparison with the bare solvent cast scaffold (SC). SEM pictures revealed spherical pore morphology for both scaffolds [Figures 34B&C]. Three dimensional (3D) images and density distribution images acquired from micro-CT showed 3D tubular wall morphology [Figures 35A&D] and density distribution [Figures 35B&E] with and without SNP incorporation.

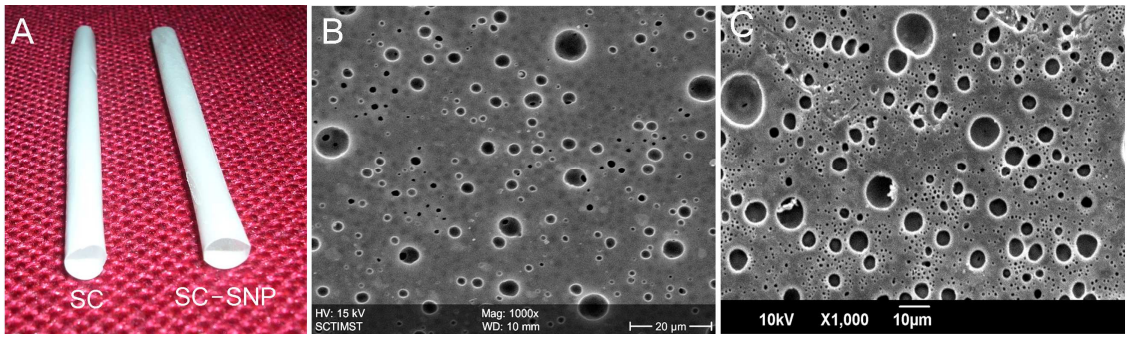

Figure 34: Macroscopic and microscopic view of solvent cast scaffolds with and without SNP: A, Photograph of samples **B & C** are SEM images of SC and SC-SNP scaffolds respectively

4.2.3. Porosity characteristics

Inverted images obtained from micro-CT analysis showed the distribution of pores within the scaffold [Figures 35C&F]. Pore size histogram revealed SC and SC-SNP scaffolds to contain ~88 % and ~87 % pores respectively in 12-24 µm range [Figure 36]. SC-SNP scaffold was found to have ~ 45 % pores in < 12 µm and ~43 % pores in 12-24 µm size whereas SC scaffold had ~69 % and ~18 % pores in < 12 and 12-24 µm sizes, respectively. Similar pore volumes of ~78 % and ~79 % were found within SC and SC-SNP scaffolds upon gravimetric analysis.

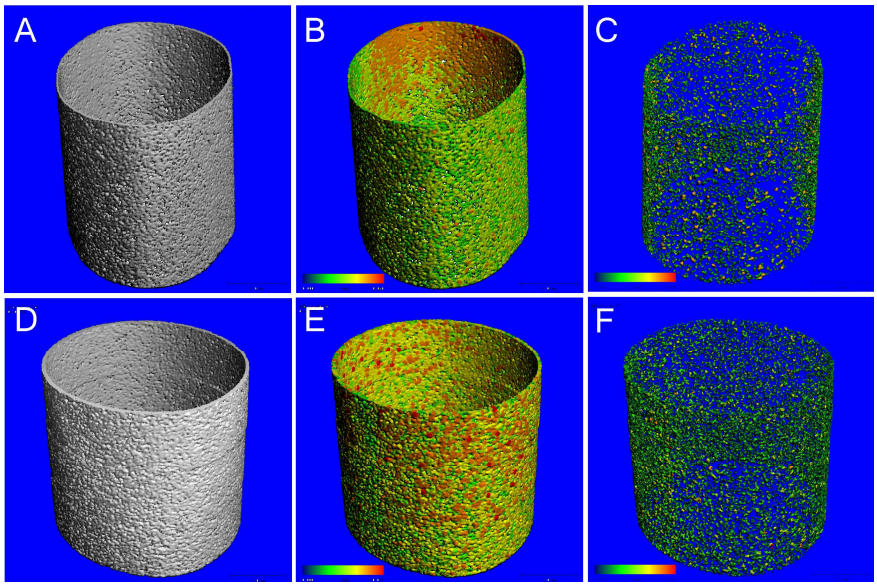

Figure 35: Micro-CT images of solvent cast scaffolds with and without SNP: A–C represents SC and **D–F** represents SC-SNP scaffolds; **A & D** are three dimensional images; **B & E** are colour coded images showing the density distribution and **C & F** are inverted images showing porosity distribution within the scaffold

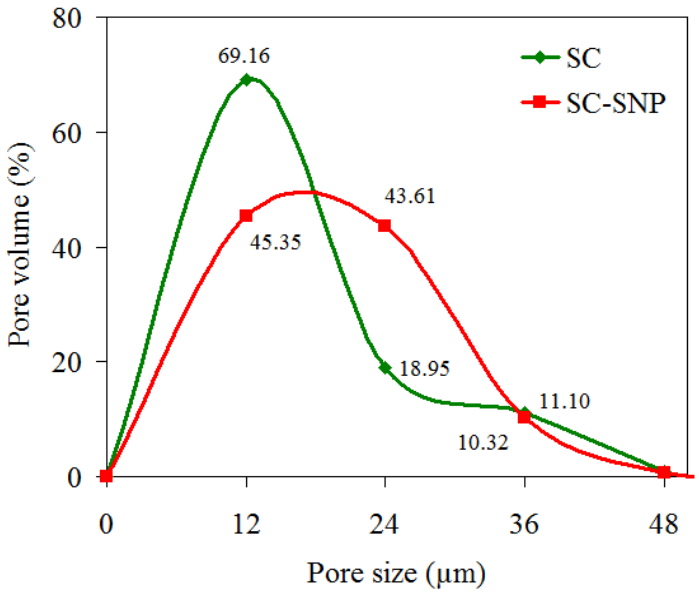

Figure 36: Graph representing pore size distribution within the scaffold with and without SNP incorporation: Triplicates were analyzed and results are given as mean ± SD values

4.2.4. Distribution and release profile of SNP

Distribution of SNP within the scaffold was illustrated by elemental mapping of silver using EDS. Red dots within the black background represent the distribution of silver within the polymer matrix [Figure 37A]. The peaks corresponding to silver were found to be low compared to those of carbon and oxygen [Figure 37B]. The release profile showed that nearly ~30 µg of SNP (~56 %) was released within 5 days of immersion in deionized water [Figure 37C].

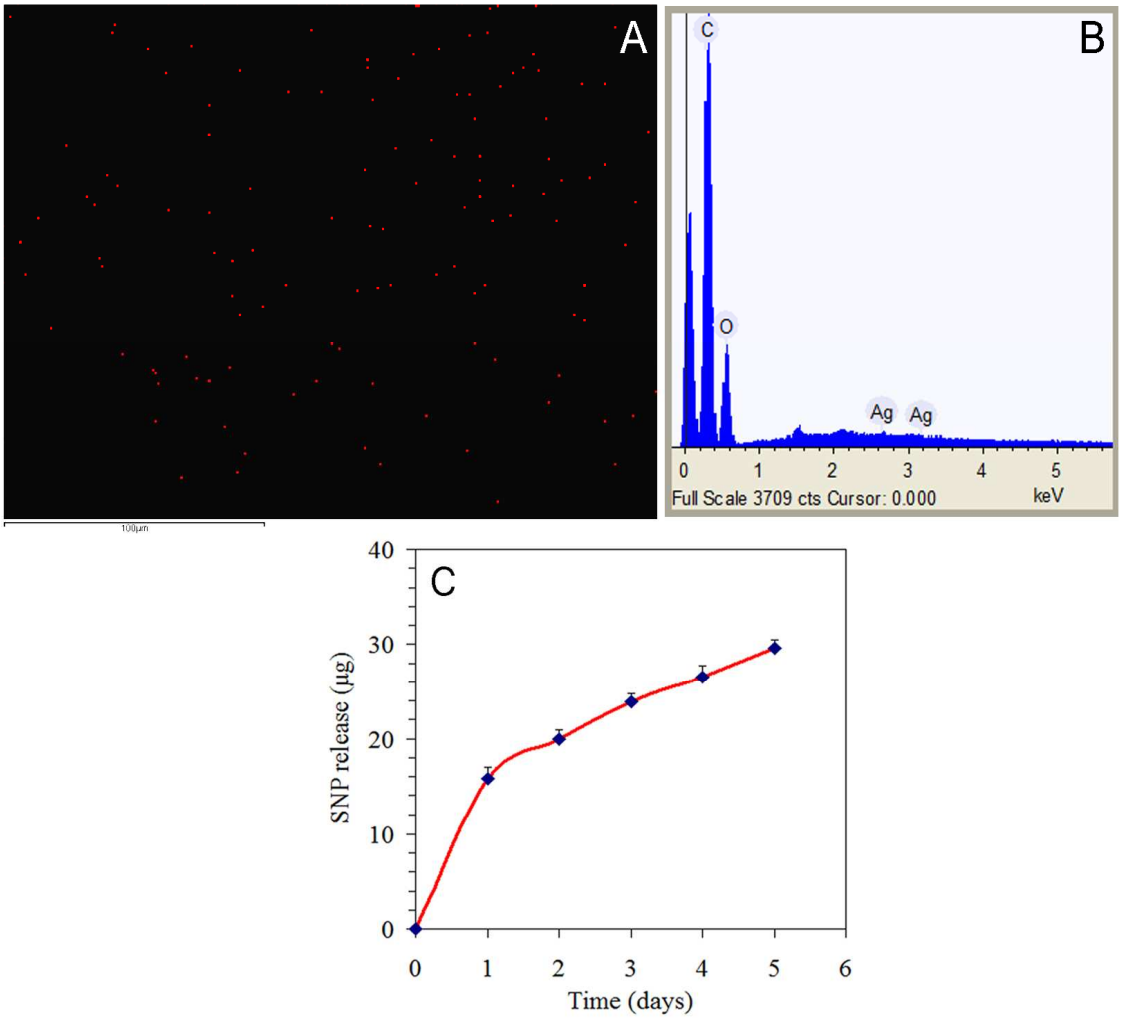

Figure 37: Distribution and release profile of SNP from PCL scaffold: A, Silver distribution mapping (scale bar = 100 µm); **B,** elemental spectra and **C,** release profile of SNP where triplicates were analyzed and result is expressed as mean ± SD values

4.2.5. *In vitro* biocompatibility of scaffolds

Analysis for cyto-compatibility using direct contact assay revealed that L929 fibroblast cells maintained normal morphology in presence of SC-SNP scaffolds similar to that in presence of bare scaffold (SC) and negative control [Figures 38A, B&C]. MTT assay showed that more than 80% cell viability was supported by both SC and SC-SNP scaffolds [Figure 38D]. Percentage hemolysis of both scaffolds was around ~0.02 %, which is within the permissible value of 0.1 %.

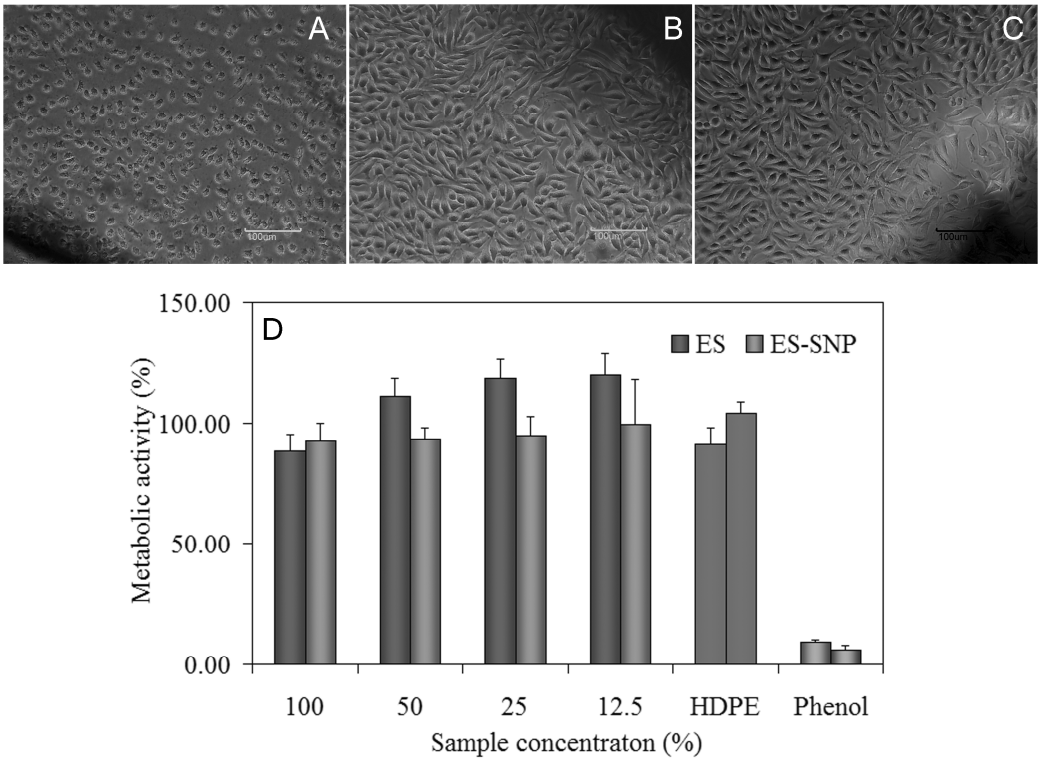

Figure 38: Evidence of cyto-compatibility of scaffolds using L929 cells: A-C represents direct contact assay; **A,** positive control; **B,** negative control; **C,** ES-SNP scaffold where scale bar = 100 µm and **D** represents results of MMT assay

4.2.6. Endothelial cell growth on scaffolds

SC-SNP scaffold was found to support the growth of endothelial cells and to form a monolayer after 3 days of static culture similar to that on SC scaffold devoid of SNP

[Figure 39]. On analysis, well-oriented actin filaments [Figures 39A&D] and cell nuclei [Figures 39B&E] were observed.

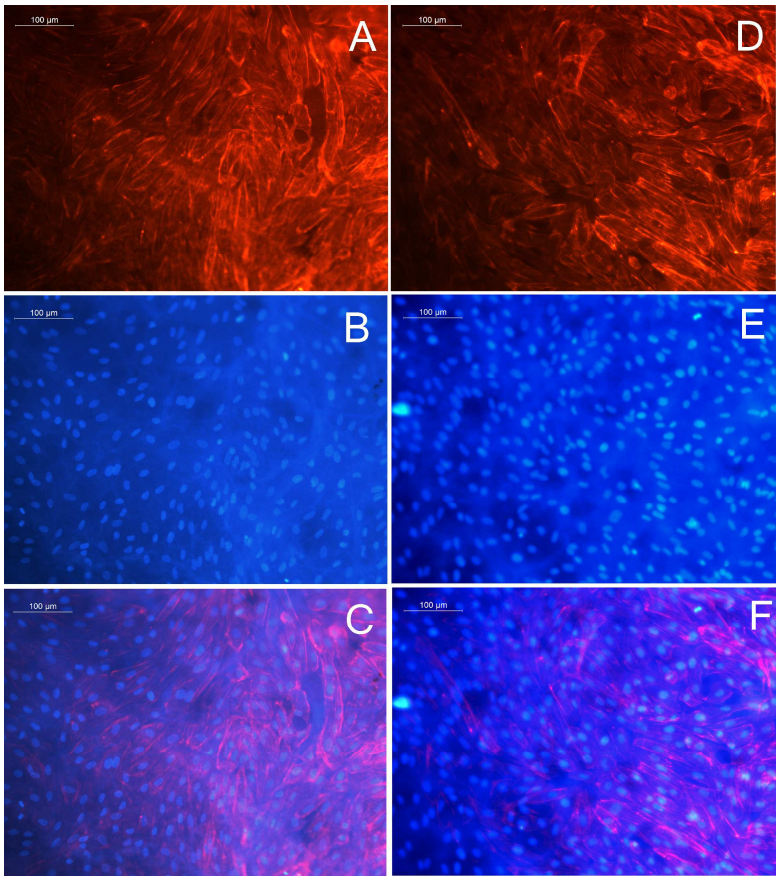

Figure 39: Fluorescent micrographs of endothelial cells grown on scaffolds after 3 days: A–C & **D–F** are corresponding to SC and SC-SNP respectively; **A & D** are actin stained, **B & E** are nuclei stained and **C & F** are merged images (scale bar = 100 µm)

4.2.7. Mechanical properties of scaffolds

The trend in tensile properties of scaffolds is shown in Figure 40. SC and SC-SNP scaffolds were observed to possess tensile strength of 3.8 ± 1.2 MPa and 3.68 ± 0.9 MPa, elasticity of 200 ± 20.5 % and 182 ± 12.6 % and modulus 36 ± 6.5 MPa and 42 ± 3.3 MPa, respectively. Burst strength values were found to be 450 ± 17 mm Hg and 420 ± 10 mm Hg for SC and SC-SNP scaffolds respectively [Figure 41A].

Suture retention strengths of 0.62 ± 0.05 N and 0.42 ± 0.03 N were obtained for SC and SC-SNP scaffolds, respectively [Figure 41B].

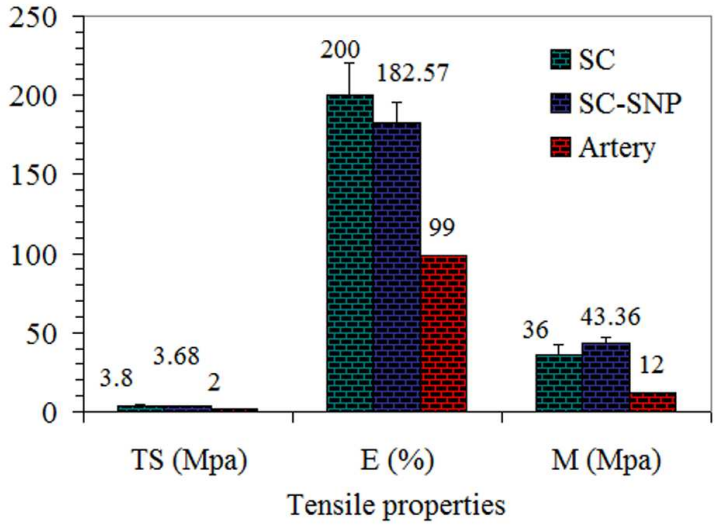

Figure 40: Variation of tensile properties as result of SNP incorporation: TS stands for tensile strength, E represent elasticity and M denotes modulus of scaffolds; Six to eight measurements were taken for each sample and values are expressed as mean ± SD

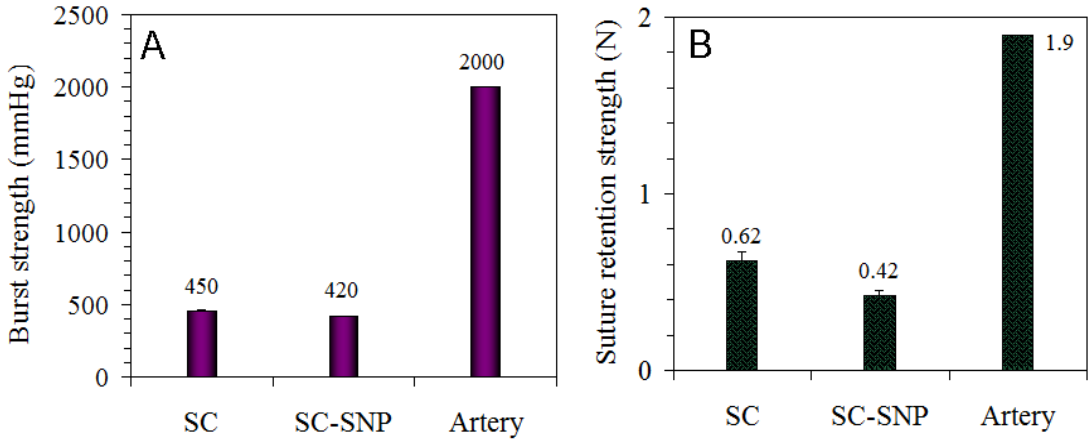

Figure 41: Mechanical strength of scaffolds of SC and SC-SNP scaffolds: A, burst strength and **B,** suture retention strength; Six to eight measurements were taken for each sample and values are expressed as mean ± SD

4.2.8. Comparative analysis of sheep artery with scaffold

In order to optimize the dimensional parameters such as inner diameter and wall thickness of scaffolds, excised sheep artery was analyzed using micro-CT. Figures 42A&B represent the 3D images and density distribution images of the artery respectively. Inner diameter and wall thickness of artery were found to be ~3.3 mm and 750 µm respectively [Figures 42C&D].

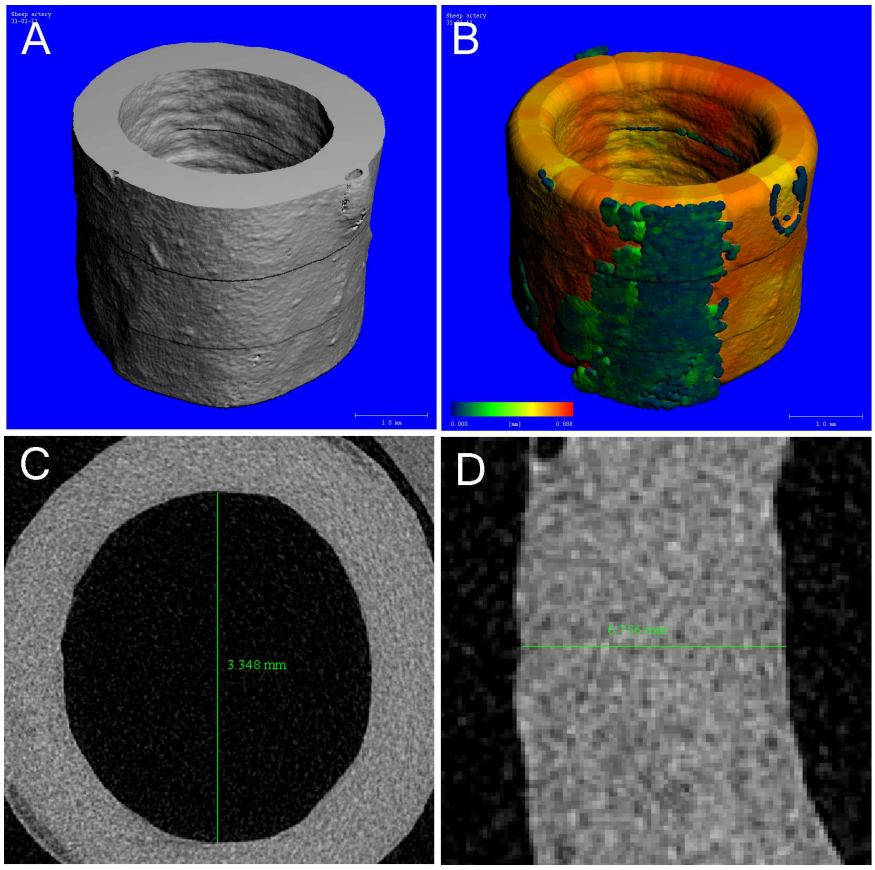

Figure 42: Data of excised sheep artery obtained from µ-CT analysis: A, three dimensional image; **B,** density distribution and **C & D** are two dimensional images indicating inner diameter and wall thickness of artery respectively

4.3. Optimization of ES scaffold properties

Optimization of electrospinning parameters for constructing a fibrous mat with appropriate physico-mechanical properties is a critical step in blood vessel tissue engineering. Electrospun tubular scaffolds having an inner diameter of 4 mm and length of ~70 mm designated as ES-1, ES-3 and ES-5 were fabricated by varying the flow rate as 1 ml/hr, 3 ml/hr and 5 ml/hr respectively [Figure 43].

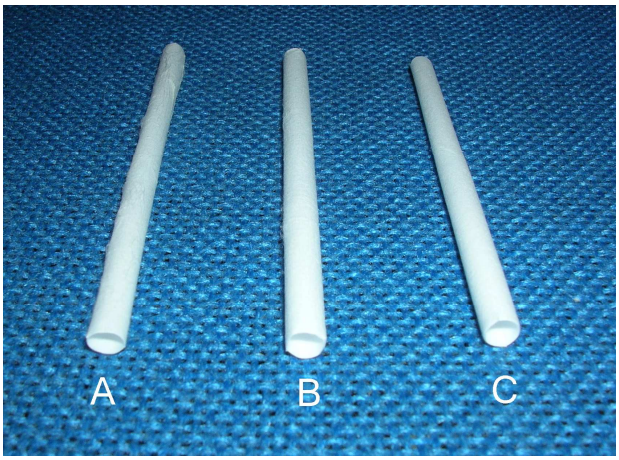

Figure 43: Macroscopic view of tubular electrospun scaffolds: A, ES-1; **B,** ES-3 and **C,** ES-5; scaffolds fabricated by varying flow rates during electrospinning

4.3.1. Scaffold wall thickness and porosity characteristics

Two dimensional slice images obtained using micro-CT showed the wall thickness of electrospun scaffolds increasing with change in flow rate [Figures 44A,D&G]. The average wall thicknesses obtained were 318 ± 21 µm, 534 ± 30 µm and 717 ± 28 µm for ES-1, ES-3 and ES-5 scaffolds, respectively under a constant electrospinning time of 15 minutes [Figure 45]. Pore size analysis revealed that the majority of pores in all scaffolds lay within the size range of 12-60 µm [Figure 46].

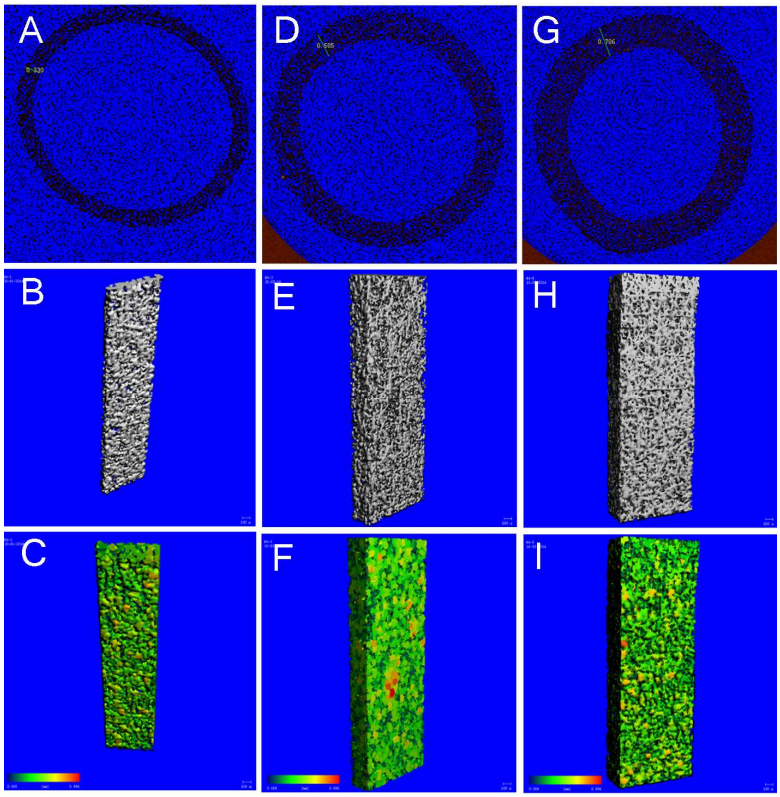

Figure 44: Micro-CT images of scaffold structure: A–D stands for ES-1; **D–F** represents ES-3 and **G–I** represents ES-5 scaffolds; **A, D & G** are two dimensional slice images representing the cross section of scaffolds; **B, E & H** are three dimensional images and **C, F & I** are colour coded inverted images showing porosity distribution within the scaffold

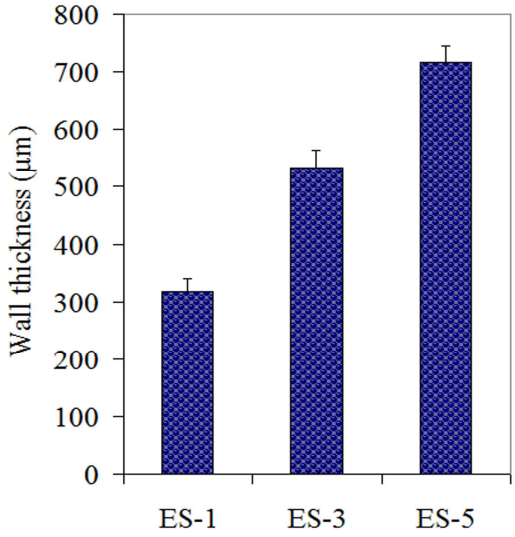

Figure 45: Variation of wall thickness of tubular scaffolds with flow rate: measurements were taken from five different sites of the same scaffold and expressed as mean ± SD

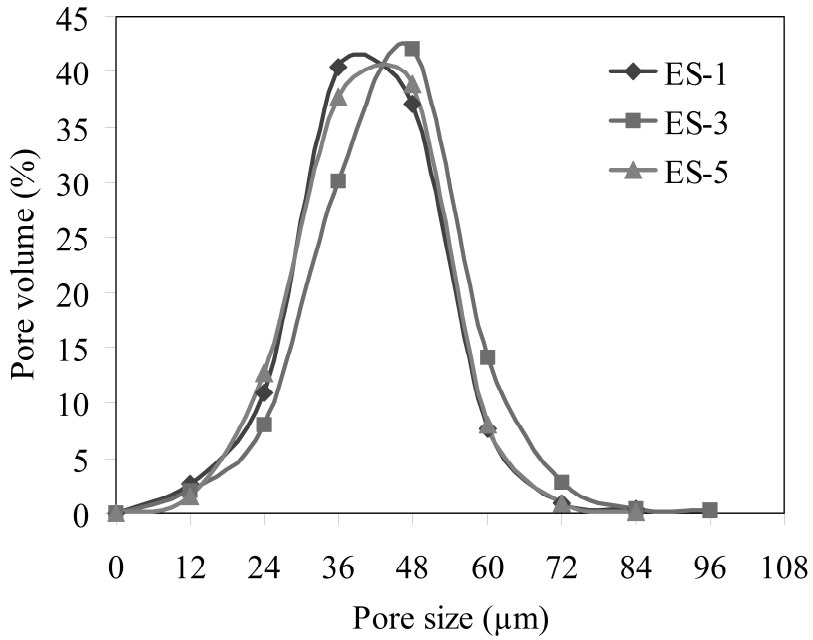

Figure 46: Pore size histogram of different electrospun scaffolds: three measurements were taken for each sample and graph was plotted using mean ± SD values

4.3.2. Evaluation of tensile properties

Tensile strength of the scaffolds was found to improve with increasing flow rate [Figure 47]. The values increased from 2.49 ± 0.16 MPa to 3.18 ± 0.03 MPa and to 4.25 ± 0.59 MPa for ES-1, ES-3 and ES-5 scaffolds, respectively [Figure 47A]. Measured elasticity also improved similarly from 183 ± 75 % to 723 ± 23 % and to 761 ± 25 % for ES-1, ES-3 and ES-5 scaffolds, respectively [Figure 47B]. Electrospun scaffolds exhibited comparable modulus values such as 28.91 ± 5.4 MPa, 28.54 ± 0.2 MPa and 33.19 ± 11.2 MPa for ES-1, ES-3 and ES-5 scaffolds [Figure 47C]. As compared to other scaffolds, ES-3 was found to possess uniform tubular wall thickness and better elasticity properties. Figure 48 compares the burst and suture retention strength values of ES-3 fibrous matrix [5545 ± 636 mmHg and 2.24 ± 0.05 N] to that of native blood vessels [Figure 48].

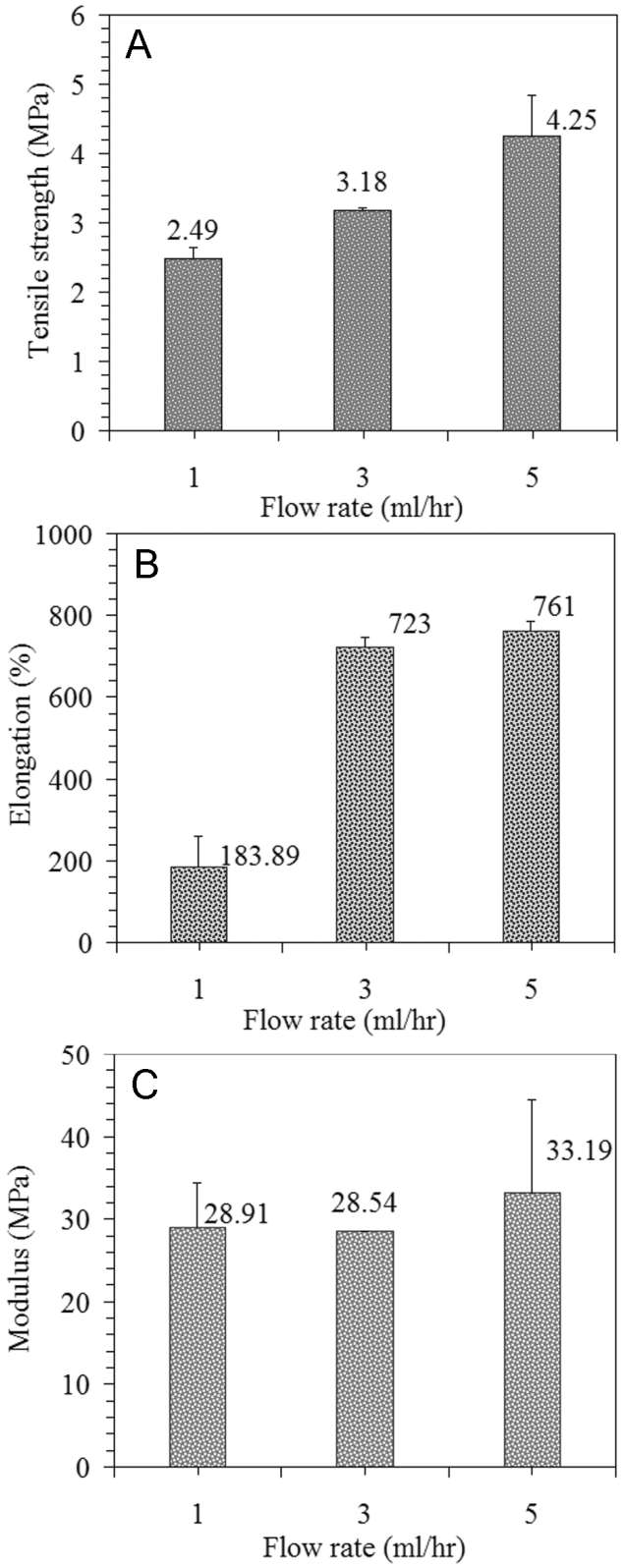

Figure 47: Variation of tensile properties of scaffolds with flow rate: Six to eight measurements were taken and results are expressed as mean ± SD values

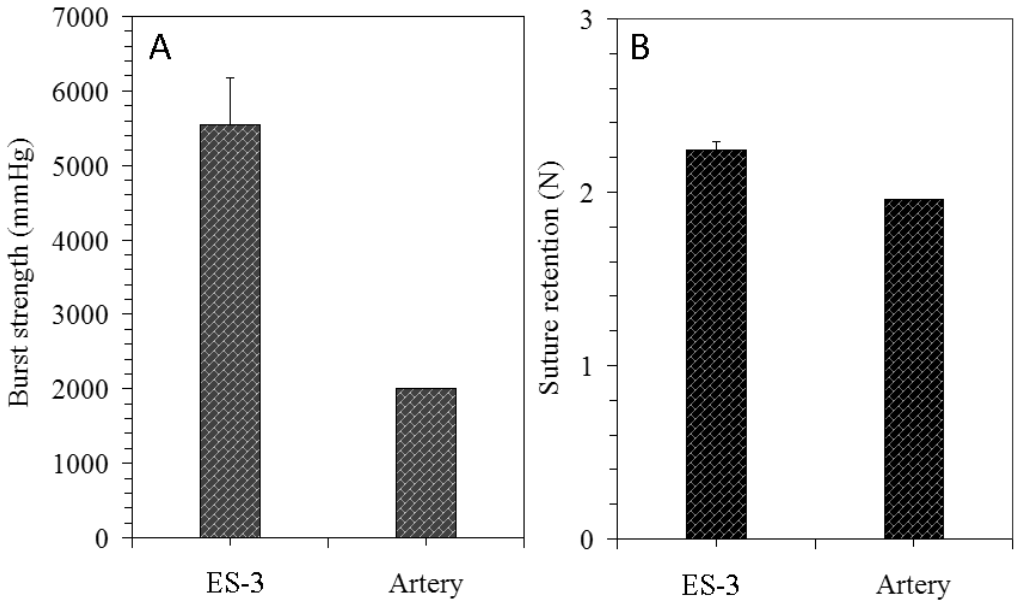

Figure 48: Mechanical properties of electrospun scaffold: A, burst strength and **B,** suture retention strength; Six to eight measurements were taken and results are expressed as mean ± SD

4.3.3. *In vitro* degradation characteristics

The degradation profile of ES-3 scaffold in terms of reduction in mass, molecular weight and mechanical strength is shown in Figures 49 & 50.

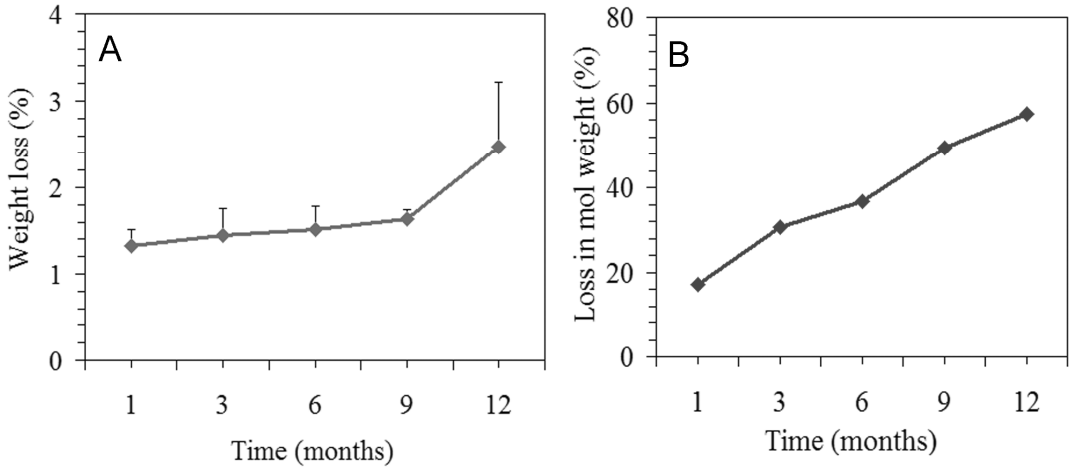

Figure 49: Degradation properties of electrospun scaffolds: **A,** gravimetric weight loss and **B,** molecular weight loss; For measuring weight loss eight samples were tested and triplicates were analyzed using GPC and the graphs were plotted using mean ± SD values

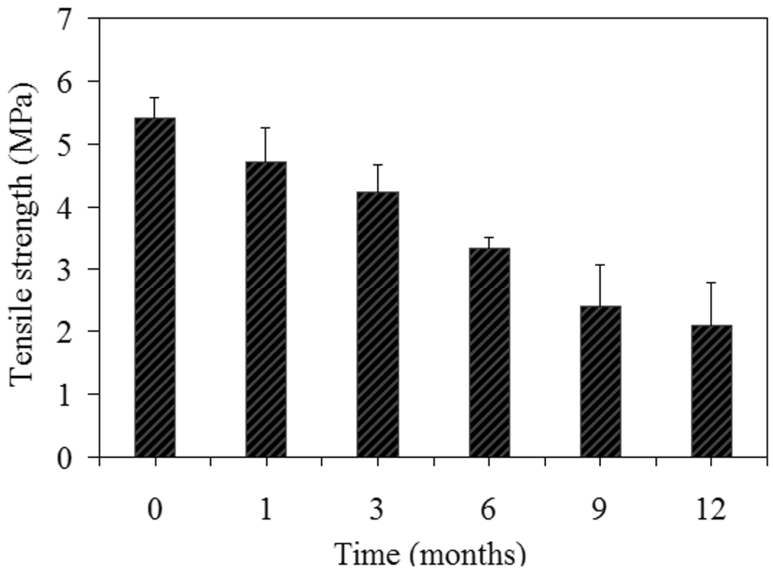

Figure 50: Tensile strength of electrospun scaffolds during degradation: Eight samples were tested and the graph was plotted using mean ± SD values

The electrospun scaffolds showed only ~3 % gravimetric weight loss [Figure 49A] even though considerable reduction in molecular weight was observed (~57 %) after one year degradation [Figure 49B]. Figure 50 shows the progressive reduction in tensile strength with increasing degradation period. However, ES-3 fibrous matrix was found to maintain mechanical integrity even after completing one year degradation.

4.4. Evaluation of ES scaffold properties after SNP incorporation

4.4.1. Scaffold macrostructure

Electrospun tubular scaffold of PCL fibrous matrix without (ES) and with SNPs (ES-SNP) are shown in Figure 51. Two dimensional slice images obtained from the micro-CT analysis illustrated the cross-sectional view of both scaffolds [Figures 52A&E]. Maintaining a constant electrospinning time of 15 minutes, wall

thicknesses of 591 µm and 270 µm were obtained for ES and ES-SNP scaffolds respectively.

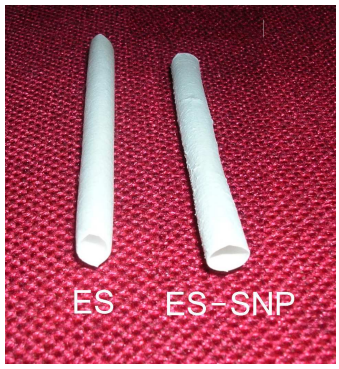

Figure 51: Macroscopic view of SNP incorporated and bare electrospun scaffolds

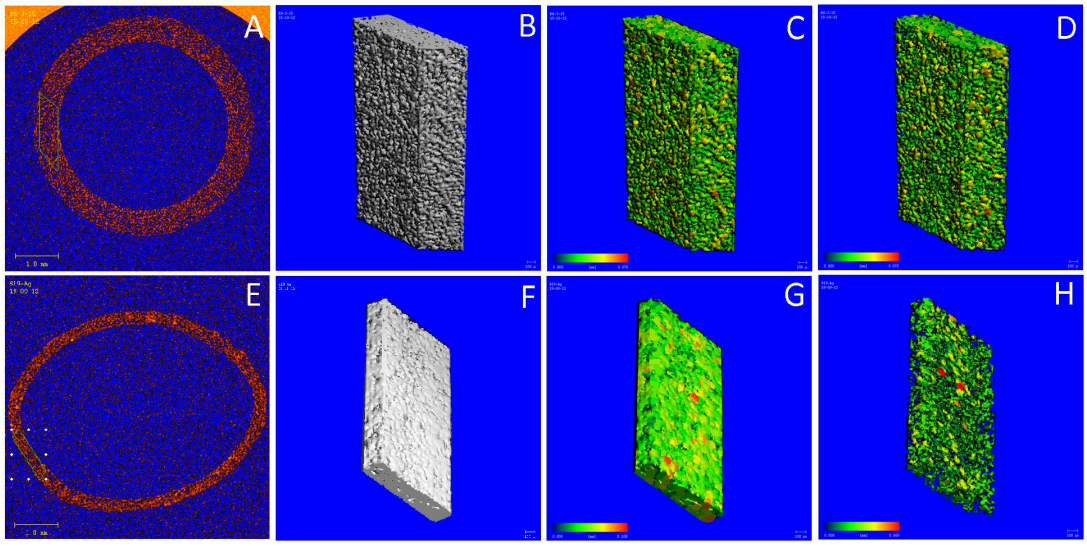

Figure 52: : Micro-CT images of electrospun scaffolds with and without SNP: A–D represents ES and **E–H** represents ES-SNP scaffolds; **A & E** are two dimensional images; **B & F** are three dimensional images; **C & G** are colour coded images showing the density distribution and **D & H** are inverted images showing porosity distribution within the scaffold

4.4.2. Fiber morphology and scaffold porosity characteristics

SEM images revealed the junctions between the ES fibers to be fused whereas ES-SNP scaffolds contained free fibers [Figures 53A-D]. Image J analysis showed ES

scaffold as consisting of fibers whose diameter varied from 3 to 10 µm with an average diameter of 6.34 ± 1.51 µm [Figure 54]. The average fiber diameter of ES-SNP scaffold was found to be 0.81 ± 0.4 µm with values ranging from 0.3 to 1.8 µm.

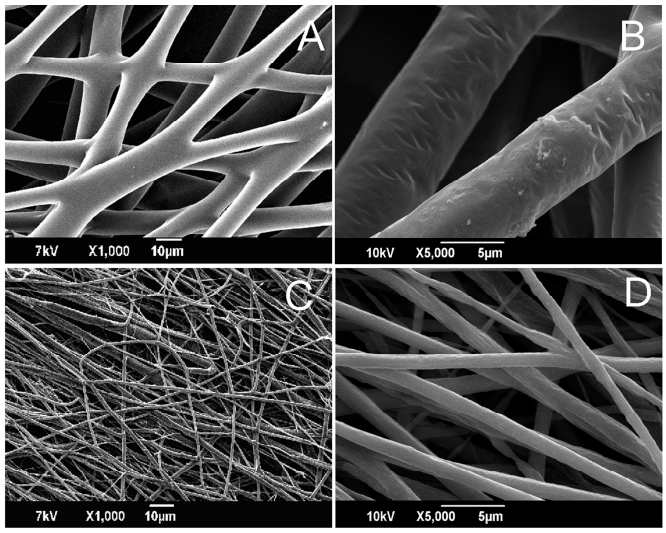

Figure 53: Surface topography of ES and ES-SNP electrospun matrices: A–B represent ES and **C–D** represents ES-SNP scaffolds; **A & C** show lower and **B & D** higher magnifications

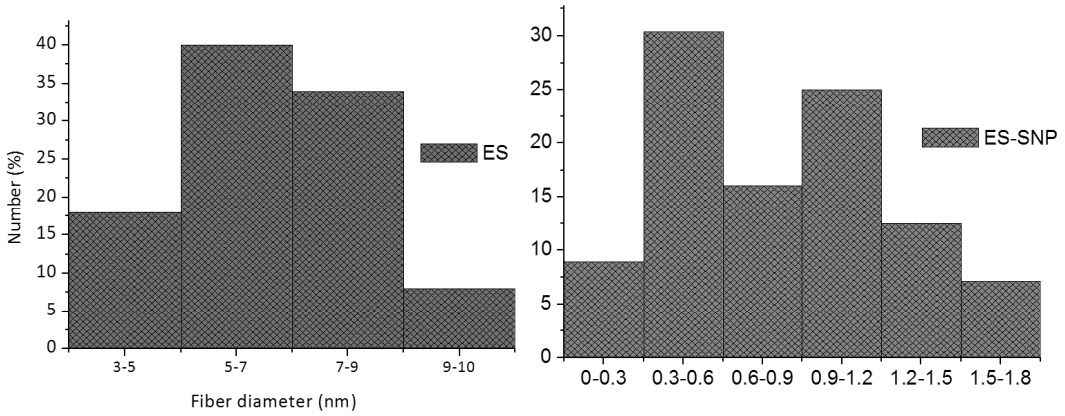

Figure 54: Fiber diameter histogram of ES and ES-SNP scaffolds: measurements were taken from ~30 different sites of SEM images and histogram was plotted; mean values are given in the text

The distribution of pores within scaffolds was demonstrated by inverted images obtained from micro-CT analysis [Figures 52D&H]. Pore size histogram demonstrates that SNP incorporation played a major role in the observed shift in pore

size distribution within the electrospun matrix [Figure 55]. The bare ES scaffold had 92% pores in 24-60 µm range whereas ES-SNP scaffold had 98% pores within 12-36 µm. Total porosity of 87.5 ± 6.4 % and 81.6 ± 2.9 % were found to be present in ES-1 and ES-SNP scaffolds respectively [Table 6].

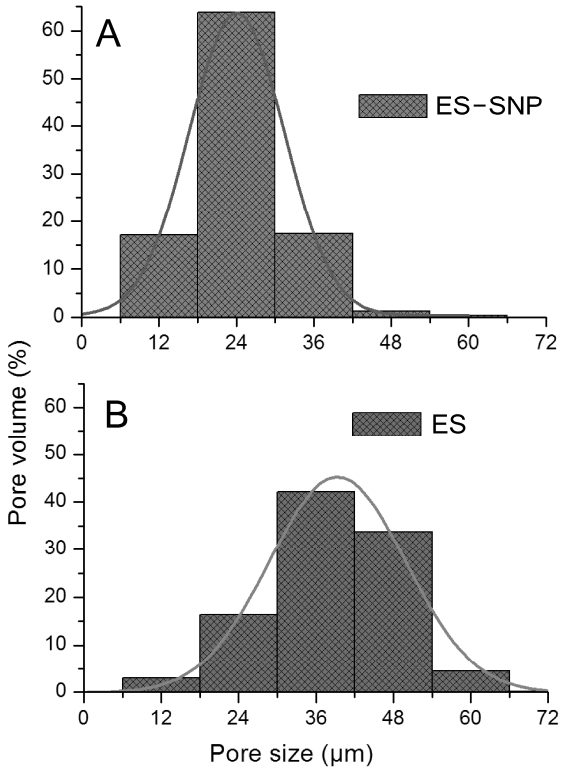

Figure 55: Pore size histogram of ES and ES-SNP electrospun scaffolds: histogram was plotted using data obtained from triplicate scaffolds

4.4.3. Distribution and release profile of SNPs

EDS analysis revealed the peaks corresponding to silver (Ag) had a lower intensity than those of carbon and oxygen [Figure 56A]. However ~0.092% Ag was found to be present in ES-SNP matrix. The distribution of SNPs within the scaffold is shown by silver distribution mapping [Figure 56B]. Further SNP distribution on the surface of electrospun fibers is demonstrated by TEM images [Figures 56C&D]. SNP release profile showed that ~31 % SNP was released after 5 days of incubation in DI water

[Figure 56E]. Though a burst release of ~11 µg was observed on day 1, sustained release was observed thereafter. Out of 48 µg SNPs incorporated per scaffold, a total of 14.93 µg (~31 %) was detected within 5 days.

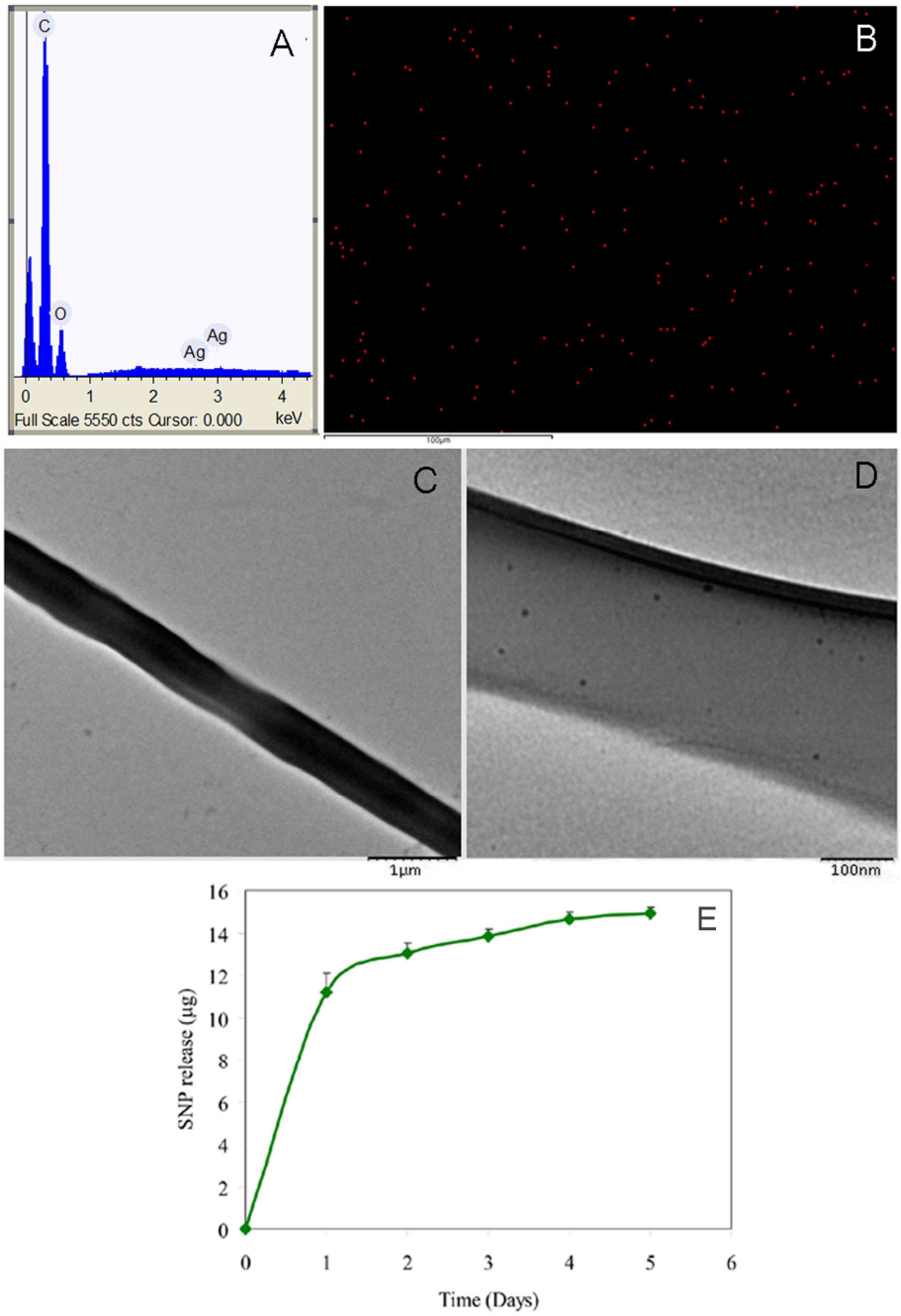

Figure 56: Distribution and release profile of SNP from ES-SNP scaffold: A, EDS spectra; **B,** Mapping of silver; **C & D**, TEM images of SNPs on electrospun fibers at lower and higher magnifications respectively and **E,** release profile of SNP from polymer matrix; for which triplicates were analyzed and graph is plotted using mean ± SD values

4.4.4. Surface wettability and crystalline properties

Contact angles formed on the surface of the electrospun scaffolds are shown in Figure 57 and mean contact angles are given in Table 6. The hydrophobic nature of electrospun matrices was evident where contact angles remained above 90^o. However biological modification with fibrin resulted in lowering of contact angle with $\theta < 90^o$. Enhancement in the intensities of crystalline peaks at 21.7 and 23.9 corresponding to PCL was observed during XRD analysis after SNP incorporation [Figure 58]. XRD spectra of ES-SNP scaffold revealed characteristic peaks at 2θ values 40.6 and 43.62 corresponding (111) and (200) planes of silver.

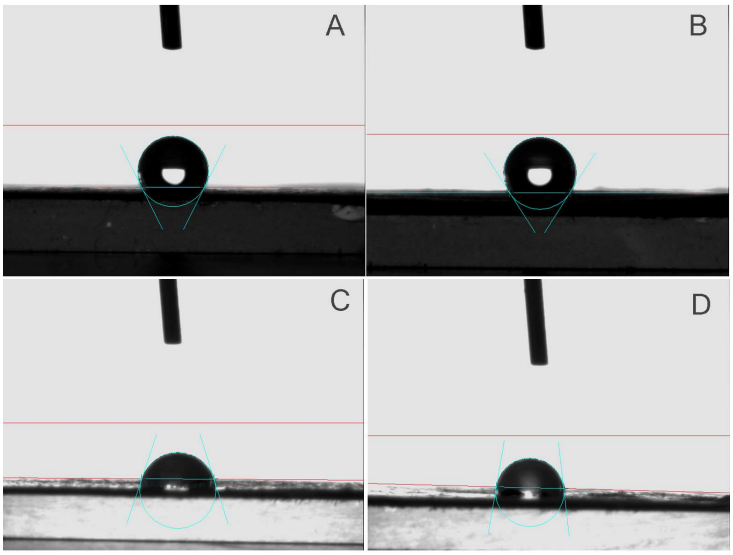

Figure 57: Representative images showing surface wettability of electrospun scaffolds: A, ES; **B,** ES-SNP; **C,** ES-fibrin coated and **D,** ES-SNP-fibrin coated scaffolds

Scaffold ID	Contact angle (θ) measured for scaffolds		Porosity (%)
	Before fibrin coating	After fibrin coating	
ES	119 ± 5	88 ± 7	87.5 ± 6.4
ES-SNP	122 ± 2	87 ± 5	81.6 ± 2.9

Table 6: Surface wettability characteristics and porosity of electrospun scaffolds

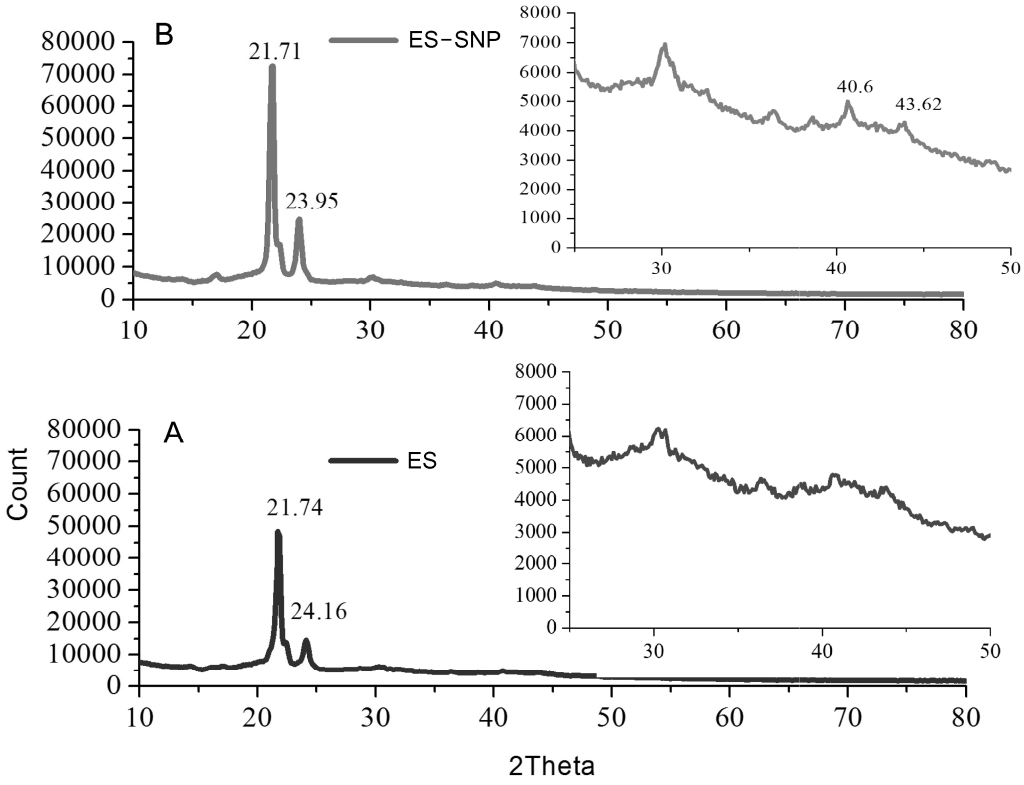

Figure 58: XRD spectra of electrospun scaffolds with and without SNP: intense peaks corresponding to PCL are visible and SNP characteristic peaks are given in the inset

4.4.5. Mechanical properties

The effect of SNP addition on the mechanical strength of PCL scaffolds is shown in Figures 59 & 60. Tensile strength values of 3.15 ± 0.3 MPa and 2.6 ± 1.7 MPa, elongation values of 830.5 ± 77.4 % and 311 ± 40.7% and modulus of 19.75 ± 3.4 MPa and 13.48 ± 1.7 MPa were obtained for ES and ES-SNP scaffolds respectively [Figures 59A-C]. The suture retention strengths were found to be 2.24 ± 0.05 N for ES scaffold and 0.61 ± 0.06 N for ES-SNP scaffold [Figure 60A]. ES scaffold could withstand a burst pressure of 5545 ± 636 mm Hg whereas ES-SNP scaffold was observed to withstand only 476 ± 79 mm Hg [Figure 60B].

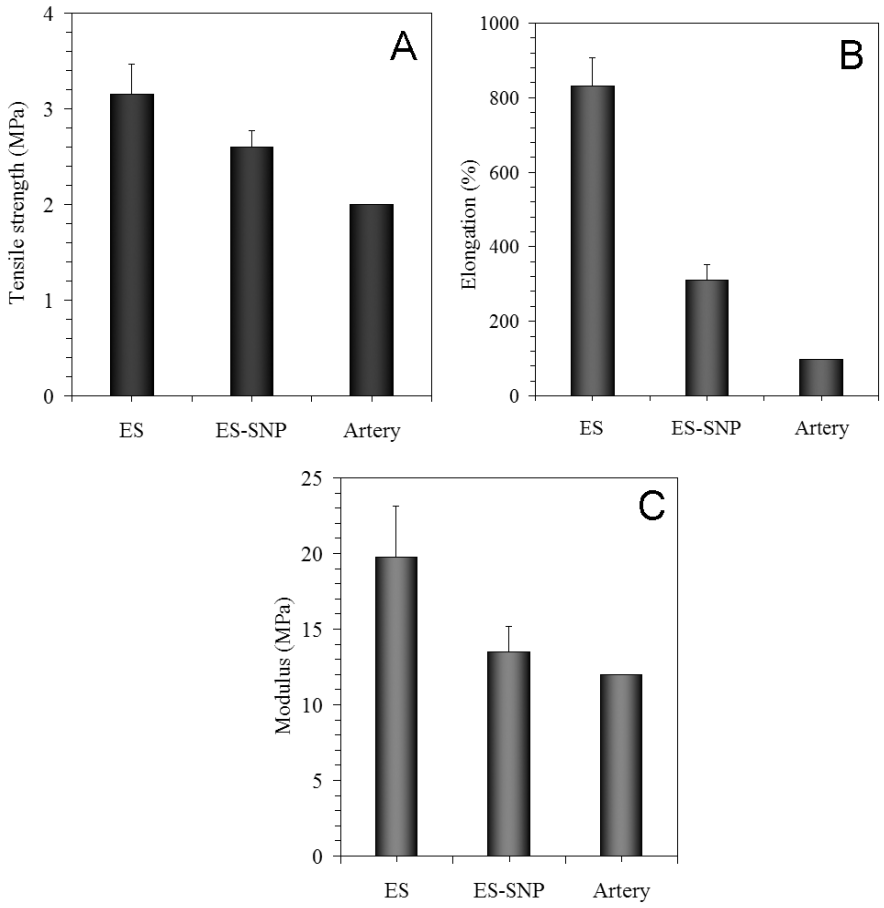

Figure 59: Tensile properties of electrospun scaffolds before and after SNP addition: A, tensile strength; **B,** elongation and **C,** modulus; Six to eight measurements were taken and results are expressed as mean ± SD values

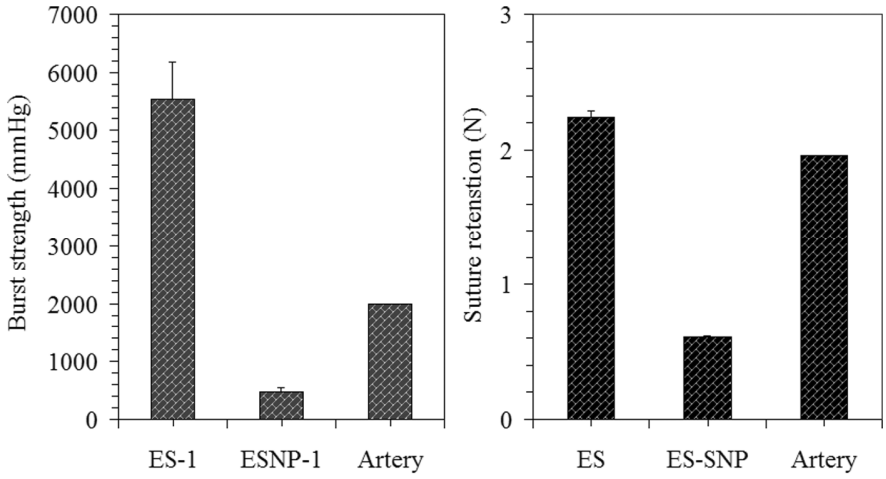

Figure 60: Mechanical properties of electrospun scaffold as function of SNP addition: A, burst strength and **B,** suture retention strength; Six to eight measurements were taken and results are expressed as mean ± SD values

4.4.6. Cytotoxic behaviour

Direct contact assay demonstrated that SNP present in the scaffold did not induce any toxic effects and scaffolds were found to be cyto-compatible compared to negative control [Figures 61A-C]. The normal spindle-shaped morphology of L929 fibroblast cells was maintained when cultured in presence of both scaffolds. Cells on positive control (PVC discs) were found to lose their normal morphology and changed to spherical shape. MTT assay showed that both types of scaffolds have more than 80 % cell viability compared to negative control HDPE [Figure 61D].

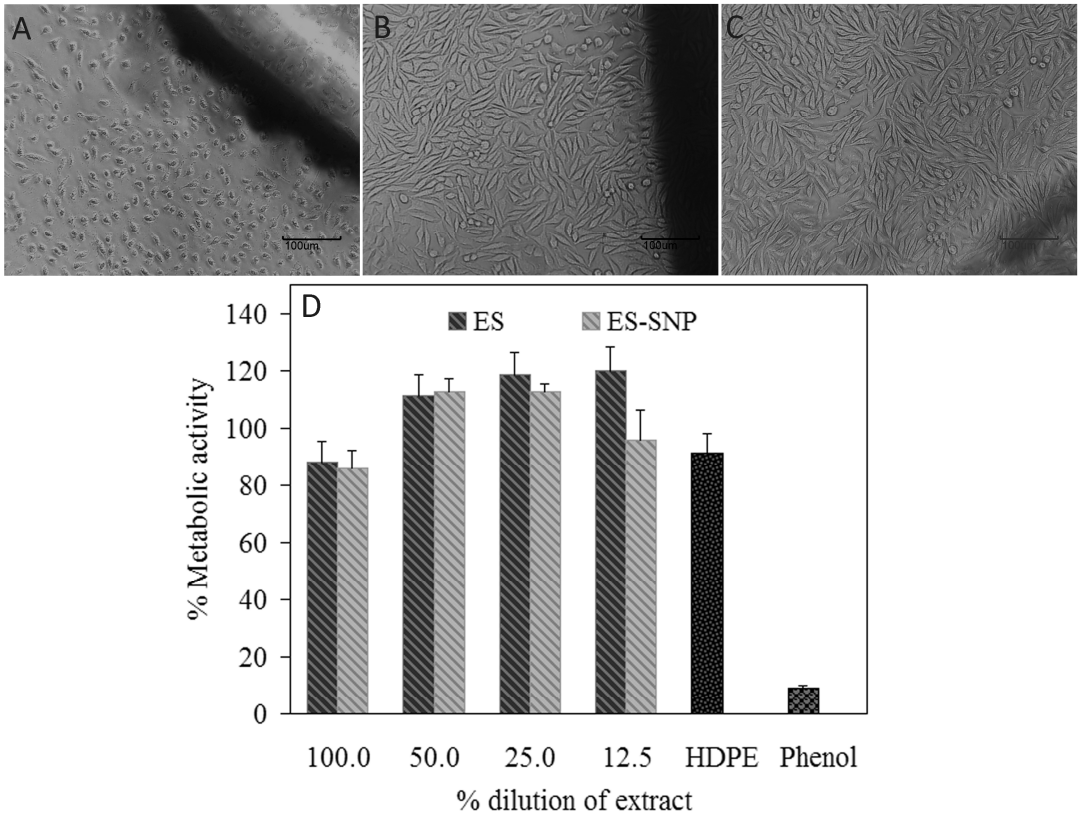

Figure 61: Cyto-compatibility data of PCL scaffolds using L929 fibroblast cells: A-C represents direct contact assay and **D** represents MTT assay; **A,** positive control; **B,** negative control and **C,** ES-SNP scaffold (scale bar = 100 µm)

4.4.7. EC adhesion and proliferation

Fibrin-modified PCL scaffolds were found to support endothelial cell growth. Endothelial cell adhesion on scaffolds was demonstrated by actin and nuclear-stained microscopic images of cells cultured for 3 days on scaffolds [Figures 62 & 63]. Cells on ES-SNP scaffolds were found to have well-spread actin filaments [Figures 62D-F] and cells were found to grow along the fibers in the case of ES scaffolds [Figures 62A-C]. ESEM images also showed EC growth on both ES and ES-SNP scaffolds [Figure 63]. After 5 days culture, uniform coverage of cells was observed on both scaffolds [Figure 64].

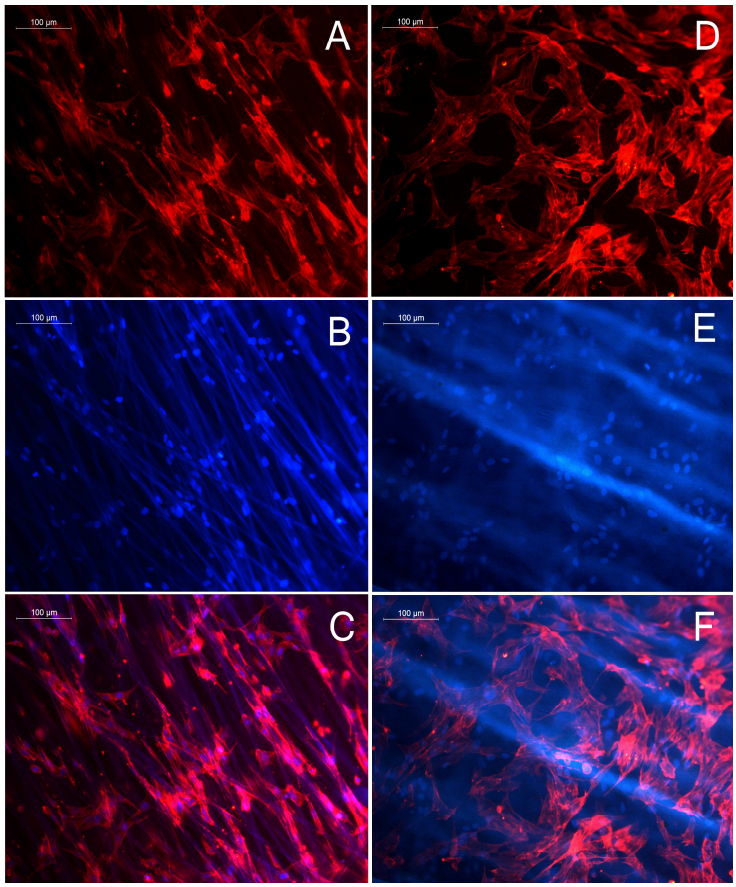

Figure 62: Fluorescent microscopic images of endothelial cells grown on electrospun scaffolds for 3 days: A–C & D–F correspond to ES and ES-SNP scaffolds respectively; **A & D** are actin stained; **B & E** are nuclei stained and **C & F** are merged images (scale bar = 100 µm)

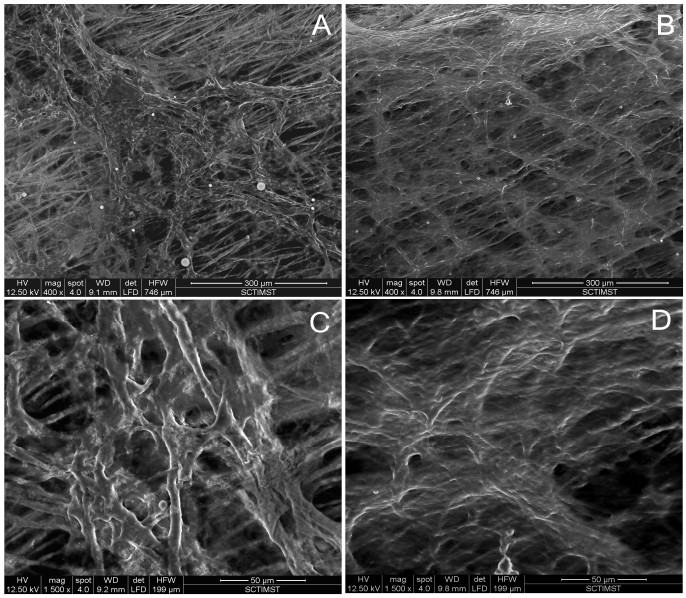

Figure 63: ESEM images of EC seeded scaffolds after 3 days culture: A & C represent ES scaffold and **B & D** represent ES-SNP scaffold; [Scale bar (A-B) = 300 µm & (C-D) = 50 µm]

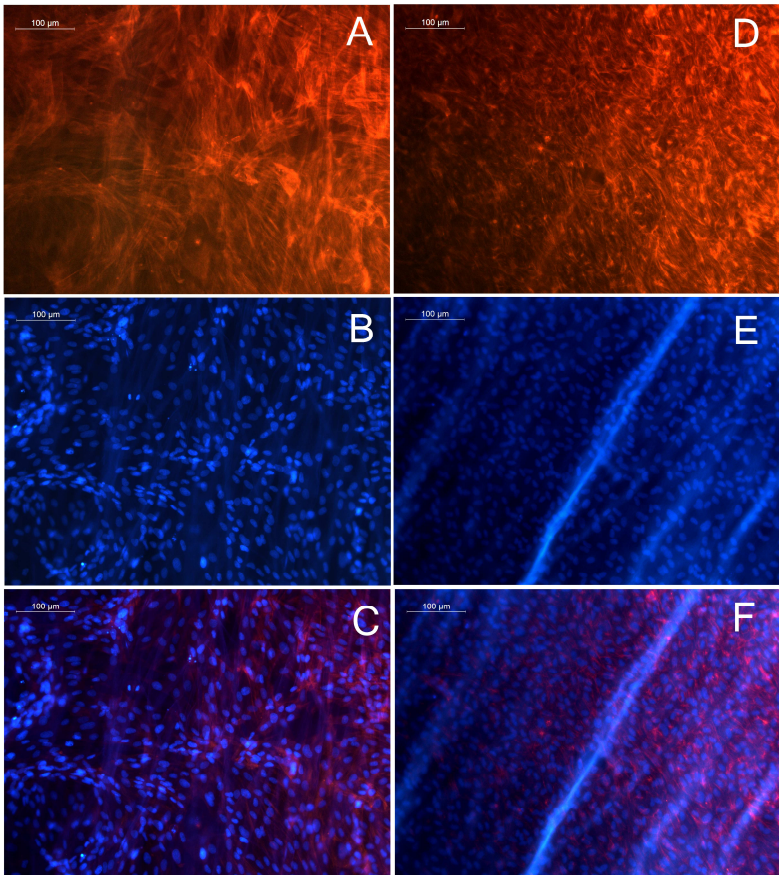

Figure 64: Fluorescent microscopic images of endothelial cells grown on electrospun scaffolds for 5 days: A–C & D–F images correspond to ES and ES-SNP scaffolds respectively; **A & D** are actin stained; **B & E** are nuclei stained and **C & F** are merged images (scale bar = 100 µm)

4.5. Design and evaluation of an antimicrobial bi-layered scaffold

The main objective in this section was to evaluate the hypothesised design strategy of a bi-layered scaffold with pore size gradient and antimicrobial property. The scaffolds whose properties were studied include SC, SC-SNP, ES and ES-SNP. The results are given in Table 7. The physico-chemical properties of bi-layered construct were also evaluated for their suitability for blood vessel applications.

Scaffold properties	**Solvent cast scaffolds**		**Electrospun scaffolds**	
	SC	**SC-SNP**	ES	**ES-SNP**
Pore size (µm)	12-24 (88%)	12-24 (89%)	12-60 (92%)	12-36 (98%)
Porosity (%)	~77	~79	~88	~82
Tensile Strength (MPa)	~3.8	~3.6	~3.1	~2.6
Elasticity (%)	~200	~180	~830	~310
Suture retention (N)	~0.62	~0.5	~2.2	~0.6
Burst strength (mmHg)	~450	~432	~5545	~476
Surface roughness (nm)	198.81	115.47	---	1268
Surface texture	Smooth	Smooth	More fibrous	Less Fibrous
EC growth	Uniform	Uniform	Non-uniform	Uniform

Table 7: Overall properties of scaffold systems based on solvent casting and electrospinning

4.5.1. Bi-layered scaffold construction

Tubular bi-layered scaffolds of 4 mm inner diameter and 70 mm length were successfully fabricated by combining SCPL and electrospinning techniques [Figure 65A]. The design strategy for developing an antimicrobial BS scaffold was tested by comparing properties of scaffold systems. The luminal layer of BS scaffold was constituted by SC-SNP layer which possessed spherical pore morphology as shown

in Figure 65B and abluminal layer fabricated as ES scaffold possessed highly porous fibrous mats [Figure 65C]. The construction of the graft was evidenced from the two dimensional slice images [Figures 66A,E&I]. The overall wall thickness of the construct was found to be ~450 µm.

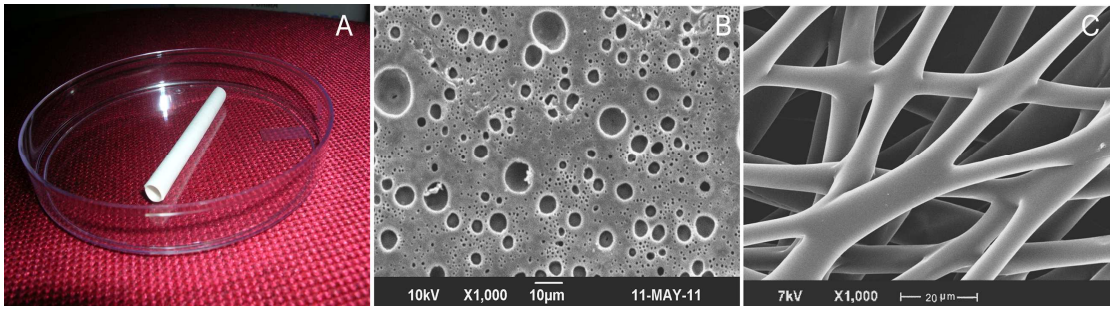

Figure 65: Macroscopic and microarchitecture of bi-layered scaffold: A, Photograph of BS scaffold, **B & C** are SEM images of luminal and abluminal layer of scaffold

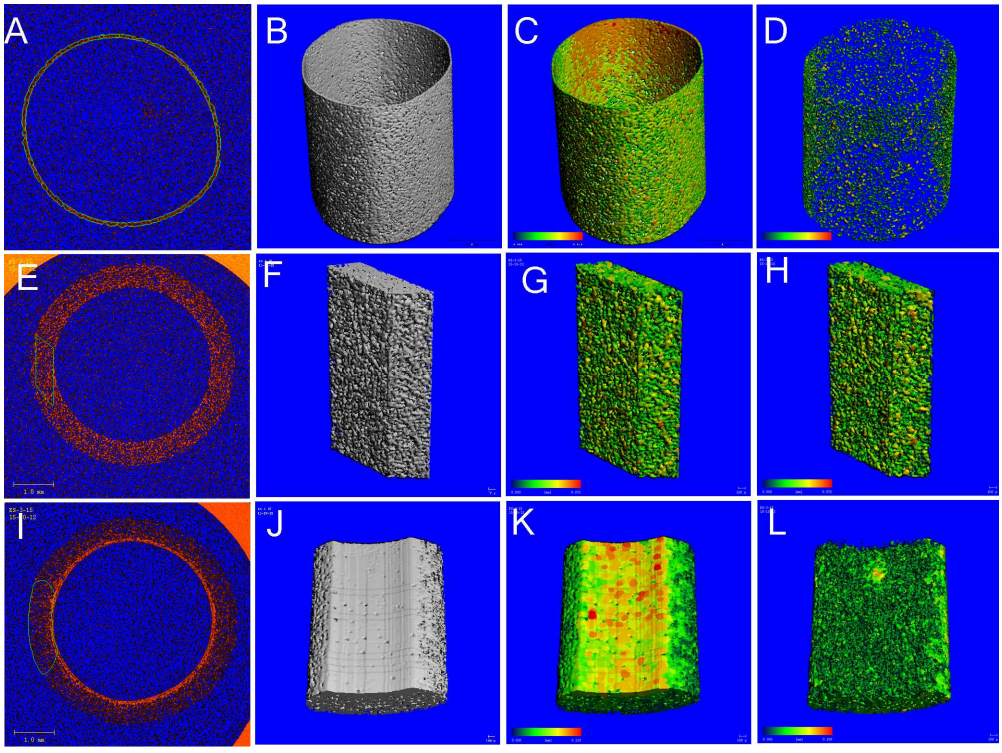

Figure 66: Micro-CT images of bi-layered scaffold: A–D represents SC-SNP; **D–H** represents ES and **I–L** represents BS scaffolds; **A, E & I** are two dimensional slice images; **B, F & J** are three dimensional images; **C, G & K** are colour coded images showing the density distribution and **D, H & L** are inverted images showing porosity distribution within the scaffold

4.5.2. Evaluation porosity characteristics

From micro-CT analysis, it could be seen that a gradient in pore size and porosity were present within the tubular BS wall. The inner layer was found to possess the majority of pores (~89 %) in 12-24 µm range and the outer layer had much broader pores, which lay in 12-60 µm size range [Figure 67]. The overall pore volumes present in luminal and abluminal layers were ~79 % and ~88 % respectively.

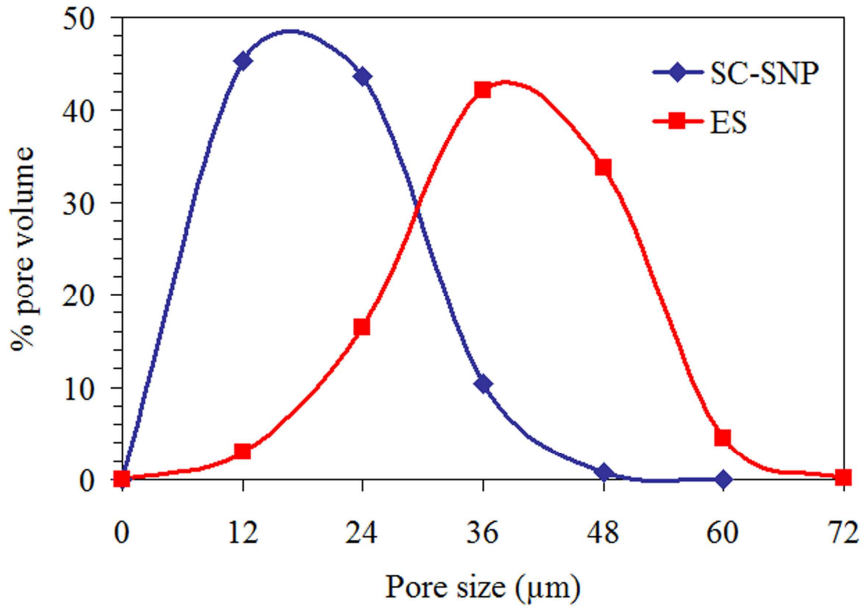

Figure 67: Histogram representing pore size distribution at luminal and abluminal layers of BS scaffold: measurement was done using three samples for each scaffold and histogram plotted

4.5.3. Evaluation of mechanical properties

From micro-CT analysis, it could be seen that a gradient in pore size and porosity were present within the tubular BS wall. The inner layer was found to possess the majority of pores (~89 %) in 12-24 µm range and the outer layer had much broader pores, which lay in 12-60 µm size range [Figure 67]. The overall pore volumes present in luminal and abluminal layers were ~79 % and ~88 % respectively.

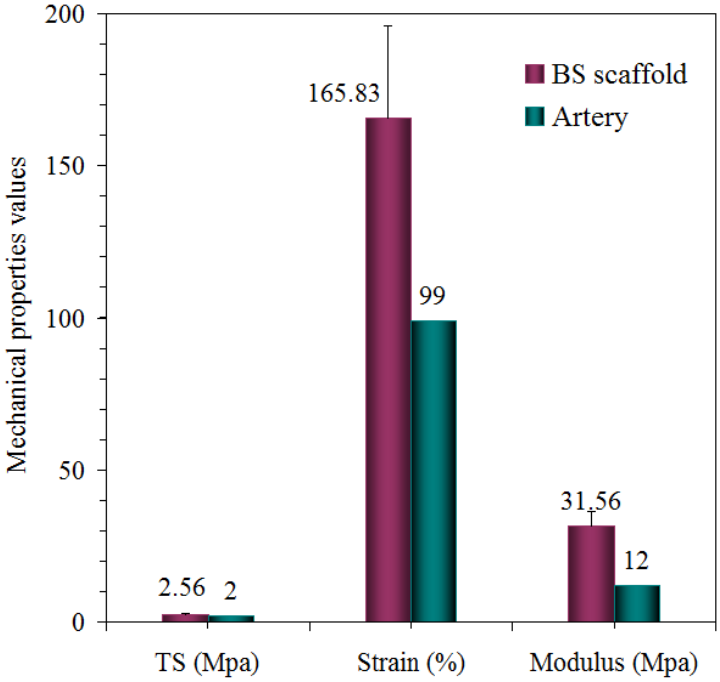

Figure 68: Tensile properties of BS scaffold compared with that of native artery: Six to eight measurements were taken and results are expressed as mean ± SD

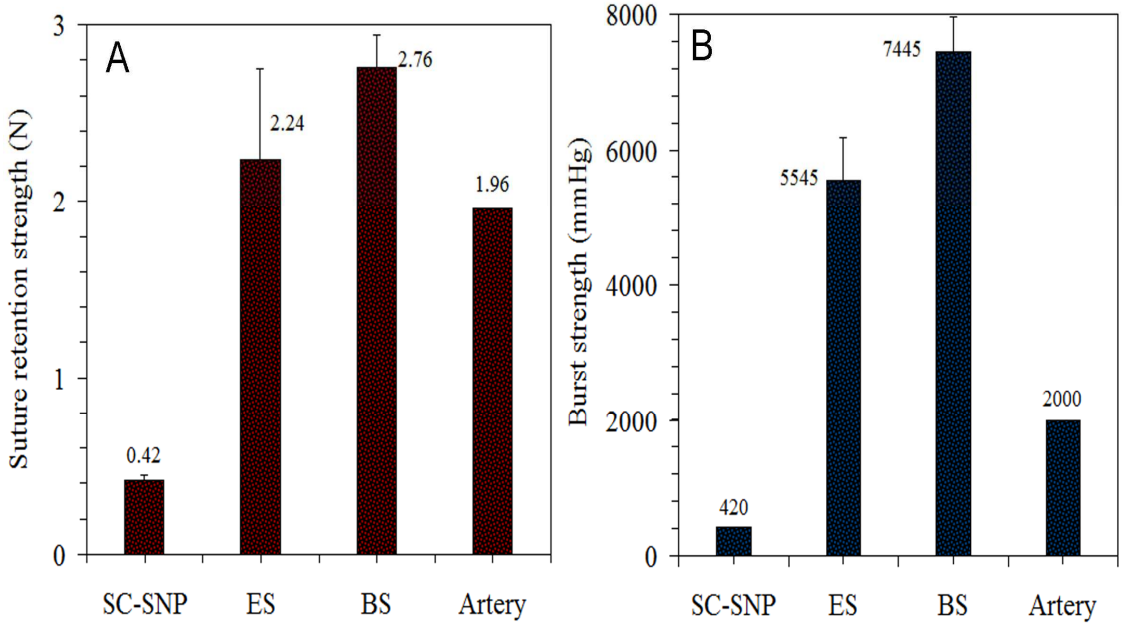

Figure 69: Mechanical properties of BS scaffold compared with that of native artery and individual layers: A, suture retention strength and **B,** burst strength; Six to eight measurements were taken and results are expressed as mean ± SD

4.5.4. Antimicrobial activity of scaffolds

Antimicrobial activity of SNP incorporated lumen was demonstrated using the standard agar diffusion method [Figure 70]. The clear zone around the samples represented the zone of inhibition which was found to be 16 mm for *Staphylococcus aureus* and 12 mm for *Escherichia coli*. Control (Gentamycin; 10 µg) exhibited 32 mm and 24 mm clear zone against the respective bacterial strains while bare SC scaffolds were found to be devoid of any clear zone.

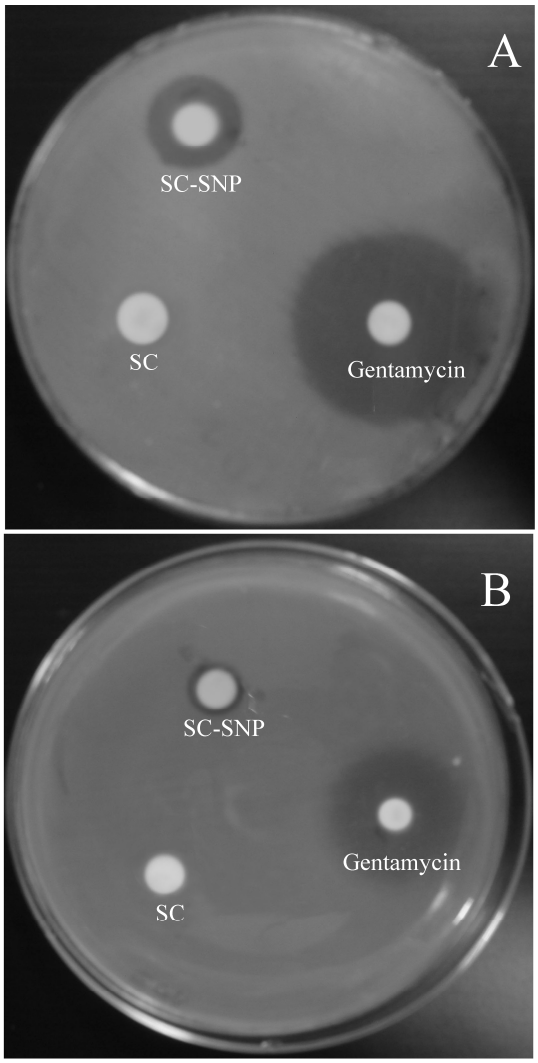

Figure 70: Representative images showing antimicrobial activity of SNP incorporated scaffolds: (A) *Staphylococcus aureus* and (B) *Escherichia Coli*

4.5.5. Growth of EC and SMC on BS scaffold

Endothelial and smooth muscle cells were differentiated from PBMNCs isolated from rabbit blood. EC and SMC were characterized by `cobblestone' morphology [Figure 70A] and `hill and valley' structure [Figure 70B]. After co-culturing these cells on BS scaffolds in a perfusion bioreactor, it was seen that EC aligned along the direction of flow [Figure 71A] whereas SMC grew on the fibrous abluminal layer [Figure 71B].

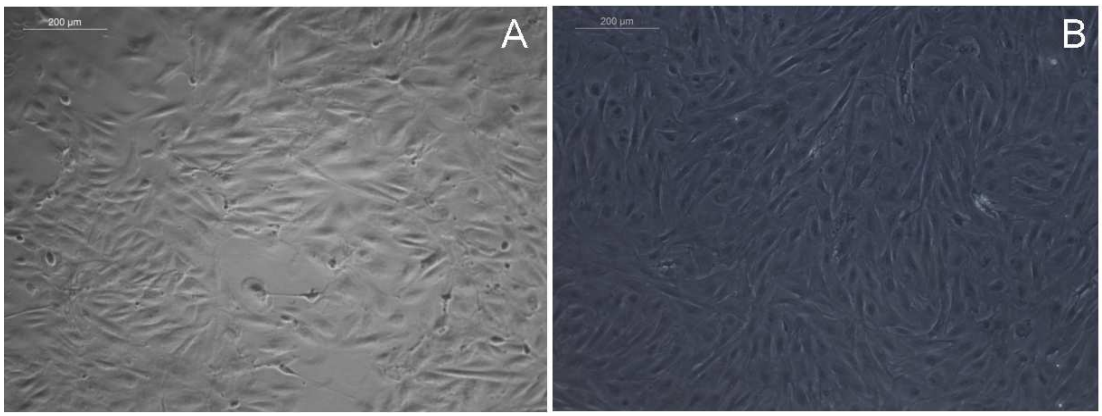

Figure 71: Microscopic images showing morphology of rabbit vascular cells: A, endothelial cells and **B,** smooth muscle cells

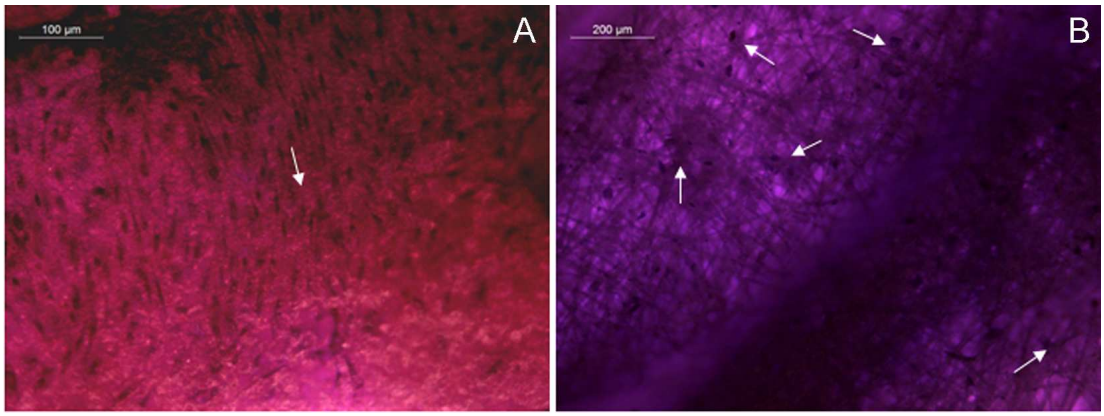

Figure 72: Microscopic images demonstrating the growth of cells on BS scaffold after bioreactor culture: A, EC on luminal layer and **B,** SMC on abluminal layer

CHAPTER 5

DISCUSSION

Chapter 5 includes the discussion and interpretation of the study results as detailed in the previous chapter. The major findings of this study are correlated with published literature in the relevant field and interpretation made wherever possible. The limitations of the study have been identified and future prospects are outlined.

5.1. Fabrication of SC scaffold and optimization of properties

The polymer matrix (PCL) and porogen (PEG) chosen for the study are both FDA approved biocompatible polymers (Ghoroghchian *et al*., 2006, Woodward *et al*., 1985). Since total degradation of PCL requires longer time period (>24months), it has been recommended for long term implantation applications such as vascular grafts (Valence *et al*., 2012). PCL also possesses good mechanical strength which plays a crucial role in the functioning of a small diameter graft. Commonly used porogens like sodium chloride have limitations such as encapsulation by hydrophobic polymer which causes incomplete removal of porogens from the polymer matrix. Use of PEG as a porogen in PCL scaffolds has already been reported earlier by our group (Pankajakshan *et al*., 2008). The hydrophilic character of PEG allows leaching of porogen from the hydrophobic PCL matrix easily while immersed in water resulting in the formation of a highly porous matrix devoid of porogen. Since concentration and molecular weight of PEG can influence the properties of solvent cast scaffolds, this study was conducted to elucidate this.

5.1.1. Effect of PEG concentration on scaffold properties

It was demonstrated that SCPL technique could be successfully used to prepare PCL conduits on stainless steel mandrels of 4 mm inner diameter and 80 mm length. While the casting process is similar to the dip coating process, the film thickness is expected to be directly proportional to the viscosity and concentration of the polymer solution employed (Uchida *et al*., 2008, Yimsiri P & Mackley, 2006). In tune with the reported observation (Wan *et al*., 2001), increasing PEG content in PCL system (4:1 to 4:4 ratios) is found to improve scaffold wall thickness proportionate to solution viscosity. Wan *et al* has reported that at high solution viscosity, there is the possibility of film imperfections such as waves and furrows to occur whereas low viscosity could result in excessive sagging of the dip coating solution (Wan *et al*., 2001). Concentration optimization is essential to obtain uniform downward flow of the coating solution over a mandrel under gravity. In the present study, PCL solutions with 4:4 PCL:PEG ratio is found to provide optimal viscosity for fabricating conduits with better thickness and tubular consistency. At lower concentrations of PEG (4:3, 4:2 and 4:1) wall thicknesses of tubular scaffolds are non-uniform when compared with scaffolds of 4:4 PCL-PEG ratio [Table 5].

The successive increase in porosity of PCL scaffolds with incremental PEG content is consistent with earlier reports that scaffold porosity is proportional to porogen concentration (Yu *et al*., 2008). Since interconnected porosity is very difficult to achieve through the SCPL method, many tissue engineering efforts modified this method by combining it with gas foaming (Kim *et al*., 2006) and phase separation (Cai *et al*., 2002) during fabrication of scaffolds. It was previously

observed that when SCPL is combined with salt fusion, PLGA scaffolds with well interconnected pores and 98 % porosity could be achieved (Murphy *et al.,* 2002). In the present study, it was observed that PEG loading in PCL at 4:3 and 4:4 concentrations introduces pore interconnectivity in PCL matrix using simple SCPL technique [Figures 19(C-D) & 20(C-D)]. This might be due to proper dispersion of both components at higher PCL-PEG ratios resulting in uniform polymer-porogen mixture. In PEG8000 containing scaffolds, rise in porogen concentration resulted in narrowing of pore size distribution whereas the effect is reversed in case of scaffolds with PEG3400 which is accompanied by the appearance of larger pores [Figures 19, 20 & 21].

Since hydrophilicity greatly depends on the surface architecture of the scaffold, nanofibrous PCL is reported to have contact angle greater than 100^{o} (Nguyen *et al*., 2013) while films show contact angle values below 100^{o} (Vance *et al*., 2004). In this study, we found that porous scaffolds have hydrophilic surfaces with contact angle < 80^{o}. Since hydrophilicity of the scaffolds is inversely correlated to their surface roughness (Martins *et al*., 2009), lower contact angle values of scaffolds with PEG3400 may be attributed to their better surface smoothness compared to scaffolds with PEG8000. Low molecular weight of PEG3400 may be instrumental in enhancing proper miscibility of the polymer-porogen mixture leading to better processing capacity. Investigations on the effect of the solvent casting process on crystalline properties of scaffolds revealed that slow solvent evaporation process affects semi-crystalline value (Barbanti *et al*., 2008) for bare PCL (58 %) which supports the observations of Tang *et al* that solvent evaporation allows

nucleation and formation of crystallites in PCL which in turn increases the crystalline nature of scaffold after solvent casting (Tang *et al*., 2004). Barbanti *et al* have shown that crystallinity of PCL reaches upto 62 % in solvent casting with sodium citrate porogens (Barbanti *et al*., 2008). In this study also, the crystallinity of solvent cast PCL scaffolds tends to lie in the same range.

Tensile strength (TS) values are found to be slightly lower for all scaffold systems containing PEG8000 compared to scaffolds with PEG3400. Narrower pore size distribution can be accounted by relatively higher TS values of scaffolds containing PEG3400 compared to those with PEG8000. TS of scaffold is found to reduce with successive PEG addition, though the change is statistically insignificant (p value < 0.05). Studies on electrospun PCL scaffolds also showed the dependence of porosity on TS in a similar manner where mechanical properties are found inversely related to scaffold porosity (Yu *et al*., 2008). Earlier work by Dorati *et al* has been reported as to how the physico-chemical properties of scaffold were affected by porogen incorporation when fabricating scaffolds using SCPL. They constructed solvent cast PLGA scaffolds using sucrose and salt as porogens and found that each porogen had a distinct influence on porosity characteristics, compressive strength and degradation properties of scaffolds (Dorati *et al*., 2010). We have attempted to modify the properties of tubular PCL scaffolds by varying porogen concentration for blood vessel applications using a porogen with different molecular weights.

Scaffolds with 4:4 PCL/PEG ratio (SC4 & SC8) which possess better wall thickness and conformability, high porosity and hydrophilic characteristics along

with required mechanical strength were chosen for endothelial cell culture studies. These scaffolds were further modified with bio-mimetic fibrin for improving cell-scaffold interaction. Previous studies have shown that fibrin composite matrix coating enhanced the vascular tissue generation with ECM deposition (Pankajakshan & Krishnan, 2009). The present study has shown that the topography of the scaffold lumen is found suitable for good endothelial cell coverage. The cells tend to grow across the pores and form a continuous monolayer after 3 days of static culture.

5.1.2. Influence of PEG molecular weight on scaffold degradation

The effect of PEG molecular weight on *in vitro* degradation characteristics of solvent cast PCL scaffolds (SC4 and SC8) has been studied and they are found to affect the pore size characteristics. It is found that pore size varies with porogen molecular weight. Usually in SCPL methodology, scaffold pore size is mainly determined by porogen size (Lee *et al*., 2011). The effect of porogen molecular weight upon pore size of solvent cast scaffolds has not been systematically investigated.

The pore size histogram [Figure 29] shows pore size distribution of both SC4 and SC8 scaffolds which has a prominent unimodal curve with a slight bimodal tendency (skewed right). It is clear that pore size distribution of both scaffolds do not show drastic variation after six months degradation in PBS. But in case of SC4 scaffold, the curve tends to become more bimodal after degradation accompanied by an increase in the percentage of larger pores (~10 % increase in 24-48 μm pore size and only ~9 % increase for pore size of < 12 μm). However, SC8 scaffold does not show this behavior, where degradation tends to increase pores with < 24 μm size by about 20 %. Considerable increase of pores of larger size was not noticed and the

curve remained narrower compared to that of SC4 after degradation for 6 months. This observation indicates that SC8 scaffold with narrower pore size distribution maintains its morphological features during the degradation compared to SC4. Even though, the percentage of pores (< 24 μm) increases for SC8 compared to SC4 as a result of degradation, the pore size distribution tends to remain narrower for SC8 scaffold. Polymer to porogen ratio (4:4) was the same for both scaffolds, but the pore volume of SC4 is found to be higher compared to SC8 (p value < 0.05).

Scaffold (SC8) with smaller pore size (< 24 μm) has demonstrated more endothelial cell attachment, collagen and elastin deposition after 30 days of dynamic culture (Mathews *et al*., 2012). The enhancement of the pore percentage in the same preferred range during degradation is not found to affect the morphology of the SC8 scaffold and may not affect the cell functionality when implanted *in vivo*, but is expected to provide more space for tissue in-growth and ECM deposition. Thickness distribution images show that both scaffolds have uniform wall thickness [Figure 30]. From the histogram, it is clear that the curve has shifted more towards the lower thickness range for SC4 compared to SC8 scaffold after 6 months. The enhancement of pore size with decreased wall thickness can be regarded as an indication of enhanced degradation rate of SC4 compared to SC8 scaffold.

Tensile and suture retention strength of SC8 scaffold is found to be superior to SC4 scaffold (p value < 0.05) and the mechanical properties are found to be dependent on scaffold pore size before degradation. However, changes in tensile and suture retention strength after 6 months degradation are not found significant for SC8 scaffold (p value > 0.05) compared to SC4 (p value < 0.05) which shows

deterioration in properties (Figure 22). This behaviour of SC4 and SC8 scaffolds may be attributed due to the changes in pore morphology during degradation. In the case of SC4, formation of ~10 % larger pores (24-48 µm) may have facilitated anisotropy in pore distribution throughout the scaffold wall. This results in reduction of mechanical strength whereas in SC8 scaffold uniform distribution of pores [< 24 µm] is evidently supported by SEM and micro-CT data resulting only in insignificant loss in strength (p value > 0.05).

Mass loss and molecular weight loss of the scaffolds indicate that they degrade by bulk degradation kinetics as reported for PCL (Lam *et al*., 2007). Degradation happens by polymer chain cleavage resulting in reduction of molecular weight; though slow diffusion of degradation by-products results in minor weight loss. The degree of initial mass loss of scaffolds compared to molecular weight loss is lower and further mass loss is expected to occur only in the advanced period of degradation (Lam *et al*., 2008). While both scaffolds show negligible weight loss, SC4 scaffold show significant molecular weight loss compared to SC8 scaffold, which may be an indication of the higher degradation rate of SC4. Therefore, SC8 scaffold which exhibited better retention in porosity characteristics and mechanical properties after six months degradation was chosen for further studies.

5.2. Solvent cast scaffold properties after SNP incorporation

Poly (ethylene glycol) protected SNP was synthesized and characterized in the laboratory. Several studies have shown that poly(N-vinylpyrrolidone) (PVP), poly(acrylonitrile) (PAN) and cellulose acetate (CA) can serve as protecting agents during silver nanoparticle synthesis (Yang *et al*., 2003, Son *et al*., 2006, Jin *et al*.,

2005). Mandal *et al* reported the preparation of silver nanoparticles by capping with PEG/Triton X100 system (Mandal *et al*., 2012). In the present study, we found that PEG not only acts as protecting agent for silver, but also improves the miscibility of nanoparticle solution with the hydrophobic poly (caprolactone) matrix.

Silver nanoparticles could be incorporated successfully into the solvent cast SC8 scaffold system (denoted as SC-SNP). SC-SNP scaffold is found to demonstrate a macroscopic appearance similar to that of the bare scaffold (denoted as SC). SEM images demonstrated that SNP incorporation does not result in significant alteration in scaffold microstructure. Inverted images exhibit the interconnected porosity within scaffolds. The pore size histogram shows that majority of the pores present in both scaffolds lie between 12-24 µm [Figure 36]. As a result of SNP incorporation, ~24 % of pores < 12 µm shifted to 12-24 µm range. The slight bimodal tendency of the pore size histogram of SC scaffold is found to diminish and change to a unimodal distribution. This may be due to the presence of PEG mixture (200 & 3400) which was integrated into the PCL matrix as part of SNP solution, which in turn may have resulted in slight variation in pore size distribution of SC-SNP scaffold compared to that of SC.

Nanoparticles are found to be distributed uniformly throughout the scaffold which exhibited an initial burst release of 15 µg during first 24 hrs of immersion. Thereafter a sustained release is observed where > 50 % of SNPs got released from the solvent cast matrix within 5 days of immersion. It is expected that further SNP release may take place during the advanced periods of immersion. Presence of elemental silver at high concentrations can induce cytotoxic effects on cells

(Madhavan *et al*., 2011). The preliminary biocompatibility evaluation shows that SNP scaffolds are cyto- and hemo- compatible and comparable with that of bare SC scaffold. Moreover, fibrin coated SC-SNP scaffold supported good endothelial cell coverage on the scaffold surface and the cells form a monolayer after 3 days of static culture.

On the whole, the mechanical properties of solvent cast scaffolds show reduction after SNP incorporation. Still, physical properties such as tensile strength, elasticity and modulus for both scaffolds are found to be suitable for blood vessel tissue engineering applications. However, suture retention and burst strength values are found not matching that of native blood vessels. Analysis of the dimensional parameters of scaffold and sheep artery shows that both of them possess comparable inner diameters (~4 mm). However, the wall thickness of solvent cast scaffold is found to be very low (~80 µm) in comparison with that of sheep artery (~750 µm). Human artery and sephenous vein have been reported as having wall thicknesses of 350-750 µm and 250 µm respectively (L'Heureux *et al*., 2006). Moreover, the seeding and culture of smooth muscle cells on the abluminal side of scaffold is found to be difficult due to limited wall thickness. The scaffolds with comparable wall thickness may provide more space for SMC proliferation and ECM deposition to generate a mechanically stable graft. Further work on this platform showed that it is unable to improve the tubular wall thickness better than this limiting value, which is regarded as the drawback of SCPL methodology. This is the reason for choosing to modify the solvent cast scaffold by improving the wall thickness. This in turn was

expected to facilitate the suture retention strength, burst strength and handling characteristics of the graft.

5.3. Optimization of electrospun scaffold properties

Fibrous tubular scaffolds were fabricated by varying the flow rate of electrospinning while optimizing the parameters such as collector to needle distance, voltage and mandrel rotation speed. The concentration and spinning flow rate are reported to influence the fiber diameter of electrospun scaffolds (Solimann *et al*., 2011). In the present study, the concentration of polymer solution has been optimized to get uniform fibers without any bead formation. The variation of micro-structural parameters and mechanical properties of electrospun scaffolds have been studied with respect to flow rate of electrospinning.

Analysis of pore size characteristics have shown that the fibrous matrices possess much broader pore size distribution (majority of the pores are of 12-60 µm size) compared to solvent cast scaffolds. Increase in flow rate has been reported to enhance the fiber diameter which in turn can increase scaffold pore size (Zong *et al.*, 2002, Liu *et al*., 2009). However, the current study shows that variation of flow rate from 1 to 5 ml/hr has not altered the pore size of electrospun scaffolds significantly. The thickness of the tubular scaffold shows significant increase with flow rate. Increasing flow rate may have caused enhancement of the fiber density at the Taylor cone resulting in alteration of fiber diameter and thereby maintaining similar scaffold pore size characteristics.

The electrospun matrices are found to show superior tensile properties compared to those of the native vessel. The uniformity and handling characteristics of ES-3 scaffold is found to be better than those of ES-1 and ES-5. Burst strength and suture retention properties of ES-3 scaffold are found to be superior to those of solvent cast scaffolds and native artery. ES-3 has demonstrated significant reduction in molecular weight of scaffolds after one year of degradation. Since the electrospun matrices are made up of much higher molecular weight PCL (80000) compared to solvent cast scaffolds (PCL 42500), the mass loss is found to be negligible compared to molecular weight reduction. This suggests that electrospun matrices also follow bulk degradation kinetics similar to solvent cast scaffolds as reported for PCL scaffolds (Lam *et al*., 2007). Degradation is found to significantly reduce tensile strength, while maintaining the mechanical integrity necessary for blood vessel applications even after one year of degradation.

Several reports have shown that nanofibrous matrices enhance cell adhesion and proliferation potentials better than microfiber counter parts (Thapa *et al*., 2003, Kim & Kim, 2007, Liu *et al*., 2009). Recent studies have shown that the relationship between fiber diameter and cellular interactions to be much more complex especially at a micrometer scale (Thapa *et al*., 2003, Pham *et al*., 2006). Reports have suggested that smaller pore size associated with nanofibrous scaffolds may be instrumental in restricting the cellular infiltration and growth into the scaffold structure. However this is facilitated by the large pore size of microfiber scaffolds (Pham *et al*., 2006, Chen *et al*., 2007, Balguid *et al*., 2009). Over and above this, the fiber diameter can influence the mechanical as well as degradation characteristics of electrospun

scaffolds. Published literature indicates that microfibers possess better mechanical properties and stable degradation characteristics than nanofibrous matrices (Soliman *et al*., 2007, Shum & Mak, 2003). In the present study, electrospun PCL matrices have been designed with fibers in the micrometer range. This electrospun matrix is found to possess appropriate mechanical properties and stable degradation characteristics for blood vessel tissue engineering.

5.4. Electrospun scaffold properties after SNP incorporation

Silver nanoparticles were immobilized successfully into the fibrous matrix using electrospinning technique. The efficacy of imparting antimicrobial activity into PLLA (Xu *et al*., 2006), PLGA (Fortunati *et al*., 2011) and PCL (Nirmala *et al*., 2012) has been reported earlier for many biomedical applications. However the effect of the metal particle solution on the architectural properties of the fiber mat has not been fully elucidated by earlier studies. When PCL scaffold was fabricated by adding silver loaded zirconium phosphate nanoparticles for wound dressing applications, the fiber diameter distribution was found to shift towards larger values (Duan *et al*., 2007). This was explained as being due to the enhancement in viscosity of electrospinning solution by the addition of nanoparticles. Later, Jia *et al* observed that the fiber diameter gradually reduced with nanoparticle content while fabricating ultrafine PCL matrices containing poly(vinyl pyrrolidone) stabilized silver nanoparticles (Jia *et al*., 2011). They observed that polymer solution conductivity increases as a direct function of silver content, which in turn reduced the fiber diameter. Studies on poly-(3-hydroxybutyrate-co-3-hydroxyvalerate) (PHBV) electrospun scaffolds containing silver nanoparticles up to 1 % loading demonstrated

that the fiber morphology of PHBV-SNP scaffolds was comparable to that of bare PHBV scaffolds (Xing *et al*., 2010). However the average fiber diameter slightly decreased from 770 ± 40 nm to 630 ± 20 nm.

In the present study, the addition of a small quantity of SNP solution (0.1 %) into PCL/DCM system is found to cause appreciable changes in electrospun fiber diameter morphology. Since increase in solution conductivity has been reported proportional to silver content in the polymer solution (Ohkawa *et al*., 2006), SNP addition into PCL/DCM system was expected to make a significant impact on the electrospinning process of PCL scaffolds. Increased conductivity of SNP-PCL solution may have resulted in stretching of ES-SNP fibers towards the collector mandrel with much greater force compared to bare PCL solution. Furthermore, accumulation of charges within the polymer jet can lead to an increase in the alignment of polymer chains within the fibers (Zhao *et al*., 2004). As a result, the crystalline peaks corresponding to PCL in ES-SNP scaffold are found to enhance with respect to E-1. Besides, PEG is reported to have a plasticizing effect on high molecular weight polymers (Lim *et al*., 2003), as a result of which PCL solution viscosity might have reduced after PEG-SNP addition. The enhanced conductivity along with the reduced solution viscosity of SNP-PCL solution may have contributed to significant decrease in the fiber diameter of ES-SNP scaffolds, which in turn reduced their wall thickness.

The smaller fiber diameter may have led to the shift in scaffold pore size distribution to lower range after SNP incorporation which is concordant with the previous studies that pore size of electrospun scaffolds can increase with fiber

diameter (Eichhorn & Sampson, 2005). Contact angle studies have shown the hydrophobic nature of scaffolds as reported earlier for electrospun PCL scaffolds (Yan *et al*., 2013). No distinct variation is observed in the contact angle values of scaffold before and after SNP incorporation (p value >0.05). However, fibrin modification is found to improve the surface wettability of scaffolds, which has critical role in improving the cell growth potential of synthetic polymers (Pankajakshan *et al*., 2008).

Electrospun-nanoparticle scaffold (ES-SNP) shows release of uniformly distributed SNPs in a sustained manner into the medium. It is inferred that a major portion of SNPs (69 %) could have got entrapped within the bulk of electrospun fibers. This is expected to facilitate controlled release of SNPs embedded within the electrospun fibers during the extended periods of immersion. ES-SNP scaffolds were expected to maintain the antimicrobial activity for a more prolonged period of time than that of SC-SNP scaffold. The released SNPs showed no cytotoxic effect on L929 fibroblast cells as indicated by direct contact and MTT assay. The hemo-compatible nature of fibrous matrix was found to be unaffected after SNP incorporation.

Electrospun matrices with and without SNP integration have demonstrated distinct differences in EC growth. The lower pore size distribution of ES-SNP is (12-36 µm) found suitable for EC growth which confirms our earlier observation on solvent cast scaffolds. In addition, the matrix with smaller ES-SNP fibers (~810 nm diameter) may have higher surface area with more cell binding sites compared to those with larger ES fibers (~6340 nm diameter). In an earlier study, Kwon *et al* also

observed that Human Umbilical Cord Endothelial cells (HUVEC) were well attached and showed better proliferation on poly(L-lactide-co-ε-caprolactone) (PLCL) electrospun scaffolds with average fiber diameters of 300 nm and 1200 nm compared to those with 7000 nm in diameter (Kwon *et al*., 2005). Properties such as strength, elongation and modulus tend to show variation for ES-SNP compared to ES (p value < 0.05). However, both scaffolds are found to possess superior tensile properties compared to native artery though lower suture retention and burst strength values are noticed SNP incorporation. The lowering of mechanical properties can be correlated to the lower fiber diameter of ES-SNP since mechanical properties are stated to facilitate the increase in electrospun fiber diameter (Hajiali *et al*., 2011).

5.5. Design and evaluation of an antimicrobial bi-layered scaffold

While comparing the properties of four scaffold systems (Table 7), it can be seen that SC, SC-SNP, ES-SNP scaffolds possess favourable pore size distribution (> 85 % pores within 12-24 µm size) to facilitate good endothelialization in *in vitro* conditions (Sections 4.1.1.5, 4.2.4 & 4.4.7). ES scaffold is found to have better tensile strength, elasticity, suture retention and burst strength than other scaffold systems with broader pore size distribution (12-60 µm size). In order to derive a design strategy for fabricating an antimicrobial bi-layered scaffold with pore size gradient and required mechanical properties, SC-SNP and ES-SNP scaffolds were considered for constructing the luminal layer while ES was chosen for the abluminal layer. Since surface smoothness can facilitate the hemo-compatibility of grafts (Klee & Hocker, 1999), the surface roughness parameter of SC-SNP and ES-SNP were also

compared; SC-SNP layer having smooth surfaces was further chosen for constructing the graft lumen.

Bi-layered graft (BS) was thus fabricated by combining SCPL and electrospinning techniques. Micro-CT evaluation has shown that BS scaffold is composed of comparably thinner solvent cast lumen (~80 µm) surrounded by thicker, highly porous fibrous ablumen [Figures 66(A, E & I)]. It is established that a pore size gradient and optimum porosity exist across the BS scaffold. While narrower pore size distribution of luminal layer is expected to facilitate endothelization, lower porosity and pore size of SC-SNP layer may restrict the growth of SMCs into the inner side of the graft. The proliferation of SMCs into the graft lumen has been considered as a major cause of intimal hyperplasia, a major failure mode of vascular grafts (Geary *et al*., 1994, Chan-Park *et al*., 2009,). Evaluation of mechanical properties shows that tensile properties such as tensile strength, elasticity, retention and burst strength values of scaffolds are better than that required for native artery. The previous investigations on degradation characteristics have demonstrated that solvent cast and electrospun layers have stable degradation kinetics which may be suitable for long-term implantable applications.

In order to generate an infection-resistant graft, SNP incorporated lumen was designed for the bi-layered construct. The antimicrobial property of the graft was evaluated against gram positive and gram negative bacteria such as Staphylococcus aureus (ATCC 25923) and Escherichia coli (ATCC 25922), which are commonly employed to study the antimicrobial activity of materials (Xu *et al*., 2006, Li *et al*., 2009). Distinct clear zones could be seen for the scaffold in both cases, where the

maximum zone of inhibition was demonstrated against S.aureus. It was also reported that silver nanoparticles can restrict the growth of other bacteria such as Pseudomonas aeroginosa, Klebsiella pneumonia, Bacillus cereus, Proteus mirabilis (Rujitanaroj, *et al*., 2008, Xing *et al*., 2010, Mandal *et al*., 2012). Lala *et al* suggested that SNPs can interact with the building elements of bacterial membrane which leads to structural changes, degradation and finally to bacterial death (Lala *et al*., 2007).

Significant progress has been made in recent years in improving the differentiation and organization of vascular cells by exposing the construct to hemodynamic forces *in vitro* (Hoerstrup *et al*., 2001, Baguneid *et al*., 2004, Niklason *et al*., 2001). In this study, the co-culture system of EC and SMC has been demonstrated in BS scaffold using a perfusion bioreactor. In flow conditions, ECs are found to align along the direction of flow similar to native blood vessels. Malek *et al* suggested that endothelial cells experience long-term morphological changes in response to simulated culture conditions under the flow (Malek & Izumo, 1996). Endothelium undergoes a transition from a polygonal cobblestone-like structure under static conditions to a uniformly spindle-shaped aligned monolayer in the pulsatile conditions similar to its *in vivo* state. The formation of a stable and healthy endothelium on the graft lumen may facilitate the generation of a thrombus resistant bi-layered graft. Long term culture of the graft may have facilitated the growth and re-organization of SMCs with deposition of ECM components such as collagen, elastin and glycosaminoglycans which can lead to the generation of mechanically stable media on the abluminal side of the bi-layered graft.

The current study has investigated the importance of scaffold micro-structural parameters while constructing a bi-layered small diameter tissue engineered vascular graft with appropriate mechanical properties and degradation characteristics. It has demonstrated that the optimization of microstructure has a detrimental effect on the *in vitro* performance of the vascular construct. Integration of antimicrobial activity into the graft proved to be effective against a broad spectrum of microbes. An attempt to define the design strategies of a small diameter vascular scaffold with emphasis on micro-structure, macro-structure, mechanical and degradation properties and infection resistance has been the focus of this study.

5.6. Limitations of the study

In the present study, the microstructure of solvent cast graft lumen has been optimized in terms of endothelial cell growth. However the study has not delineated the influence of electrospun micro-architecture on SMC growth and deposition of ECM components such as collagen and elastin. The fabricated bi-layered scaffold is found to possess required tensile strength, elasticity and burst strength for blood vessel tissue engineering. Graft compliance is another mechanical aspect which needs to be addressed for the bi-layered grafts. In addition, the present study is limited to the *in vitro* degradation of the scaffold which may further be influenced by the presence of enzymes and the hemodynamic environment when implanted *in vivo*.

5.7. Future perspectives

The influence of pore size on SMC growth and ECM deposition should be elucidated under perfusion flow culture conditions. As graft compliance can be enhanced by the

deposition of elastin on the blood vessel wall, it should be evaluated as a function of SMC growth and ECM deposition. The correlation of mechanical properties of the graft in terms of scaffold degradation and ECM deposition may be advantageous to predict the performance of the graft. Finally the pre-conditioned grafts need to be evaluated in animal models to understand the performance of the bi-layered constructs *in vivo*, by which correlation of scaffold degradation under *in vitro* and *in vivo* conditions can be made.

CHAPTER 6

SUMMARY AND CONCLUSION

6.1. Summary

Disease conditions that affect small diameter blood vessels are becoming a major concern all over the world. Conventional treatment modalities mainly employ autologous grafts or synthetic grafts for repairing occluded blood vessels and each of these types of grafts are associated with drawbacks such as limited availability and high failure rates due to thrombosis. Recent advances in vascular research have focussed on bioengineered vessels with the aid of biomaterial scaffolds and autologous vascular cells. Reports suggest that scaffolds based on both natural and synthetic polymers are suitable for vascular tissue engineering. Due to the complexities associated with small diameter vascular graft construction, none of the approaches have achieved complete success till date. Scaffold specifications play a major role in the successful construction of bioengineered grafts. It is reported that specific porosity characteristics are required for each cell type for facilitating cellular adhesion, proliferation and ECM deposition. Native blood vessel is multi-layered and cellular penetration and tissue formation at each level have specific requirements. Researchers have laid emphasis on multi-layered scaffold designs which mimic native blood vessel architecture. The mechanical properties and degradation characteristics of scaffolds may also be influenced by their microstructure. Organization of various cells in multiple interfaces can be attained by designing a gradient pore size within the scaffold wall in the case of vascular tissue generation.

Simultaneous consideration of scaffold macrostructure and microstructure, which have not been endorsed earlier, may be a better design criterion for a small diameter vascular construct.

The main focus of the present study was to design a bi-layered scaffold based on poly(ε-caprolactone) with optimized pore size gradient across the scaffold wall while satisfying the mechanical and degradation characteristics required for blood vessel application. This has been achieved by combining SCPL and electrospinning where the fabrication parameters were optimized properly. Moreover, successful development of TE construct can be influenced by microbial contamination during the *in vitro* culture periods which is another concern in vascular tissue engineering. One strategy for overcoming this difficulty is the incorporation of a broad spectrum antimicrobial agent during the scaffold fabrication which can provide the scaffold with infection resistance. Silver nanoparticles (SNP) have gained great attention in the biomedical field owing to their broad spectrum antimicrobial effect. The feasibility of SNP incorporation into solvent cast and electrospun scaffolds has been evaluated in the current study while monitoring scaffold properties before and after SNP addition.

The porogen used in this study PEG is found to be very effective as it could generate interconnected porosity within PCL matrix. The major advantage of choosing this porogen is that appropriate size could be chosen to obtain required porosity characteristics in addition to its biocompatibility and miscibility with the non-aqueous polymer solutions. Its concentration is found to influence the tubular scaffold wall properties. Optimization of PEG content was done to obtain solvent

cast scaffolds with better tubular conformability and wall thickness, required porosity characteristics and mechanical properties. Pore size distribution of these scaffolds varied with changes in the porogen molecular weight.

In tissue engineering efforts, scaffold presence is required till new tissue is generated and become functional. In the case of vascular constructs, the requirement is long term because it has to resist the hemodynamic forces. Therefore, PCL, a long degrading polymer was chosen for the study and the degradation kinetics was evaluated to ensure that the polymer would remain stable till functional tissue generation is complete. Since porosity is important for vascular tissue engineering, its effect of degradation kinetics is an important aspect of this study. The porogen size was found to be critical in determining the degradation kinetics. Silver nanoparticles were prepared, characterized and incorporated into the optimized solvent cast scaffold system. It was found that SNPs are distributed uniformly throughout the scaffold which exhibited a sustained release from the matrix. Scaffolds were found to be cyto and hemo-compatible and supported good coverage of endothelial cells. SNP incorporation did not alter the scaffold microstructure significantly, but the pore size distribution shows a slight shift from bimodal to unimodal curve. Both scaffolds are found to possess appropriate tensile properties for blood vessel applications. The lower burst and suture retention strengths of SNP incorporated scaffolds may be due to limited wall thickness. Upon comparison of sheep artery and developed scaffold using micro CT, inner diameters of both are found to be comparable.

Electrospinning protocol for scaffold fabrication was optimized. It was observed that the flow rate did not influence pore size distribution, but the tensile properties and uniformity of tubular scaffold wall were affected. The experiments were useful for standardizing the protocol to obtain the appropriate scaffold specifications. The selected scaffold matrix showed appropriate burst strength and suture retention properties prescribed for blood vessels. Only after 1 year of *in vitro* degradation, the mechanical properties of the scaffold showed a significant reduction. By this time, the tissue growth is expected to take over the vessel strength. Therefore the optimized matrix architecture is likely to be the best option for vascular tissue engineering applications.

The incorporated SNP was found to be released in a sustained manner. Therefore it is likely to prevent microbial contamination during the process of *in vitro* vascular tissue construction. SNP was found to influence the surface topography which resulted in significant alteration of fiber morphology and diameter and also resulted in narrower pore size distribution. Mechanical properties such as tensile strength, burst strength and suture retention strength were found to be dependent on fiber diameter. The crystalline nature of PCL showed enhancement after SNP incorporation due to the better dragging effect of PCL-SNP solution. Both electrospun matrices were found to have hydrophobic surfaces which became hydrophilic in nature after modifying the scaffold with fibrin bio-mimetic matrix. The *in vitro* experiment shows that incorporation of SNP does not have any toxic effects on L929 and primary endothelial cells. Endothelial cell adhesion and

proliferation are found to be pronounced in the SNP-incorporated hybrid scaffold compared to the bare scaffold.

Bi-layered scaffold design strategy has been derived by comparing the properties of the scaffold systems that were developed. BS scaffold could be successfully fabricated by combining SCPL and electrospinning techniques. Micro-structural analysis demonstrated that pore size gradient present within the scaffold wall facilitates growth of EC and SMC. Mechanical properties of scaffold such as strength, elasticity, burst strength and suture retention capability were found to be comparable to the properties of native blood vessel. Incorporation of SNP into solvent cast layer was found to impart an antimicrobial effect against a number of bacterial strains. The growth of EC and SMC on the bi-layered scaffold has been demonstrated by employing a co-culture system using a perfusion bioreactor. Endothelial cells tend to align along the direction of flow while SMCs grow on the abluminal portion of the graft. Overall the current study has looked in depth at the significance of the microstructure of an antimicrobial, bi-layered scaffold in vascular tissue engineering which still remains an unconquered challenging area.

6.2. Conclusions

The conclusions derived from the present study are as follows

1. Microstructure of solvent cast scaffolds is optimized by altering concentration and molecular weight of PEG

2. Solvent cast scaffolds fabricated with 4:4 PCL-PEG ratio possess better wall thickness, tubular consistency, high porosity, hydrophilic characteristics and optimum tensile properties for blood vessel applications
3. PEG3400 porogen incorporation resulted in optimum pore size distribution needed for vascular tissue engineering compared to scaffolds containing PEG8000
4. Scaffolds containing PEG3400 exhibit better retention in porosity and mechanical characteristics after being subjected to *in vitro* degradation upto 6 months
5. SNP incorporation does not result in significant variation of properties of solvent cast scaffolds
6. SNP incorporation does not affect the cyto or hemo-compatibility characteristics of electrospun matrix
7. Good endothelial coverage was established on both SC and SC-SNP scaffolds
8. Limited scaffold wall thickness correlates to lower suture retention strength and burst strength of the solvent cast scaffolds
9. Variation of electrospinning parameters is instrumental in generating fibrous mat
10. After SNP incorporation, electrospun scaffolds show significant alteration in the microarchitectural parameters
11. Uniform coverage of endothelial cells is obtained on the hybrid scaffolds even after SNP incorporation unlike bare scaffold
12. Silver nanoparticle incorporation altered the mechanical properties of electrospun scaffolds

13. Bi-layered scaffold with pore size gradient within the scaffold wall could be successfully developed by integrating SCPL and electrospinning
14. Bi-layered scaffold is found to have adequate mechanical properties to be used for small diameter blood vessel applications
15. Co-culture system of rabbit-derived EC and SMC within the bi-layered scaffold was demonstrated using a perfusion bioreactor.
16. Endothelial cells got aligned in the direction of flow on the graft lumen
17. The Smooth muscle cells could grow on the electrospun fibrous ablumen
18. Biologically modified bi-layered scaffold may be highly recommended for small diameter vascular graft application.

BIBLIOGRAPHY

Asahara T, Murohara T, Sullivan A, Silver M, van der Zee R, Li T, Witzenbichler B, Schatteman G, Isner JM (1997) Isolation of putative progenitor endothelial cells for angiogenesis. *Science.* 275: 964-7.

Badylak S, Liang A, Record R, Tullius R, Hodde J (1999) Endothelial cell adherence to small intestinal submucosa: An acellular bioscaffold. *Biomaterials*. 20: 2257-63.

Baguneid M, Murray D, Salacinski HJ, Fuller B, Hamilton G, Walker M, Seifalian AM (2004) Shear-stress preconditioning and tissue-engineering-based paradigms for generating arterial substitutes. *Biotechnol Appl Biochem*. 39:151-7.

Balguid A, Mol A, van Marion MH, Bank RA, Bouten CV, Baaijens FP (2009) Tailoring fiber diameter in electrospun poly(epsilon-caprolactone) scaffolds for optimal cellular infiltration in cardiovascular tissue engineering. *Tissue Eng Part A.* 15: 437-44.

Barbanti SH, Santos AR Jr, Zavaglia CA, Duek EA (2004) Porous and dense poly(L-lactic acid) and poly(D,L-lactic acid-co-glycolic acid) scaffolds: *In vitro* degradation in culture medium and osteoblasts culture. *J Mater Sci Mater Med.* 15: 1315-21.

Barbanti SH, Zavaglia CA, Duek EA (2008) Effect of salt leaching on PCL and PLGA (50/50) resorbable scaffolds. *Mat. Res*. 11: 75-80.

Benditt EP, Schwartz SM (1988) Blood vessels. In: Rubin E, Faber JL (eds) *Pathology*, JP Lippincott Publishers, Philadelphia, pp. 452-495.

Bilodeau K, Mantovani D (2006) Bioreactors for tissue engineering: focus on mechanical constraints. A comparative review. *Tissue Eng.* 12: 2367-83.

Brennan MP, Dardik A, Hibino N, Roh JD, Nelson GN, Papademitris X, Shinoka T, Breuer CK (2008) Tissue-engineered vascular grafts demonstrate evidence of growth and development when implanted in a juvenile animal model. *Ann Surg.* 248: 370-7.

Cai Q, Yang J, Bei J, Wang S (2002) A novel porous cells scaffold made of polylactide–dextran blend by combining phase-separation and particle-leaching techniques. *Biomaterials.* 23: 4483-92.

Campbell GR and Campbell JH (2007) Development of tissue engineered vascular grafts. *Curr. Pharm. Biotechnol*. 8: 43-50.

Chan-Park MB, Shen JY, Cao Y, Xiong Y, Liu Y, Rayatpisheh S, Kang GC, Greisler HP (2009) Biomimetic control of vascular smooth muscle cell morphology and phenotype for functional tissue-engineered small-diameter blood vessels. *J Biomed Mater Res A.* 88: 1104-21.

Chen G, Ushida T and Tateishi T (2002) Scaffold Design for Tissue Engineering. *Macromol. Biosci*. 2: 67-77.

Chen M, Patra PK, Warner SB, Bhowmick S (2007) Role of fiber diameter in adhesion and proliferation of nih 3t3 fibroblast on electrospun polycaprolactone scaffolds. *Tissue Eng.* 13: 579-87.

Chen VJ, Ma PX (2006) The effect of surface area on the degradation rate of nano-fibrous poly(L-lactic acid) foams. *Biomaterials.* 27: 3708-15.

Chlupac J, Filova E, Bacakova L (2009) Blood vessel replacement: 50 years of deveopment and tissue engineering paradigms in vascular surgery. *Physiol Res.* 58: S119-39.

Cunha-Reis C, TuzlaKoglu K, Baas E, Yang Y, El Haj A, Reis RL (2007) Influence of porosity and fibre diameter on the degradation of chitosan fibre-mesh scaffolds and cell adhesion. *J Mater Sci Mater Med*. 18: 195-200.

Deterling RA, Bhonslay SB (1955) An evaluation of synthetic materials and fabrics suitable for blood vessel replacement. *Surgery*. 38: 71-89

Devine C, Mccollum C (2004) The north west femoropopliteal trial participants: Heparin-bonded Dacron and polytetrafuoroethylene for femoforopoplileal bypass: five years results of a perspective randomized multi-centre clinical trial. *J Vasc Surg.* 40: 924-31.

Dorati R, Colonna C, Genta I, Modena T, Conti B (2010) Effect of porogen on physico-chemical properties and degradation performance of PLGA scaffolds, *Polym. Degrad. and Stabil*. 95, 694-701.

Dong Y, Liao S, Ngiam M, Chan CK, S Ramakrishna (2009) Degradation behaviors of electrospun resorbable polyester nanofibers. *Tissue engineering Part B.* 15: 333-51.

Duan Y, Jia J, Wang S, Yan W, Jin L, Wang Z (2007) Preparation of antimicrobial poly(ε-caprolactone) electrospun nanofibers containing silver-loaded zirconium phosphate nanoparticles. *J. Appl. Polym. Sci.* 106: 1208-14.

Eichhorn SJ, Sampson WW (2005) Statistical geometry of pores and statistics of porous nanofibrous assemblies. *J. R. Soc. Interface*. 2: 309-18.

Eldsater C, Erlandsson B, Renstad R, Albertsson A-C, Karlsson S (2000) The biodegradation of amorphous and crystalline regions in film-blown poly(e-caprolactone). *Polymer.* 41: 1297-1304.

Faries PL, Logerfo FW, Arora S, Pulling MC, Rohan DI, Campbell DR, Gibbons GW, Pomposelli FB (2000) Arm vein conduit is superior to composite prosthetic-autogenous grafts in lower extremity revascularization. *J vasc surg*. 31: 1119-27.

Fortunati E, Latterini L, Rinaldi S, Kenny JM, Armentano I (2011) PLGA/Ag nanocomposites: *In vitro* degradation study and silver ion release. *J Mater Sci Mater Med.* 22: 2735-44.

Gaudio CD, Bianco A, Folin M, Baiguera S, Grigioni M (2009) Structural characterization and cell response evaluation of electrospun PCL membranes: Micrometric versus submicrometric fibers. *J Biomed Mater Res A.* 89: 1028-39.

Geary RL, Kohler TR, Vergel S, Kirkman TR, Clowes AW (1994) Time course of flow-induced smooth muscle cell proliferation and intimal thickening in endothelialized baboon vascular grafts. *Circ Res*. 74: 14-23.

Giesche H (2006) Mercury porosimetry: A general (practical) overview. *Part. Part. Syst. Charact.* 23: 9-19.

Ghoroghchian PP, Li G, Levine DH, Davis KP, Bates FS, Hammer DA, Therien MJ (2006) Bioresorbable vesicles formed through spontaneous self-assembly of amphiphilic poly(ethylene oxide)-block-polycaprolactone. *Macromolecules.* 39: 1673-75.

Go AS, Mozaffarian D, Roger VL, Benjamin EJ, Berry JD, Borden WB, Bravata DM, Dai S, Ford ES, Fox CS, Franco S, Fullerton HJ, Gillespie C, Hailpern SM, Heit JA, Howard VJ, Huffman MD, Kissela BM, Kittner SJ, Lackland DT, Lichtman JH, Lisabeth LD, Magid D, Marcus GM, Marelli A, Matchar DB, McGuire DK, Mohler ER, Moy CS, Mussolino ME, Nichol G, Paynter NP, Schreiner PJ, Sorlie PD, Stein J, Turan TN, Virani SS, Wong ND, Woo D and Turner MB (2013) Heart disease and stroke statistics-2013 update: A report from american heart association. *Circulation.* 127: e6- e245.

Gorbet MB, Sefton MV (2004) Biomaterial-associated thrombosis: roles of coagulation factors, complement, platelets and leukocytes. *Biomaterials.* 25: 5681-703.

Gross RE, Hurwitt ES (1948) Preliminary observations on the use of human arterial grafts in the treatment of certain cardiovascular defects. *N Engl J Med*. 239: 578.

Gupta R, Guptha S, Joshi R, Xavier D (2011) Translating evidence into policy for cardiovascular disease control in India. *Health Research Policy and Systems.* 9: 1-12.

Gui L, Muto A, Chan SA, Breuer CK, Niklason LE (2009) Development of decellularized human umbilical arteries as small-diameter vascular grafts. *Tissue Eng Part A.* 15: 2665-76.

Hajiali H, Shahgasempour S, Jamal MR, Peirovi H (2011) Electrospun PGA/gelatin nanofibrous scaffolds and their potential application in vascular tissue engineering. *Int J Nanomedicine*. 6: 2133-41.

Han F, Jia X, Dai D, Yang X, Zhao J, Zhao Y, Fan Y and Yuan X (2013) Performance of a multilayered small-diameter vascular scaffold dual-loaded with VEGF and PDGF. *Biomaterials.* 34: 7302-13.

Han J, Lazarovici P, Pomerantz C, Chen X, Wei Y, Lelkes PI (2011) Co-electrospun blends of PLGA, gelatin, and elastin as potential nonthrombogenic scaffolds for vascular tissue engineering. *Biomacromolecules.* 12: 399-408.

Hasan A, Memic A, Annabi N, Hossain M, Paul A, Dokmeci MR, Dehghani F, Khademhosseini A (2014) Electrospun scaffolds for tissue engineering of vascular grafts. *Acta Biomater*. 10: 11-25.

He W, Yong T, Teo WE, Ma Z, Ramakrishna S (2005) Fabrication and endothelialization of collagen-blended biodegradable polymer nanofibers: Potential vascular graft for blood vessel tissue engineering. *Tissue Eng*. 11: 1574-88.

Herring M, Gardner A, Glover J (1978) A single-staged technique for seeding vascular grafts with autogenous endothelium. *Surgery.* 84: 498-504.

Ho ST, Hutmacher DW (2006) A comparison of micro CT with other techniques used in the characterization of scaffolds. *Biomaterials.* 27: 1362-76.

Hoenig MR, Campbell GR, Rolfe BE, Campbell JH (2005) Tissue engineered blood vessels: alternative to autologous grafts. *Arterioscler Thromb Vasc Biol*. 25: 1128-34.

Hoerstrup SP, Zund G, Sodian R, Schnell AM, Grunenfelder J, Turina MI (2001) Tissue engineering of small caliber vascular grafts. *Eur J Cardiothorac Surg*. 20: 164-9.

Hutmacher DW (2000) Scaffolds in tissue engineering of bone and cartilage. *Biomaterials.* 21: 2529-43.

Huynh T, Abraham G, Murray J, Brockbank K, Hagen PO, Sullivan S (1999) Remodeling of an acellular collagen graft into a physiologically responsive neovessel. *Nat Biotechnol*. 17: 1083-6.

Innocente F, Mandracchia D, Pektok E, Nottelet B, Tille JC, de Valence S, Faggian G, Mazzucco A, Kalangos A, Gurny R, Moeller M, Walpoth BH (2009) Paclitaxel-eluting biodegradable synthetic vascular prostheses: A Step Towards Reduction of Neointima Formation?. *Circulation*. 120: S37-45.

Jena A, Gupta K (2003) Liquid extrusion techniques for pore structure evaluation of nonwovens. *International nonwoven journal.* 12: 45-53.

Jeong SI, Kwon JH, Lim JI, Cho SW, Jung Y, Sung WJ, Kim SH, Kim YH, Lee YM, Kim BS, Choi CY, Kim SJ (2005) Mechano-active tissue engineering of vascular smooth muscle using pulsatile perfusion bioreactors and elastic PLCL scaffolds. *Biomaterials.* 26: 1405-11.

Jia Y, Liu Q, Zhu X (2011) Preparation of ultrafine poly(ε-caprolactone) fibers containing silver nanoparticles via electrospinning method. *Advanced Materials Research.* 332*:* 1235-8.

Jin WJ, Lee HK, Jeong EH, Park WH, Youk JH (2005) Preparation of polymer nanofibers containing silver nanoparticles by using poly (N-vinylpyrrolidone). *Macromol Rapid Commun*. 26: 1903-7.

Kanda K, Matsuda T (1994) *In vitro* reconstruction of hybrid arterial media with molecular and cellular orientations. *Cell.* 3: 537-45.

Kapfer X, Meichelboeck W, Groegler FM (2006) comparison of carbon impregnated and standard ePTFE prostheses in extra-anatomical anterior tibial artery bypass: A prospective randomized multicentre study. *Eur J Vasc Endovasc Surg.* 32: 155-168.

Karageorgiou V, Kaplan D (2005) Porosity of 3D biomaterial scaffolds and osteogenesis. *Biomaterials.* 26: 5474-91.

Karande TS, Ong JL, Agrawal CM (2005) Diffusion in musculoskeletal tissue engineering scaffolds: design issues related to porosity, permeability, architecture, and nutrient mixing. *Ann Biomed Eng.* 32: 1728-43.

Kaushal S, Amiel GE, Guleserian KJ, Shapira OM, Perry T, Sutherland FW, Rabkin E, Moran AM, Schoen FJ, Atala A, Soker S, Bischoff J, Mayer JE Jr (2001) Functional small-diameter neovessels created using endothelial progenitor cells expanded *ex vivo*. *Nat Med*. 7: 1035-40.

Kim G, Kim W (2007) Highly porous 3d nanofiber scaffold using an electrospinning technique. *J Biomed Mater Res B Appl Biomater.* 81: 104-10.

Kim SS, Park MS, Jeon O, Choi CY, Kim BS (2006) Poly(lactide-co-glycolide)/hydroxyapatite composite scaffolds for bone tissue engineering. *Biomaterials*. 27: 1399-409.

Klee D, Hocker H (1999) Polymers for biomedical applications: improvement of the interface compatibility. In: Eastmond GC, Hocker H, Klee D (eds) *Biomedical Applications Polymer Blends*, Springer, New York, pp 1-57.

Koch S, Flanagan TC, Sachweh JS, Tanios F, Schnoering H, Deichmann T, Ella V, Kellomaki M, Gronloh N, Gries T, Tolba R, Schmitz-Rode T, Jockenhoevel S (2010) Fibrin-polylactide-based tissue-engineered vascular graft in the arterial circulation. *Biomaterials.* 31: 4731-9.

Konig G, McAllister TN, Dusserre N, Garrido SA, Iyican C, Marini A, Fiorillo A, Avila H, Wystrychowski W, Zagalski K, Maruszewski M, Jones AL, Cierpka L, de la Fuente LM, L'Heureux N (2009) Mechanical properties of completely autologous human tissue engineered blood vessels compared to human saphenous vein and mammary artery. *Biomaterials.* 30: 1542-50.

Kwon IK, Kidoaki S, Matsuda T (2005) Electrospun nano- to microfiber fabrics made of biodegradable copolyesters: structural characteristics, mechanical properties and cell adhesion potential. *Biomaterials*. 26: 3929-39.

Lala NL, Ramaseshan R, Bojun L, Sundarrajan S, Barhate RS, Ying-Jun L, Ramakrishna S (2007) Fabrication of nanofibers with antimicrobial functionality used as filters: protection against bacterial contaminants. *Biotechnol Bioeng*. 97: 1357-65.

Lam CX, Teoh SH, Hutmacher HW (2007) Comparison of the degradation of polycaprolactone and polycaprolactone-(β-tricalcium phosphate) scaffolds in alkaline medium, *Polym. Int.* 56: 718-28.

Lam CX, Savalani MM, Hutmacher DW (2008) Dynamics of *in vitro* polymer degradation of polycaprolactone-based scaffold: accelerated versus simulated physiological conditions. *Biomed Mater*. 3: 034108.

Lam CX, Hutmacher DW, Schantz JT, Woodruff MA, Teoh SH (2009) Evaluation of polycaprolactone scaffold degradation for 6 months *in vitro* and *in vivo*. *J Biomed Mater Res A*. 90: 906-19.

Langer R, Vacanti JP (1993) Tissue engineering. *Science*. 260: 920-926.

Lantz GC, Badylak SF, Coffey AC, Geddes LA, Blevins WE (1990) Small intestinal submucosa as a small-diameter arterial graft in the dog. *J Invest Surg*. 3: 217-27.

Lee KW, Stolz DB, Wang Y (2011) Substantial expression of mature elastin in arterial walls. *Proc Natl Acad Sci U S A*. 108: 2705-10.

Lee M, Wu BM, Dunn JC (2008) Effect of scaffold architecture and pore size on smooth muscle cell growth. *J Biomed Mater Res A*. 87:1010-6.

Leukers B, Gulkan H, Irsen SH, Milz S, Tille C, Schieker M, Seitz H (2005) Hydroxyapatite scaffolds for bone tissue engineering made by 3D printing. *J Mater Sci Mater Med*.16: 1121-4.

L'Heureux N, Paquet S, Labbe R, Germain L, Auger FA (1998) A completely biological tissue-engineered human blood vessel. *FASEB J*. 12: 47-56.

L'Heureux N, Dusserre N, Konig G, Victor B, Keire P, Wight TN, Chronos NA, Kyles AE, Gregory CR, Hoyt G, Robbins RC, McAllister TN (2006) Human tissue-engineered blood vessels for adult arterial revascularization. *Nat Med*. 12: 361-5.

L'Heureux NL, Dusserre N, Marini A, Garrido S, Fuente L, McAllister T (2007) Technology insight: the evolution of tissue engineered vascular grafts- From research to clinical practice. *Cardiovascular medicine* 7: 1119-27.

Li L, Li Y, Li J, Yao L, Mak AF, Ko F, Qin L (2009) Antibacterial properties of nanosilver PLLA fibrous membranes. *Journal of nanomaterials.* 2009: 1-5.

Liao CJ, Chen CF, Chen JH, Chiang SF, Lin YJ, Chang KY (2002) Fabrication of porous biodegradable polymer scaffolds using a solvent merging/particulate leaching method. *J Biomed Mater Res*. 59: 676-81.

Lim KY, Kim DH, Paik U, Kim SH (2003) Effect of molecular weight of polyethylene glycol on the plasticization of green sheets composed of ultrafine BaTiO3 particles and poly(vinyl butyral). *Mater. Res. Bull.* 38: 1021-32.

Lin AS, Barrows TH, Cartmell SH, Guldberg RE (2003) Microarchitectural and mechanical characterization of oriented porous polymer scaffolds. *Biomaterials.* 24: 481-9.

Liu Y, Ji Y, Ghosh K, Clark RA, Huang L, Rafailovich MH (2009) Effects of fiber orientation and diameter on the behavior of human dermal fibroblasts on electrospun PMMA scaffolds. *J Biomed Mater Res A* 90: 1092-106.

Lopez PP, Ginzberg E (2008) Vascular trauma. In: Nortan JA, Barie PS, Bollinfer RR, Chang AE, Lowry S, Mulvihill SJ, Pass HI, Thompson RW (eds), *Surgery: Basic science and clinical evidence*. Springer, New York, pp. 521-544.

Lu S, Zhang P, Sun X, Gong F, Yang S, Shen L, Huang Z, Wang C (2013) Synthetic ePTFE grafts coated with an anti-CD133 antibody-functionalized heparin/collagen multilayer with rapid *in vivo* endothelialization properties. *ACS Appl Mater Interfaces.* 5: 7360-9.

Lyman DJ, Fazzio FJ, Voorhees H, Robinson G, Albo D Jr (1978) Compliance as a factor effecting the patency of a copolyurethane vascular graft. *J Biomed Mater Res.* 12: 337-45.

Ma PX (2004) Scaffolds for tissue engineering. *Materilas today.* 7: 30-40.

Ma Z, Kotaki M, Inai R, Ramakrishna S (2005) Potential of nanofiber matrix as tissue-engineering scaffolds. *Tissue Eng*. 11: 101-9.

Maciag T, Cerundolo J, Ilsley S, Kelley PR, Forand R (1979) An endothelial cell growth factor from bovine hypothalamus: identification and partial characterization. *Proc. Natl Acad. Sci. USA.* 76: 5674-8.

Mandal A, Meda V, Zhang WJ, Farhan KM, Gnanamani A (2012) Synthesis, characterization and comparison of antimicrobial activity of PEG/TritonX-100 capped silver nanoparticles on collagen scaffold. *Colloid surfaces B.* 90: 191-6.

Madhavan RV, Rosemary MJ, Nandkumar MA, Krishnan KV, Krishnan LK (2011) Silver nanoparticle impregnated poly(ε-caprolactone) scaffolds: optimization of antimicrobial and noncytotoxic concentrations. *Tissue Eng Part A.* 17: 439-49.

Malek AM, Izumo S (1996) Mechanism of endothelial cell shape change and cytoskeletal remodeling in response to fluid shear stress. *J Cell Sci.* 109: 713-26.

Mansfield PB, Wechezak AR, Sauvage LR (1975) Preventing thrombus on artificial vascular surfaces: true endothelial cell linings. *Trans.Amer.Soc.Artif.Intern. Organs*. 21: 264-72.

Martins A, Pinho ED, Faria S, Pashkuleva I, Marques AP, Reis RL, Neves NM (2009) Surface modification of electrospun polycaprolactone nanofiber meshes by plasma treatment to enhance biological performance. *Small.* 5: 1195-206.

Mathews A, Columbus S, Krishnan VK, Krishnan LK (2012) Vascular construction on poly(caprolactone) scaffolds by dynamic seeding: effect of pore size. *J. Tissue Eng. Regen. Med.* 6: 451-61.

Matthews JA, Wnek GE, Simpson DG, Bowlin GL (2002). Electrospinning of collagen nanofibers. *Biomacromolecules.* 3: 232-238.

Meinhart JG, Schense JC, Schima H, Gorlitzer M, Hubbell JA, Deutsch M, Zilla P (2005) Enhanced endothelial cell retention on shear-stressed synthetic vascular grafts precoated with RGD-cross-linked fibrin. *Tissue Eng.* 11: 887-95.

Melchels FP, Feijen J, Grijpma DW (2009) A poly(D,L-lactide) resin for the preparation of tissue engineering scaffolds by stereolithography. *Biomaterials.* 30: 3801-9.

Michaels AD, Chatterjee K (2002) Angioplasty versus bypass surgery for coronary artery disease. *Circulation.* 106: e107-e190.

Mikos AG, Bao Y, Cima LG, Ingber DE, Vacanti JP, Langer R (1993) Preparation of poly(glycolic acid) bonded fiber structures for cell attachment and transplantation. *J Biomed Mater Res*. 27: 183-9.

Mohan D, Melvin JW (1982) Failure properties of passive human aortic tissue. *J. Biomech.* 15: 887-902.

Murphy SV, Atala A (2014) 3D bioprinting of tissues and organs. *Nat Biotechnol*. 32: 773-85.

Murphy WL, Dennis RG, Kileny JL, Mooney DJ (2002) Salt Fusion: An approach to improve pore interconnectivity within tissue engineering scaffolds. *Tissue Eng.* 8: 43-52.

Nerem R, Alexander R, Chappell D. Medford R, Varner S, Taylor W (1998) The study of the influence of flow on vascular endothelial biology. *Am J Med Sci.* 316: 169-75.

Niklason LE, Gao J, Abbott WM, Hirschi KK, Houser S, Marini R, Langer R (1999) Functional arteries grown *in vitro*. *Science*. 284: 489-93.

Niklason LE, Abbott W, Gao J, Klagges B, Hirschi KK, Ulubayram K, Conroy N, Jones R, Vasanawala A, Sanzgiri S, Langer R (2001) Morphologic and mechanical characteristics of engineered bovine arteries. *J Vasc Surg*. 33: 628-38.

Nguyen TH, Bao TQ, Park I, Lee BT (2013) A novel fibrous scaffold composed of electrospun porous poly(ε-caprolactone) fibers for bone tissue engineering, *J. Biomater Appl*. 28: 514-28.

Nicolaides AN (1985) Haemodynamic aspects of vascular grafting. *Acta Chir Scand Suppl.* 529: 7-16.

Nirmala R, Kang HS, Park HM, Navamathavan R, Jeong IS, Kim HY (2012) Silver-loaded biomimetic hydroxyapatite grafted poly(ε-caprolactone) composite nanofibers: a cytotoxicity study. *J. Biomed. Nanotechnol*. 8: 125-32.

Odelius K, Hoglund A, Kumar S, Hakkarainen M, Ghosh AK, Bhatnagar N, Albertsson AC (2011) Porosity and pore size regulate the degradation product profile of polylactide. *Biomacromolecules* 12: 1250-8.

Oh SH, Kang SG, Lee JH (2006) Degradation behavior of hydrophilized PLGA scaffolds prepared by melt-molding particulate-leaching method: comparison with control hydrophobic one. *J Mater Sci Mater Med*. 17: 131-7.

Ohkawa K, Minato KI, Kumagai G, Hayashi S, Yamamoto H (2006) Chitosan nanofiber. *Biomacromolecules.* 7: 3291-4.

Pankajakshan D, Krishnan V K, Krishnan LK (2007) Vascular tissue generation in response to signaling molecules integrated with a novel poly(epsilon-caprolactone)-fibrin hybrid scaffold. *J Tissue Eng Regen Med*. 1: 389-97.

Pankajakshan D, Philipose LP, Palakkal M, Krishnan K, Krishnan LK (2008) Development of a fibrin composite-coated poly(ε-caprolactone) scaffold for potential vascular tissue engineering applications. *J Biomed Mater Res B Appl Biomater*. 87B: 570-9.

Pankajakshan D, Krishnan LK (2009) Design of fibrin matrix composition to enhance endothelial cell growth and extracellular matrix deposition for *in vitro* tissue engineering. *Artif Organs.* 33: 16-25.

Pankajakshan D, Agrawal DK (2010) Scaffolds in tissue engineering of blood vessels. *Can J Physiol Pharmacol*. 88: 855-73.

Patel A, Fine B, Sandig M, Mequanint K (2006) Elastin biosynthesis: the missing link in tissue engineered blood vessels. *Cardiovasc Res.* 71: 40-49.

Pavcnik D, Obermiller J, Uchida BT, Alstine WV, Edwards JM, Landry GJ, Kaufman JA, Keller FS, Rosch J (2009) Angiographic evaluation of carotid artery grafting with prefabricated small- diameter, small intestinal submucosa graftts in sheep. *Cardiovasc Intervent Radiol*.32: 106-113.

Pektok E, Nottelet B, Tille JC, Gurny R, Kalangos A, Moeller M, Walpoth BH (2008) Degradation and healing characteristics of small-diameter poly(epsilon-caprolactone) vascular grafts in the rat systemic arterial circulation. *Circulation*. 118: 2563-70.

Pham QP, Sharma U, Mikos AG (2006) Electrospun poly(ε-caprolactone) microfiber and multilayer nanofiber/microfiber scaffolds: characterization of scaffolds and measurement of cellular infiltration. *Biomacromolecules*. 7: 2796-805.

Rademacher A, Paulitschke M, Meyer R, Hetzer R (2001) Endothelialization of PTFE vascular grafts under flow induces significant cell changes. *Int J Artif Organs.* 24: 235-42.

Ratcliffe D (2000) Tissue engineering of vascular grafts. *Matrix biology*. 19: 353-7.

Resmi KR, Krishnan LK (2002) Protease action and generation of beta-thromboglobulin-like protein followed by platelet activation. *Thromb Res.* 106: 229-36.

Rezai N, Podor TJ, McManus BM (2004) Bone marrow cells in the repair and modulation of heart and blood vessels: emerging opportunities in native and engineered tissue and biomechanical materials. *Artif Organs*. 28: 142-51.

Rnjak-Kovacina J, Weiss AS (2011) Increasing the pore size of electrospun scaffolds. *Tissue Eng Part B: Reviews.* 17: 365-372.

Rogers L, Said SS, Mequanint K (2013) The effects of fabrication strategies on 3D scaffold morphology, porosity, and vascular smooth muscle cell response, *J. Biomater.Tissue Eng.* 3, 300-11.

Roh JD, Nelson GN, Brennan MP, Mirensky MT, Yi T, Hazlett TF, Tellides G, Sinusas AJ, Pober JS, Saltzman WM, Kyriakides TR, Breuer CK (2008) Small-diameter biodegradable scaffolds for functional vascular tissue engineering in the mouse model. *Biomaterials.* 29: 1454-63.

Rujitanaroj P, Pimpha N, Supaphol P (2008) Wound-dressing materials with antibacterial activity from electrospun gelatin fiber mats containing silver nanoparticles. *Polymer*. 49: 4723-32.

Ross R (1993) The pathogenesis of atherosclerosis: a perspective for the 1990s. *Nature.* 362: 801-9.

Rubanyi GM (1993) The role of endothelium in cardiovascular homeostasis and diseases. *J Cardiovasc Pharmacol*. 4: S1-S14.

Ruoslahti E, Pierschbacher MD (1987) New Perspectives In cell adhesion RGD and integrins. *Science.* 238: 491-7.

Sahoo S, Ang LT, Goh JC, Toh SL (2010) Growth factor delivery through electrospun nanofibers in scaffolds for tissue engineering applications. *J Biomed Mater Res A*. 93: 1539-50.

Sarkar S, Salacinski HJ, Hamilton G, Seifalian AM (2006) The mechanical properties of infrainguinal vascular bypass grafts: their role in influencing patency. *Eur J Vasc Endovasc Surg.* 31: 627-36.

Schwarz K, Epple M (1998) Hierarchically structured polyglycolide- A biomaterial mimicking natural bone. *Macromol. Rapid Commun*. 19: 613-7.

Seliktar D, Nerem RM, Galis ZS (2003) Mechanical strain-stimulated remodeling of tissue-engineered blood vessel constructs. *Tissue Eng.* 9: 657-66.

Shin YM, Lim JY, Park JS, Gwon HJ, Jeong SI, and Lim YM (2014) Radiation-induced biomimetic modification of dual-layered nano/microfibrous scaffolds for vascular tissue engineering. *Biotechnol. Bioprocess Eng.* 19: 118-25.

Shinoka T, Shum-Tim D, Ma PX, Tanel RE, Isogai N, Langer R, Vacanti JP, Mayer JE Jr (1998) Creation of viable pulmonary artery autografts through tissue engineering. *J Thorac Cardiovasc Surg.* 115: 536-45.

Shin'oka T, Matsumura G, Hibino N, Naito Y, Watanabe M, Konuma T, Sakamoto T, Nagatsu M, Kurosawa H (2005) Midterm clinical result of tissue-engineered vascular autografts seeded with autologous bone marrow cells. *J Thorac Cardiovasc Surg.* 129: 1330-8.

Shoichet MS (2010) Polymer scaffolds for biomaterial applications. *Macromolecules.* 43: 581-91.

Shum AW, Mak AF (2003) Morphological and biomechanical characterization of poly(glycolic acid) scaffolds after *in vitro* degradation. *Polym Degrad Stabil.* 81: 141-9.

Siedlecki CA, Marchant RE (1998) Atomic force microscopy for characterization of the biomaterial interface. *Biomaterials.* 19: 441-54.

Sill TJ, Recum HA (2008) Electrospinning: Applications in drug delivery and tissue engineering. *Biomaterials*. 29: 1989-2006.

Simper D, Stalboerger PG, Panetta CJ, Wang S, Caplice NM (2002) Smooth muscle progenitor cells in human blood. *Circulation.* 106: 1199-204.

Soliman S, Sant S, Nichol JW, Khabiry M, Traversa E, Khademhosseini A (2011) Controlling the porosity of fibrous scaffolds by modulating the fiber diameter and packing density. *J Biomed Mater Res A.* 96: 566-74.

Soletti L, Hong Y, Guan J, Stankus JJ, El-Kurdi MS, Wagner WR, Vorp DA (2010) A bilayered elastomeric scaffold for tissue engineering of small diameter vascular grafts. *Acta Biomater*. 6: 110-22.

Son WK, Youk JH, Park WH (2006) Antimicrobial cellulose acetate nanofibers containing silver nanoparticles. *Carbohydrate Polym* 65: 430-4.

Soyer T, Lempinen M, Cooper P, Norton L, Eiseman B (1972) A new venous prosthesis. *Surgery.* 72: 864-72.

Sreerekha PR ,Divya P, Krishnan LK (2006) Adult stem cell homing and differentiation *in vitro* on composite fibrin matrix. *Cell Prolif.* 39: 301-12.

Stankus JJ, Guan J, Fujimoto K, Wagner WR (2006) Microintegrating smooth muscle cells into a biodegradable, elastomeric fiber matrix. *Biomaterials*. 27: 735-44.

Starzl TE (2003) A trip south. In: Starzl TE (ed), *The Puzzle People: Memoirs of a Transplant Surgeon*, University of Pittsburgh Press, Pittsburgh, pp.47-58.

Suh SW, Shin JY, Kim J, Kim J, Beak CH, Kim DI, Kim H, Jeon SS, Choo IW (2002) Effect of different particles on cell proliferation in polymer scaffolds using a solvent-casting and particulate leaching technique. *ASAIO J*. 48: 460-4.

Sumpio BE, Riley JT, Dardik A (2002) Cell in focus: Endothelial cell. *Int J Biochem Cell Biol.* 34: 1508-12.

Swenne CL, Borowiec J, Carlsson M, Lindholm C (2006) Prediction of risk factors for surgical wound infection in sephenous vein harvesting leg in patients undergoing coronary artery bypass. *Thorac cardiovasc surg.* 54: 300-6.

Taboas JM, Maddox RD, Krebsbach PH, Hollister SJ (2003) Indirect solid free form fabrication of local and global porous, biomimetic and composite 3D polymer-ceramic scaffolds. *Biomaterials*. 24: 181-94.

Tang ZG, Black RA, Curran JM, Hunt JA, Rhodes NP, Williams DF (2004) Surface properties and biocompatibility of solvent-cast poly(ε-caprolactone) films. *Biomaterials.* 25: 4741-8.

Thapa A, Webster TJ, Haberstroh KM (2003) Polymers with nano-dimensional surface features enhance bladder smooth muscle cell adhesion. *J Biomed Mater Res A.* 67: 1374-83.

Thomas LV, Nair PD (2011) (Citric acid-co-polycaprolactone triol) polyester: A biodegradable elastomer for soft tissue engineering. *Biomatter*. 1: 81-90.

Tranquillo RT, Girton TS, Bromberek BA, Triebes TG, Mooradian DL (1996) Magnetically orientated tissue-equivalent tubes: application to a circumferentially orientated media-equivalent. *Biomaterials.* 17: 349-57.

Tu C, Cai Q, Yang J, Wan Y, Bei J, Wang S (2003) The fabrication and characterization of poly(lactic acid) scaffolds for tissue engineering by improved solid-liquid phase separation. *Polym. Adv. Technol.* 14: 565-73.

Uchida T, Ikeda S, Oura H, Tada M, Nakano T, Fukuda T, Matsuda T, Negoro M, Arai F (2008) Development of biodegradable scaffold based on patient specific arterial configuration. *J. Biotech*. 133: 213-8.

Valence S, Tille J, Mugnai D, Mrowczynski W, Gurny R, Moller M, Walpoth BH (2012) Long term performance of a poly(caprolactone) vascular grafts in rat abdominal aorta. *Biomaterials.* 33: 38-47.

Vance RJ, Miller DC, Thapa A, Haberstroh KM, Webster TJ (2004) Decreased fibroblast cell density on chemically degraded poly-lactic-co-glycolic acid, polyurethane and polycaprolactone. *Biomaterials.* 25: 2095-103.

Vanhoutte PM (1989) Endothelium and control of vascular function. State of the art lecture. *Hypertension.* 13: 658-67.

Voorhees AB Jr, Jeretzki A, Blakemore AH (1952) The use of tubes constructed from vinyon "N" cloth in bridging arterial defects. *Ann Surg.* 135: 332-36.

Walluscheck KP, Steinhoff G, Kelm S, Haverich A (1996) Improved endothelial cell attachment on ePTFE vascular grafts pretreated with synthetic RGD-containing peptides. *Eur J Vasc Endovasc Surg*. 12: 321-30.

Walpoth BH, Rogulenko R, Tikhvinskia E, Gogolewski S, Schaffner T, Hess OM, Althaus U (1998) Improvement of patency rate in heparin-coated small synthetic vascular grafts. *Circulation.* 98: II319-23.

Wan AC, Mao HQ, Wang S, Leong KW, Ong LK, Yu H (2001) Fabrication of poly(phosphoester) nerve guides by immersion precipitation and the control of porosity. *Biomaterials*. 22: 1147-56.

Wang H, Feng Y, Zhao H, Xiao R, Lu J, Zhang L, Guo J (2012) Electrospun hemocompatible PU/gelatin-heparin nanofibrous bilayer scaffolds as potential artificial blood vessels. *Macromol. Res.* 20: 347-50.

Wen X, Zhang N (2006) Biomaterials for tissue engineering. In: Shi D (ed) *Introduction to biomaterials*, World scientific publishing Co. Pvt. Ltd, Singapore, pp 214.

Weinberg CB, Bell E (1986) A blood vessel model constructed from collagen and cultured vascular cells. *Science.* 231: 397-400.

Williams C, Wick TM (2004) Perfusion bioreactor for small diameter tissue-engineered arteries. *Tissue Eng*. 10: 930-41.

Williams D (1999) *The Williams Dictionary of Biomaterials*. Liverpool University Press, Liverpool, pp. 283.

Williams JM, Adewunmi A, Schek RM, Flanagan CL, Krebsbach PH, Feinberg SE, Hollister SJ, Das S (2005) Bone tissue engineering using polycaprolactone scaffolds fabricated via selective laser sintering. *Biomaterials* 26: 4817-27.

Williamson MR, Black R, Kielty C (2006) PCL-PU composite vascular scaffold production for vascular tissue engineering: attachment, proliferation and bioactivity of human vascular endothelial cells. *Biomaterials*. 27: 3608-16.

Woodfield TB, Van Blitterswijk CA, De Wijn J, Sims TJ, Hollander AP, Riesle J (2005) Polymer scaffolds fabricated with pore-size gradients as a model for studying the zonal organization within tissue-engineered cartilage constructs. *Tissue Eng*. 11: 1297-311.

Woodward SC, Brewer PS, Moatamed F, Schindler A, Pitt CG (1985) The intracellular degradation of poly(epsilon-caprolactone). *J Biomed Mater Res*. 19: 437-44.

Wu L, Ding J (2005) Effects of porosity and pore size on *in vitro* degradation of three-dimensional porous poly(D,L-lactide-co-glycolide) scaffolds for tissue engineering. *J Biomed Mater Res A*. 75: 767-77.

Xing ZC, Chae WP, Baek JY, Choi MJ, Jung Y, Kang IK (2010) *In vitro* assessment of antibacterial activity and cytocompatibility of silver-containing PHBV nanofibrous scaffolds for tissue engineering. *Biomacromolecules*. 11, 1248-53.

Xu C, Yang F, Wang S, Ramakrishna S (2004a) *In vitro* study of human vascular endothelial cell function on materials with various surface roughness. *J Biomed Mater Res A.* 71: 154-61.

Xu C, Inai R, Kotaki M, Ramakrishna S (2004b) Electrospun nanofiber fabrication as synthetic extracellular matrix and its potential for vascular tissue engineering. *Tissue Eng.* 10: 1160-8.

Xu X, Yang Q, Wang Y, Yu H, Chen X, Jing X (2006) Biodegradable electrospun poly(L-lactide) fibers containing antibacterial silver nanoparticles. *European Polymer Journal*. 42: 2081-87.

Yan D, Jones J, Yuan X, Xu X, Sheng J, Lee JC, Ma G, Yu Q (2013) Plasma treatment of random and aligned electrospun PCL nanofibers. *J. Med. Biol. Eng*. 33: 171-8.

Yang J, Shi G, Bei J, Wang S, Cao Y, Shang Q, Yang G, Wang W (2002) Fabrication and surface modification of macroporous poly(L-lactic acid) and poly(L-lactic-co-glycolic acid) (70/30) cell scaffolds for human skin fibroblast cell culture. *J Biomed Mater Res*. 62: 438-46.

Yang QB, Li DM, Hong YL, Li ZY, Wang C, Qiu SL, Wei Y (2003) Preparation and characterization of a PAN nanofibre containing Ag nanoparticles via electrospinning. *Synth Met.* 137: 973-4.

Yang S, Leong KF, Du Z, Chua CK (2001) The Design of scaffolds for use in tissue engineering. part I. traditional factors. *Tissue Eng.* 7: 679-89.

Yoon JJ, Park TG (2001) Degradation behaviors of biodegradable macroporous scaffolds prepared by gas foaming of effervescent salts. *J Biomed Mater Res.* 55: 401-8.

Yu DG, Zhou J, Chatterton NP, Li Y, Huang J, Wang X (2012) Polyacrylonitrile nanofibers coated with silver nanoparticles using a modified coaxial electrospinning process. *Int J Nanomedicine*. 7: 5725-32.

Yu H, Matthew HW, Wooley PH, Yang SY (2008) Effect of porosity and pore Size on microstructures and mechanical properties of poly-ε-Caprolactone hydroxyapatite composites. *J. Biomed. Mater. Res B Appl. Biomater*. 86: 541-7.

Yimsiri P, Mackley MR (2006) Spin and dip coating of light emitting polymer solutions: matching experiment with modelling. *Chem. Eng. Sci*. 61: 3496-505.

Yow KH, Ingram J, Korossis SA, Ingram E, Vanniasinkam SH (2006) Tissue engineering of vascular conduits. *British Journal of Surgery.* 93: 652-61.

Zein I, Hutmacher DW, Tan KC, Teoh SH (2002) Fused deposition modeling of novel scaffold architectures for tissue engineering applications. *Biomaterials.* 23:1169-85.

Zeltinger J, Sherwood JK, Graham DA, Müeller R, Griffith LG (2001) Effect of pore size and void fraction on cellular adhesion, proliferation, and matrix deposition. *Tissue Eng*. 7: 557-72.

Zhang J, Wu L, Jing D, Ding J (2005) A comparative study of porous scaffolds with cubic and spherical macropores. *Polymer*. 46: 4979-85.

Zhang L, Zhou J, Lu Q, Wei Y, Hu S (2008) A novel small-diameter vascular graft*: In vivo* behavior of biodegradable three-layered tubular scaffolds. *Biotechnol. Bioeng.* 99: 1007-15.

Zhao S, Wu X, Wang L, Huang Y (2004) Electrospinning of ethyl-cyanoethyl cellulose/tetrahydrofuran solutions. *J. Appl. Polym. Sci*. 91: 242-6.

Zong XH, Kim K, Fang DF, Ran SF, Hsiao BS, Chu B (2002) Structure and process relationship of electrospun bioabsorbable nanofiber membranes. *Polymer*. 43: 4403-12.

LIST OF PUBLICATIONS

Original Papers

1. **Soumya Columbus**, Lissy K Krishnan and Kalliyana Krishnan V (2014) Relating pore size variation of poly(ε-caprolactone) scaffolds to molecular weight of porogen and evaluation of scaffold properties after degradation. *Journal of Biomedical Materials Research Part B: Applied Biomaterials.*102: 789-796 (IF- 2.328).

2. **Soumya Columbus**, Lissy K Krishnan and Kalliyana Krishnan V (2014) Modulating the properties of poly(ε-caprolactone) scaffolds by altering porogen molecular weight and concentration for blood-vessel tissue engineering. *Journal of Biomaterials and Tissue Engineering* 4: 450-458 (IF- 1.167).

3. Asha S. Mathews, **Soumya Columbus**, Kalliyana Krishnan V and Lissy K Krishnan (2012) Vascular tissue construction on poly(ε-caprolactone) scaffolds by dynamic endothelial cell seeding: effect of pore size. *Tissue Engineering and Regenerative Medicine* 6: 451-461 (IF- 4.428).

4. Ragaseema VM, **Soumya Columbus**, Renu Ramesh and Lissy K Krishnan (2014) Potential of tissue engineered blood vessel as model to study the effect of flow and wall thickness on cellular communication. *Current Tissue Engineering* 3: 39-46.

5. **Soumya Columbus**, Renu Ramesh, Renjith P Nair, Lissy K Krishnan and Kalliyana Krishnan V. Alteration of electrospun scaffold properties by silver nanoparticle incorporation: evaluation for vascular graft applications (Under communication).

6. **Soumya Columbus**, Renjith P Nair, Lissy K Krishnan and Kalliyana Krishnan V. Internal microarchitecture influences the properties of bi-layered poly(ε-

caprolactone) scaffolds for constructing tissue engineered small diameter blood vessels (Under preparation).

7. **Soumya Columbus**, Renjith P Nair, Lissy K Krishnan and Kalliyana Krishnan V. Investigation of physico-mechanical properties of solvent cast scaffold after silver nanoparticle incorporation for constructing small diameter blood vessels (Under preparation)

8. **Soumya Columbus**, Renjith P Nair, Lissy K Krishnan and Kalliyana Krishnan V. Feasibility of quantum dots incorporated poly(ε-caprolactone) scaffolds as small diameter vascular constructs (Under preparation).

Paper presentations and Conference Proceedings

1. **Soumya Columbus**, Arun Torris, Lissy K. Krishnan and Kalliyana Krishnan V "A micro-tomography (micro-CT) study on the effect of porogen concentration upon the porosity characteristics of polymer scaffolds for tissue engineering" **(Oral),** National Conference on Medical Materials (NCMM), Indian Institute Technology, Chennai, December 13-14, 2007.

2. Arun Torris , **Soumya Columbus**, Saaj US, Manitha B Nair and Kalliyana Krishnan V, "Evaluation of Biomaterials Using Micro-Computerized Tomography" published in *American Institute of Physics AIP Conference Proceedings* 1050, 68-78, 2008.

3. **Soumya Columbus**, Lissy K. Krishnan and Kalliyana Krishnan V "*In vitro* degradation study of polycaprolactone scaffolds in different media for vascular tissue engineering applications" **(Oral)**, 21st Kerala Science congress, Kerala State Council for Science, Technology and Environment, Kollam, January 28-31, 2009.

4. **Soumya Columbus**, Arun Torris, Lissy K. Krishnan and Kalliyana Krishnan V "Effect of porogen size on the pore characteristics of Polycaprolactone scaffold: A micro-CT study" **(Poster),** 1st International Conference NANO BIO (Tissue

Engineering and Stem Cell Research using Nanomaterials), Amrita Institute of Medical Sciences, Kochi, February 17-19, 2009.

5. **Soumya Columbus**, Lissy K. Krishnan and Kalliyana Krishnan V. "Evaluation of a potential biodegradable scaffold for vascular tissue engineering" **(Poster)**, International Conference on Materials Science and Technology (ICMST), Indian Institute of Space Science and Technology, Trivandrum, October 29-31, 2010.

6. **Soumya Columbus**, Lissy K. Krishnan and Kalliyana Krishnan V, "Evaluation of a potential biodegradable scaffold for vascular tissue engineering" **(Oral)**, Science competition Organized by SCTIMST in connection with Institute Day celebrations, March 12, 2011.

7. **Soumya Columbus**, Lissy K. Krishnan and Kalliyana Krishnan V, "Biodegradable polyester scaffolds for potential small diameter vascular graft applications" **(Oral)**, National seminar on Polymers in Medicine and biology (PMB), Bannari Amman Institute of Technology, Coimbatore, January 7-8, 2011.

8. Kalliyana Krishnan V, **Soumya Columbus** and Lissy K Krishnan, 'Biologically modified bi-layered antimicrobial poly(caprolactone) scaffolds for small diameter vascular graft applications" abstract published in *Tissue Engineering and Regenerative Medicine,* 6(1), 146, 2012 (DOI: 10.1002/ter.1586).

9. Lissy K Krishnan, Renu Ramesh, **Soumya Columbus** and Kalliyana Krishnan V**,** 'Functional tissue engineering of small diameter vascular graft using circulating sheep endothelial and smooth muscle progenitor cells" abstract published in *Tissue Engineering and Regenerative Medicine,* 6(1), 144, 2012 (DOI: 10.1002/ter.1586).

10. **Soumya Columbus** and Kalliyana Krishnan V, "Silver nanoparticle incorporated polycaprolactone scaffolds for small diameter vascular grafts" **(Oral)** National Seminar on Advanced Polymers (NSAP), Mahathma Gandhi College of Engineering, Thodupuzha, September 28-29, 2012.

11. **Soumya Columbus**, Lissy K. Krishnan and Kalliyana Krishnan V, "Evaluation of antimicrobial tissue engineered poly(caprolactone) scaffolds for vascular constructs" **(Oral)**, 3rd FAPS Polymer Congress and MACRO, Indian Institute of Science, Bangalore, May 15-18, 2013.

12. **Soumya Columbus**, Lissy K. Krishnan and Kalliyana Krishnan V, "Evaluation of bi-layered electrospun scaffolds for potential small diameter vascular constructs" **(Oral)** National Seminar on Biopolymers and Green composites (BPGC), Centre for Biopolymer Science and Technology (CPGC), Kochi, September 27, 2013.

CURRICULUM VITAE

Education

Ph.D. Scholar (June 2010- present) at Sree Chitra Tirunal Institute for Medical Sciences and Technology, Biomedical Technology Wing, Thiruvananthapuram, Kerala, India.

Master of Science in Polymer Chemistry (2004-2006), Department of Chemistry, St.Michael's College, Cherthala, Kerala, India (Passed with First rank).

Bachelor of Science in Chemistry (2001-2004), Department of Chemistry, St.Michael's College, Cherthala, India (Passed with First class and Distinction).

Achievements

1. ***Best oral presentation award*** on "Biodegradable polyester scaffolds for potential small diameter vascular graft applications" by Soumya Columbus, Lissy K Krishnan and V Kalliyana Krishnan in National seminar on Polymers in Medicine and biology (PMB) organized by BIT, Coimbatore 7-8th January 2011.

2. ***Best oral presentation award*** on 'Silver nanoparticle incorporated poly(caprolactone) scaffolds for small diameter vascular grafts' by Soumya Columbus, V Kalliyana Krishnan in National Seminar on Advanced Polymers (NSAP) organized by Mahathma Gandhi College of Engineering, Thodupuzha on 28-29th September 2012.

3. ***Best oral presentation award*** on 'Evaluation of bi-layered electrospun scaffolds for potential small diameter vascular constructs' by Soumya Columbus, Lissy K. Krishnan, V Kalliyana Krishnan in National Seminar on Biopolymers and Green composites (BPGC) organized by Centre for Biopolymer Science and Technology (CPGC), Kochi on 27th September 2013.

APPENDIX

PBS (1000 ml) pH 7.4

NaCl	-	8g
KCl	-	0.2g
Na_2HPO_4	-	1.44g
KH_2PO_4	-	0.24g

(Added distilled water to a final volume of 1000 ml, solution is filtered and stored at room temperature)

HBSS (1000 ml) pH- 7.4

KCl	-	0.4g
KH_2PO_4	-	0.06g
NaCl	-	8g
Na_2PO_4	-	0.0482g

(Added distilled water to a final volume of 1000 ml, solution was filtered autoclaved and stored at 4ºC)

SFM

MCDB 131	-	50ml
Antibiotics (10X)	-	500µl

(Filtered and stored at 4ºC)